

DOTTORATO DI RICERCA
IN BIOINGEGNERIA

Ciclo XXI

Settore scientifico disciplinare di afferenza: ING-IND/34

TITOLO TESI

**CARATTERIZZAZIONE BIOMECCANICA *IN VITRO*
DELLE OSSA LUNGHE DELLO SCHELETRO UMANO**

***HUMAN LONG BONES IN VITRO
BIOMECHANICAL CHARACTERIZATION***

Presentata da: Ing. MATEUSZ JUSZCZYK

Coordinatore Dottorato:
Prof. Angelo Cappello

Relatore:
Prof. Luca Cristofolini

CONTENTS

| | |
|---|----|
| SOMMARIO | 4 |
| SUMMARY..... | 7 |
| 1 INTRODUCTION..... | 10 |
| 1.1 BONE- AN ENGINEERING APPROACH..... | 11 |
| 1.1.1 CORTICAL BONE | 11 |
| 1.1.2 CANCELLOUS BONE..... | 16 |
| 1.1.3 REFERENCES | 19 |
| 1.2 LHDL PROJECT..... | 21 |
| 1.3 SCOPE OF THE THESIS | 23 |
| 1.4 STRUCTURE OF THE THESIS | 25 |
| 2 METHODOLOGY | 28 |
| 2.1. THE MARKER FOR MULTI BIOMEDICAL VISUALISATION..... | 29 |
| 2.2 COMPARISON OF THREE STANDARD ANATOMICAL REFERENCE FRAMES FOR THE TIBIA-FIBULA COMPLEX..... | 32 |
| 2.2.1 ABSTRACT | 33 |
| 2.2.2. INTRODUCTION | 34 |
| 2.2.3 MATERIALS AND METHODS | 35 |
| 2.2.3.1 SPECIMENS | 35 |
| 2.2.3.2 DEFINITION OF THE THREE REFERENCE FRAMES..... | 36 |
| 2.2.3.3 <i>IN VITRO</i> ACQUISITION | 38 |
| 2.2.3.4 STATISTICAL ANALYSIS | 39 |
| 2.2.4 RESULTS..... | 41 |
| 2.2.4.1 REPEATABILITY OF THE LANDMARKS..... | 41 |
| 2.2.4.2 REPEATABILITY OF THE REFERENCE FRAMES | 42 |
| 2.2.4.3 DIFFERENT ORIENTATION OF THE REFERENCE FRAMES..... | 43 |
| 2.2.5 DISCUSSION..... | 45 |
| 2.2.6 REFERENCES | 47 |
| 2.3 A METHOD TO IMPROVE EXPERIMENTAL VALIDATION OF FINITE-ELEMENT MODELS OF LONG BONES..... | 49 |
| 2.3.1 ABSTRACT | 50 |
| 2.3.3 MATERIALS AND METHODS | 53 |
| 2.3.4 RESULTS AND DISCUSSION..... | 63 |
| 2.3.5 CONCLUSIONS | 67 |
| 2.3.6 REFERENCES | 69 |

| | |
|---|-----|
| 2.4 IN VITRO TECHNIQUE TO DETERMINE TIME AND LOCATION OF FRACTURE INITIATION IN BONES | 71 |
| 2.4.1 INTRODUCTION | 72 |
| 2.4.2. MATERIALS | 74 |
| 2.4.2.1 CRACK-GRID APPLICATION | 74 |
| 2.4.2.2 DATA LOGGING | 75 |
| 2.4.3 ELECTRICAL TESTING OF THE CRACK-GRID | 76 |
| 2.4.4. MECHANICAL TESTING OF THE CRACK-GRID | 77 |
| 2.4.4.1 METHODS | 77 |
| 2.4.4.2 RESULTS | 78 |
| 2.4.5 TESTING OF THE CRACK-GAUGE ON SIMPLIFIED BONE SPECIMENS | 79 |
| 2.4.5.1 METHODS | 79 |
| 2.4.5.2 RESULTS | 81 |
| 2.4.6 TESTING OF THE CRACK-GAUGE ON FEMORAL METAPHYSES ... | 82 |
| 2.4.6.1 METHODS | 82 |
| 2.4.6.2 RESULTS | 83 |
| 2.4.7 DISCUSSION | 84 |
| 3 GENERAL BIOMECHANICAL CHARACTERIZATION OF LONG BONES . | 89 |
| 3.1 LHDL RELATED DATA ACQUISITION | 90 |
| 3.1.1 WHOLE-BONE STIFFNESS | 91 |
| 3.1.2 STRAIN DISTRIBUTION IN WHOLE BONES | 92 |
| 3.1.3 WHOLE-BONE STRENGTH | 93 |
| 3.2 STRUCTURAL BEHAVIOUR OF THE LONG BONES OF THE HUMAN LOWER LIMBS | 95 |
| 3.2.1 INTRODUCTION | 96 |
| 3.2.2 MATERIALS AND METHODS | 96 |
| 3.2.2.1 DESIGN OF THE EXPERIMENT | 96 |
| 3.2.2.2 SPECIMENS | 96 |
| 3.2.2.3 STRAIN MEASUREMENT | 97 |
| 3.2.2.4 <i>IN VITRO</i> LOADING | 101 |
| 3.2.5 STATISTICAL ANALYSIS | 103 |
| 3.2.3 RESULTS | 104 |
| 3.2.3.1 LINEARITY AND CREEP | 104 |
| 3.3.3.2 STIFFNESS AND STRAIN DISTRIBUTION | 104 |
| 3.2.3.3 EFFECT OF LOADING RATE | 106 |

| | |
|---|-----|
| 3.2.3.4 EFFECT OF LOADING DIRECTION | 108 |
| 3.2.4 REFERENCES | 110 |
| 4.1 STRAIN DISTRIBUTION IN THE PROXIMAL HUMAN FEMORAL METAPHYSIS | 112 |
| 4.1.2 INTRODUCTION | 115 |
| 4.1.3 MATERIALS AND METHODS | 116 |
| 4.1.3.1 TEST SPECIMENS..... | 116 |
| 4.1.3.2 STRAIN MEASUREMENT | 119 |
| 4.1.3.3 MEASUREMENT OF CORTICAL BONE THICKNESS..... | 120 |
| 4.1.3.4 ANALYSIS OF REINFORCEMENT CAUSED BY STRAIN GAUGES | 120 |
| 4.1.3.5 <i>IN VITRO</i> LOADING CONFIGURATIONS..... | 121 |
| 4.1.3.6 STATISTICS | 123 |
| 4.1.3 RESULTS | 124 |
| 4.1.4 DISCUSSION..... | 130 |
| 4.1.5 REFERENCES | 135 |
| 4.2 IN VITRO REPLICATION OF SPONTANEOUS FRACTURES OF THE PROXIMAL HUMAN FEMUR | 139 |
| 4.2.1 ABSTRACT | 140 |
| 4.2.2 INTRODUCTION | 141 |
| 4.2.3 MATERIALS AND METHODS | 143 |
| 4.2.3.1 IDENTIFICATION OF THE MOST CRITICAL LOADING SCENARIO: FE SIMULATIONS | 143 |
| 4.2.3.2 EXPERIMENTAL SETUP, MEASUREMENTS AND RECORDING | 144 |
| 4.2.3.3 ASSESSMENT OF THE TEST PROTOCOL..... | 145 |
| 4.2.4 RESULTS | 146 |
| 4.2.4.1 MOST CRITICAL LOADING SCENARIO: FE SIMULATIONS..... | 146 |
| 4.2.4.2 RESULTS FROM 10 BONE SPECIMENS..... | 148 |
| 4.2.5. DISCUSSION AND CONCLUSIONS | 150 |
| 4.2.6 REFERENCES | 153 |
| 5 CONCLUSIONS | 158 |
| CONCLUSIONS | 159 |
| APPENDIX | 160 |

Sommario

La presente tesi descrive i risultati delle ricerche svolte durante il Dottorato in Bioingegneria. L'obiettivo di questa ricerca era quello di valutare le proprietà biomeccaniche di sei ossa lunghe umane (radio, ulna, omero, femore, tibia e perone), come contributo alla creazione del "Living Human Digital Library" (LHDL). La ricerca presentata in questa tesi è stata effettuata presso il Laboratorio di Tecnologia Medica (LTM) dell'Istituto Ortopedico Rizzoli (Bologna), partner all'interno del progetto LHDL.

Un osso lungo è il principale argomento di tutti gli studi presentati in questa tesi. Ogni osso può essere considerato come tessuto, struttura e organo simultaneamente, tuttavia verranno qui presentati solo gli aspetti studiati a livello di organo. Le ossa lunghe sono state ampiamente studiate in passato e la loro biomeccanica è nota, ma finora non sono state presentate descrizioni inter-disciplinari e multi-livello dell'apparato muscolo-scheletrico umano. In realtà, il progetto LHDL mira ad indagare due cadaveri umani, partendo dal livello globale del corpo attraverso il livello organico fino quello proteico, creando un dataset multi-livello specifico dei soggetti analizzati. All'interno di questo quadro, l'obiettivo di questa tesi è stato quello di misurare, per ciascuno dei sei segmenti ossei la rigidità, la resistenza e la distribuzione delle deformazioni

Lo sviluppo di metodologie in grado di garantire elevata qualità dei dati e futura compatibilità spaziale per la fusione tra livelli strutturali è risultata essenziale all'interno di questo studio.

Pertanto, un sistema di marcatori per le diverse tecniche di imaging medico è stato sviluppato con lo scopo di aiutare la fusione tra diverse misure a livello di corpo, organi e segmenti. Utilizzando i marcatori sviluppati è stato possibile combinare dati provenienti da TAC, RMN e cinematica passiva e, inoltre, preservare le i segmenti ossei da qualsiasi rischio di danni meccanici, come ad esempio l'esecuzione di fori previsti dalla tecnica utilizzata in precedenza.

Una definizione univoca dei sistemi di riferimento della biomeccanica muscolo-scheletrica è stata estremamente importante. Soprattutto in virtù del fatto che dovevano essere svolte misure multi-livello. Pertanto tre sistemi di coordinate anatomiche sono

stati confrontati per definire quello maggiormente riproducibile per il tracciamento dei piani anatomici.

Parte degli obiettivi del laboratorio sono stati la creazione e validazione di modelli ad elementi finiti (FEM) disegnati sul soggetto. Pertanto, è stato necessario fornire alcuni dati per la definizione delle condizioni al contorno, di fondamentale importanza per una accurata validazione di modelli FEM.

Prima di tutto, allo scopo di riprodurre la posizione delle forze risultanti del giunto, durante il test *in vitro* delle ossa lunghe, è stata sviluppata una apposita cella di carico. Successivamente, per misurare il punto iniziale di frattura, necessario per la validazione dei modelli FEM per la predizione di fratture ossee, una nuova tecnica chiamata Crack Grid è stata sviluppata.

La Crack Grid ha consentito di distinguere il punto di frattura con una risoluzione spaziale di 3 mm, fornendo dati sufficientemente precisi per la convalida dei modelli FEM e fornendo ulteriori informazioni relative alla meccanica delle strutture ossee. Tuttavia questa tecnica non è limitata solo alla convalida dei modelli FEM, ad esempio può essere applicata per verificare le relazioni tra la frattura e l'orientamento del collagene nella stessa regione. Inoltre, la Crack Grid può essere applicata in altri ambiti della scienza dei materiali, come i materiali compositi, le ceramiche, ecc, dove il punto di innesco e propagazione della frattura sono temi di studio comuni. I risultati di questo studio possono essere distinti come: legati allo sviluppo dell'enciclopedia digitale prevista all'interno del progetto LHDL; ma anche risposte a specifici quesiti di ricerca.

I dati relativi alle richieste del progetto LHDL sono la distribuzione delle deformazioni di segmenti ossei interi, la rigidità e la resistenza per uno scenario definito a priori (torsione, flessione a quattro punti), dipendente dal tipo di segmento osseo.

Le relazioni di velocità e direzione di carico sono state valutate attraverso lo studio del comportamento viscoelastico e non lineare della struttura ossea.

All'interno di questa tesi sono stati condotti due studi specifici riguardanti il femore prossimale. Il primo la distribuzione delle deformazioni del femore prossimale. Si è trattato di un dettagliato studio, basato sull'utilizzo di strain-gauge, mirato alla comprensione delle capacità di carico della struttura ossea.

Il secondo studio riguarda le fratture spontanee del femore prossimale. Non esistono evidenze, né consenso scientifico, relativamente ai più rilevanti scenari di carico. Lo scopo di questo lavoro è stato quello di sviluppare e validare un metodo sperimentale per replicare *in vitro* scenari di fratture spontanee, basandosi su carichi clinicamente rilevanti.

Una combinazione di tecniche computazionali e sperimentali è stata applicata per replicare le fratture del femore prossimale con grande ripetibilità e riproducibilità. Per prima cosa è stato identificato lo scenario di carico più rilevante tramite l'utilizzo di un modello numerico. È stato poi evidenziato che non è necessario includere la funzione dei muscoli quando è in analisi la frattura del collo del femore. Il set-up sperimentale è stato poi progettato di conseguenza. Modelli di frattura clinicamente rilevanti sono stati ottenuti. Il metodo proposto può essere usato per investigare le ragioni ed i meccanismi di fallimento di femori prossimali sani ed operati.

Il lavoro svolto sino ad ora ha anche alcune applicazioni pratiche. Infatti la conoscenza pratica sviluppata testando i femori prossimali è stata applicata anche all'ottimizzazione di protesi prossimali di femore.

SUMMARY

The present thesis describes results of the research performed throughout the Ph.D. in Bioengineering. The aim of this research was to evaluate biomechanical properties of the six human long bones (radius, ulna, humerus, femur, tibia and fibula), as a contribution in the creation of the “Living Human Digital Library”(LHDL). The research presented in this thesis was carried out at the Laboratorio di Tecnologia Medica (LTM) of Istituto Ortopedico Rizzoli (Bologna), a partner to the LHDL-project.

A long bone is the main subject for all studies presented within this thesis. Each bone can be considered as a tissue, a structure and an organ simultaneously, however just the organ level is considered here. Long bones have been widely studied in the past and their biomechanics is well known, but so far there is no multi-level, inter-disciplinary description of the human musculo-skeletal apparatus. In fact, the LHDL project aimed to investigate two human cadavers from whole body level through organ level up to protein level giving a subject specific multi-level dataset. Within this framework, the goal of this thesis was to measure for each of the six bone segments whole bone stiffness, strength and strain distribution.

The development of methodologies able to ensure both high data quality and future spatial compatibility for data merging between structural levels was essential within this study.

Therefore, marker for different medical imaging techniques was developed to assist merging of different measurements of the whole body, body-segments and organs. Using the developed markers it was possible to support CT, MRI and joint passive kinematics measurements and moreover to preserve long bone segments from any mechanical damage, such as caused by drilling holes, contrary to a previously used marker technique.

A univocal definition of coordinates systems was extremely important in musculoskeletal biomechanics especially given that multi-level measurements had to be conducted. Therefore three anatomical coordinate systems were compared to define of the most reproducible coordinate system for tracing of anatomical plans.

Part of the LTM goals was the creation of subject-specific finite-element models (FEM) and to validate them. Therefore, it was necessary to provide some data to define the boundary conditions, crucial for accurate validation of the FEM. First of all, to reproduce the position of the resultant joint force during *in vitro* tests of long bones, a

load cell has been developed. Thereafter, to measure the crack initiation point, which was needed to advance FEM predicting bone fracture, a novel technique called the Crack Grid was developed.

The Crack Grid permitted to distinguish crack initiation point with 3mm spatial resolution, providing accurate data for the FEM validation and delivering extra information related to bone structure mechanics. However this technique is not limited only to the FEM validation, e.g. can be applied to verify relations between the fracture and collagen orientation in this same region. Moreover, the crack grid can be applied in the other materials science like composites, ceramics etc, where crack initiation point and fracture propagation are common subjects of study.

Results of this study can be distinguished as related to: LHDL, encyclopaedic like dataset and; specific research questions.

The data related to LHDL project demands are whole bone strain distribution, stiffness and strength for a prior chosen loading scenario, depending on the bone segment (torsion, four point bending). A loading direction and loading velocity relations were assessed providing deeper insight into bone structure non linearity and viscoelastic behaviour.

Within this thesis two specific studies addressing the proximal femur were conducted. The first one deals with strain distribution in proximal femur. It was a detailed strain-gauge based study aimed at giving an insight to understanding of proximal femur structure and its load bearing capabilities. The second one is approaching spontaneous fractures of proximal femur. There is no evidence, nor consensus on the most relevant loading scenario. The aim of this work was to develop and validate an experimental method to replicate spontaneous fractures in vitro based on clinically relevant loading. Combinations of experimental and computational techniques were applied to replicate fractures of the proximal femur with a high repeatability and reproducibility. First a numerical model indicated the most relevant loading scenario. Furthermore, it was found that it is not essential to include the muscles when investigating head–neck fractures and consequently the experimental setup was designed. Clinically relevant fracture modes were obtained. The proposed method can be used to investigate the reason and mechanism of failure of natural and operated proximal femurs.

The work done so far had also some practical application. In fact the know-how developed during testing the proximal femur was applied to testing and optimizing proximal epiphyseal replacement of the femur.

1 INTRODUCTION

1.1 Bone- an engineering approach

Bone can be considered as a tissue, an organ, a structure in this same time. However, the most relevant to the aims of this thesis are mechanical behaviours of cortical and trabecular bone.

Bone is an inhomogeneous material because it consists of various cells, organic and inorganic substances with different material properties. In mechanical terms bone is a composite material with various solid and fluid phases. The inorganic component of bone makes it hard and relatively rigid, and its organic component provides flexibility and resilience. The composition of bone varies with age, sex, type of bone, type of bone tissue and presence of bone disease.

Bone is an anisotropic material because its mechanical properties in different directions are different. That is, the mechanical response of bone is dependent upon the direction as well as the magnitude of the applied load. For example, compressive strength of bone is greater than its tensile stress. Moreover bone possesses viscoelastic (time dependent) material properties; hence the mechanical response of bone is dependent on the rate at which the loads are applied. Bone can resist rapidly applied loads much better than slowly applied loads: bone is stiffer and stronger at higher strain rates.

1.1.1 Cortical Bone

Mechanical properties of cortical bone have been well documented. Traditional mechanical testing techniques such as uniaxial tensile or compressive testing and three-points or four-points bending have been used for measuring these properties [1] as well as ultrasonic techniques, by subjecting the bone to ultrasound and measuring the velocity of the sound [2]. A typical tensile stress-strain diagram for the cortical bone is shown in figure 1.

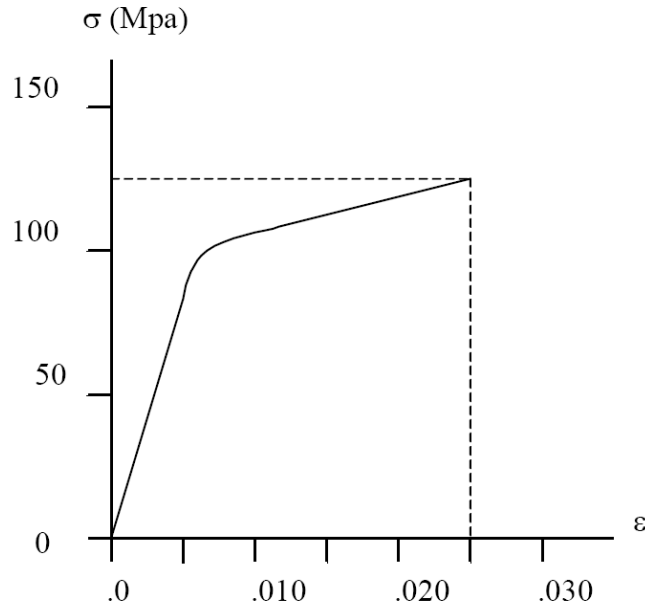


Figure 1 Tensile stress-strain diagram for human cortical bone loaded in the longitudinal direction (strain rate $\dot{\epsilon}=0.05 \text{ s}^{-1}$)

This σ - ϵ curve was drawn using the averages of the elastic modulus, strain hardening modulus, ultimate strain and ultimate stress values determined for the human femoral cortical bone by Reilly et al.[1]. Reilly et al tested specimen of bone tissues (human and bovine) under tensile and compressive loads applied in the longitudinal direction at a moderate strain rate ($\dot{\epsilon}=0.05 \text{ s}^{-1}$). The diagram that can be considered representative of the behaviour of cortical bone under tension or compression shows three distinct regions. In the initial region the behaviour is linear-elastic and the slope of the straight line is equal to the elastic or Young modulus E of the bone, which in the example is almost 17 GPa. In the intermediate region the bone exhibits a non-linear elasto-plastic behaviour. Material yielding also occurs in this region. In the final region, the bone exhibits a linearly plastic material behaviour and the σ - ϵ diagram is another straight line. The slope of this line represents the strain hardening modulus of bone tissue, which was about 0.9 GPa in the example.

The elastic modulus and the strength value are dependent on the rate at which the loads are applied[3]. This viscoelastic nature of bone can be described with the qualitative diagram plotted in Figure 2.

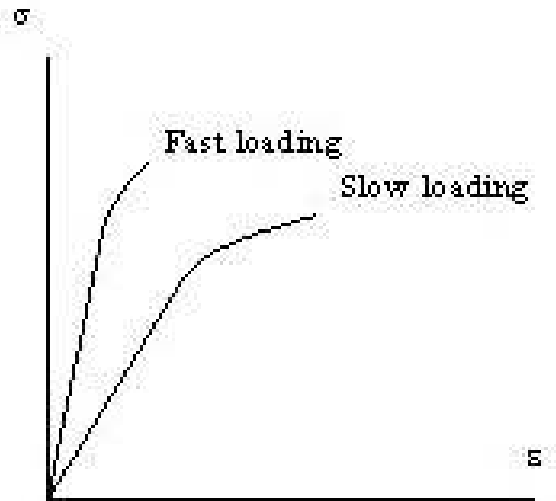


Figure 2 The strain rate dependent stress-strain curve for cortical bone tissue

The specimen of bone tissue subjected to a rapid loading generally shows an increase in bone fragility and a parallel increase in the elastic modulus. With respect to a specimen loaded more slowly, there is a reduction in the post-elastic phase (it can even lack) and in the strain to failure as well as an increase in the ultimate stress. The absorbed energy, which is proportional to the area under the σ - ϵ curve, by the bone tissue generally decreases with the strain rate.

Bone will bear a higher stress if it is loaded at a higher strain rate. Carter and Caler [4] found an empirical relationship between failure stress and strain, or stress, rate:

$$\sigma_f = 87 \dot{\sigma}^{0.053} \quad (1)$$

$$\sigma_f = 87 \dot{\epsilon}^{0.055} \quad (2)$$

The stress-strain behaviour of bone is also dependent upon the orientation of bone with respect to the loading direction. This anisotropic material behaviour can be qualitatively described by the diagram plotted in Figure3.

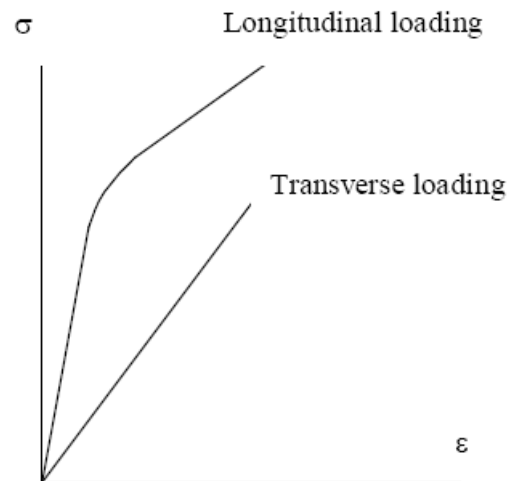


Figure 3 The direction dependent stress-strain curve for bone tissue.

The cortical bone shows a larger ultimate strength and a larger elastic modulus in the longitudinal direction than in the transverse direction. Moreover, bone specimens loaded in the transverse direction fail in a more brittle manner, without showing a considerable yielding, as compared to bone specimens loaded in the longitudinal direction.

Although the qualitative behaviour of cortical bone described previously is commonly accepted, still a great range for the values of the mechanical characteristics can be found in literature for many reasons. First of all, differences in the measured values can be due to the different treatment of specimens. It has been shown that drying bone and re-wetting it can produce differences in the results[5] as formalin fixation does [6]. Testing dry bone produces results quite different from those in wet bone: dry bone is stiffer, stronger and considerably more brittle. The dimension of the specimen influences the results as well. Very small samples produce lower values for stiffness and strength than larger samples [7]. In addition the age and health of the donor is a fundamental variable. Age may affect intrinsic properties. Osteoporotic bone may differ from 'normal' bones in ways other than the fact that is more porous: there is evidence that the collagen is different from that in similar-aged non-osteoporotic subjects [8]. Finally there are differences between bones and among different sites in the same bone. Long bones differ along their length and around their circumference. Lotz et al. [7], for example, showed that the longitudinal Young's modulus varied from 12.5 GPa to 9.6 GPa considering diaphysis specimens or metaphysis ones. In the following paragraphs values

are reported that should be considered to be valid for a well-performed test on bone obtained from a middle-aged person with no disease [9].

Stiffness

The values reported in Table1 are taken from [1,2]. In the orthotropic formulation reported, the indices 1, 2, 3 to the moduli values indicate respectively the radial, circumferential and longitudinal direction, where the longitudinal direction is the one parallel to the main axis of the femur.

Table1 Mechanical properties of cortical bone of human femur (Source [9])

| | Femur Tension | Femur Tension | Femur Compression |
|------------------------------|---------------|---------------|-------------------|
| <i>Elastic Moduli (GPa):</i> | | | |
| E_1 | 12.0 | 12.8 | 11.7 |
| E_2 | 13.4 | 12.8 | 11.7 |
| E_3 | 20.0 | 17.7 | 18.2 |
| <i>Shear Moduli (GPa):</i> | | | |
| G_{12} | 4.5 | - | - |
| G_{13} | 5.6 | 3.3 | - |
| G_{23} | 6.2 | 3.3 | - |
| <i>Poisson's ratios:</i> | | | |
| ν_{12} | 0.38 | 0.53 | 0.63 |
| ν_{13} | 0.22 | - | - |
| ν_{23} | 0.24 | - | - |
| ν_{21} | 0.42 | 0.53 | 0.63 |
| ν_{31} | 0.37 | 0.41 | 0.38 |
| ν_{32} | 0.35 | 0.41 | 0.38 |

Reilly et al [1] tested femoral specimen to determine whether the value of Young's modulus was different in tension and compression. A paired Student's 't' test showed no significant difference between the compressive and the tensile moduli at the 95% confidence level. The load-deformation traces showed no change of slope going from compression into tension and vice versa.

Calculations [10], incorporating data from non-human as well as human material, predict that Young's modulus is modestly dependent upon strain rate:

$$E = 21402 (\text{strain rate (s}^{-1}\text{)})^{0.050} \text{ MPa (3)}$$

Strength

The values reported in Table2 are taken from Keller [11].

Table2 Strength of cortical bone (Source [9])

| <i>Mode</i> | <i>Orientation</i> | <i>Breaking</i> | <i>Yield Stress</i> | <i>Ultimate strain</i> |
|-------------|--------------------|-----------------|---------------------|------------------------|
| Tension | Longitudinal | 133 | 114 | 0.031 |
| | Tangential | 52 | - | - |
| Compression | Longitudinal | 205 | - | - |
| | Tangential | 130 | - | - |
| | Shear | 67 | - | - |

As already reported, a slight dependence on strain rate has been demonstrated, which becomes significant for strain rate variation of some order of magnitude.

1.1.2 Cancellous bone

The chemical compositions of cortical and cancellous bone tissue are similar. The distinguishing characteristic of the cancellous bone is its porosity. Trabecular bone consists primarily of lamellar bone, arranged in packets that make up an interconnected irregular array of plates and rods, called trabeculae. Most mechanical properties of trabecular bone depend to a large degree on the apparent density, which is defined as the mass of bone tissue present in a unit volume of bone [12]. Volume fraction typically ranges from 0.6 for dense trabecular bone to 0.05 for porous trabecular bone [13, 14]. The (wet) tissue density for human trabecular bone is fairly constant and is in the approximate range 1.6-2.0 g/cm³. By contrast, the (wet) apparent density varies substantially and is typically in the range 0.05-1.0 g/cm³ Table3.

Table3 Typical wet apparent densities for human trabecular bone (Source [12])

| <i>Tissue source</i> | <i>Cadavers</i> | | <i>Specimens</i> | <i>Wet Apparent Density (g/cm³)</i> | |
|-----------------------|-----------------|-------------|------------------|--|--------------|
| | <i>Nr.</i> | <i>Ages</i> | <i>Nr.</i> | <i>Mean (SD)</i> | <i>Range</i> |
| Proximal Tibia | 9 | 59-82 | 121 | 0.29 (0.10) | 0.09-0.66 |
| Femur | 10 | 58-83 | 299 | 0.50 (0.16) | 0.14-1.00 |
| Lumbar Spine | 42 | 15-87 | 40 | 0.24 (0.07) | 0.11-0.47 |
| Lumbar Spine | 3 | 71-84 | 231 | 0.19 (0.08) | 0.06-0.40 |

Individual trabeculae have relatively uniform compositions that are similar to cortical bone tissue, but are slightly less mineralised and slightly more hydrated than cortical tissue. The percent volume of water, inorganic and organic component have been

reported at 27%, 38% and 35%, respectively [15], although the precise values depend on anatomical site, age and health.

The cancellous bone tissue mechanical behaviour can be qualitatively represented as in Figure 14.

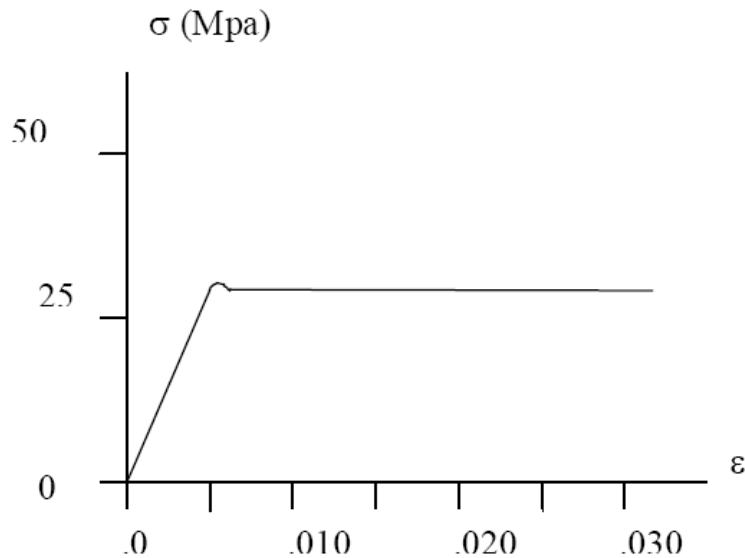


Figure 14 Compressive stress-strain curve for cancellous bone tissue

The compressive stress-strain curves of cancellous bone show an initial linear elastic region up to a strain of about 0.05. The material yielding occurs as the trabeculae begin to fracture. A plateau region of almost constant stress follows this initial elastic region until fracture, exhibiting a ductile material behaviour. After yielding, it can sustain large deformations (up to 50% strain) while still maintaining its load-carrying capacity. Thus, trabecular bone can absorb substantial energy before mechanical failure. By contrast, cancellous bone fractures abruptly under tensile forces, showing a brittle material behaviour. The energy absorption capacity is considerably higher under compressive loads than under tensile loads.

Being a heterogeneous open cell porous solid, trabecular bone has anisotropic mechanical properties that depend on the porosity of the specimen as well as the architectural arrangement of the individual trabeculae. In order to specify its mechanical properties, one must therefore specify factors such as the anatomical site, loading direction with respect to the principal orientation of the trabeculae, age and health of the donor. Young's module can vary 100-fold within a single epiphysis [16] and can vary on average by factor of three depending on loading direction [17,18]. Pathologies such as osteoporosis, osteoarthritis and bone cancer are known to affect mechanical properties [19,20]. Typically the modulus of human trabecular bone is in the range

0.010-2 GPa depending on the above factors. Strength, which is linearly and strongly correlated with modulus [16], is typically in the range 0.1-30 MPa [12].

1.1.3 References

1. Reilly DT and Burstein AH. The elastic and ultimate properties of compact bone tissue. *J Biomech* 1975; 8(6):393-405.
2. Ashman RB, Cowin SC, Van Buskirk WC, and Rice JC. A continuous wave technique for the measurement of the elastic properties of cortical bone. *J Biomech* 1984; 17(5):349-61.
3. Lakes RS and Katz JL. Viscoelastic properties of wet cortical bone--III. A non-linear constitutive equation. *J Biomech* 1979; 12(9):689-98.
4. Carter DR and Caler WE. A cumulative damage model for bone fracture. *J Orthop Res* 1985; 3(1):84-90.
5. Currey JD. The effects of drying and re-wetting on some mechanical properties of cortical bone. *J Biomech* 1988; 21(5):439-41.
6. Sedlin ED. A rheologic model for cortical bone. A study of the physical properties of human femoral samples. *Acta Orthop Scand* 1965; :Suppl(83):1-77.
7. Lotz JC, Gerhart TN, and Hayes WC. Mechanical properties of metaphyseal bone in the proximal femur. *J Biomech* 1991; 24(5):317-29.
8. Bailey AJ, Wotton SF, Sims TJ, and Thompson PW. Biochemical changes in the collagen of human osteoporotic bone matrix. *Connect Tissue Res* 1993; 29(2):119-32.
9. Currey JD. Cortical Bone, in *Handbook of Biomaterial Properties*, J Black and G Hastings, Editors. 1998, Chapman&Hall: London, UK.3-14.
10. Carter DR and Caler WE. Cycle-dependent and time-dependent bone fracture with repeated loading. *J Biomech Eng* 1983; 105(2):166-70.
11. Keller TS. Predicting the compressive mechanical behavior of bone. *J Biomech* 1994; 27(9):1159.
12. Keaveny TM. Cancellous Bone, in *Handbook of Biomaterial Properties*, J Black and G Hastings, Editors. 1998, Chapman&Hall: London, UK.15-23.
13. Kuhn JL, Goldstein SA, Feldkamp LA, Goulet RW, and Jasion G. Evaluation of a microcomputed tomography system to study trabecular bone structure. *J Orthop Res* 1990; 8(6):833-42.
14. Mosekilde L, Bentzen SM, Ortoft G, and Jorgensen J. The predictive value of quantitative computed tomography for vertebral body compressive strength and ash density. *Bone* 1989; 10(6):465-70.
15. Gong JK, Arnold JS, and Cohn SH. Composition of Trabecular and Cortical Bone. *Anat Rec* 1964; 149:325-31.

16. Goldstein SA, Wilson DL, Sonstegard DA, and Matthews LS. The mechanical properties of human tibial trabecular bone as a function of metaphyseal location. *J Biomech* 1983; 16(12):965.
17. Townsend PR, Raux P, Rose RM, Miegel RE, and Radin EL. The distribution and anisotropy of the stiffness of cancellous bone in the human patella. *J Biomech* 1975; 8(6):363-7.
18. Linde F, Pongsoipetch B, Frich LH, and Hvid I. Three-axial strain controlled testing applied to bone specimens from the proximal tibial epiphysis. *J Biomech* 1990; 23(11):1167-72.
19. Pugh JW, Radin EL, and Rose RM. Quantitative studies of human subchondral cancellous bone. Its relationship to the state of its overlying cartilage. *J Bone Joint Surg Am* 1974; 56(2):313-21.
20. Hipp JA, Rosenberg AE, and Hayes WC. Mechanical properties of trabecular bone within and adjacent to osseous metastases. *J Bone Miner Res* 1992; 7(10):1165-71.

1.2 LHDL project

This thesis was carried out as part of LTM research group activities within the Living Human Digital Library project (LHDL). Therefore this chapter will briefly present the LHDL project and related LTM responsibilities. It must to be mentioned that LHDL project is an executive part of the bigger Living Human Project (LHP).

The LHP aimed to create an *in silico* model of the human musculoskeletal apparatus able to predict how mechanical forces are exchanged internally and externally at any dimensional scale from the whole body down to the protein level. This goal has been pursued through the following steps:

- creation of a community of researchers interested in the project and in the idea of exchanging information, data and models to create a collectively owned resource
- development and implementation of a specialized infrastructure, called the Living Human Digital Library (LHDL), which makes it possible for the community members to create, share, modify the data and modeling resources that constitute the LHP.

The LHDL involved various institutions, each contributing different skills (Fig.1).

The substance of the LHP and was biomechanical data, and therefore the data collection was a fundamental step of the LHDL project. Only two of LHDL project participants were involved in data collection. The ULB has granted two human cadavers, subjects to this functional-anatomical and multi-level study. The ULB has also provided all anatomical measurements, like whole body CT and MRI or passive kinematics.

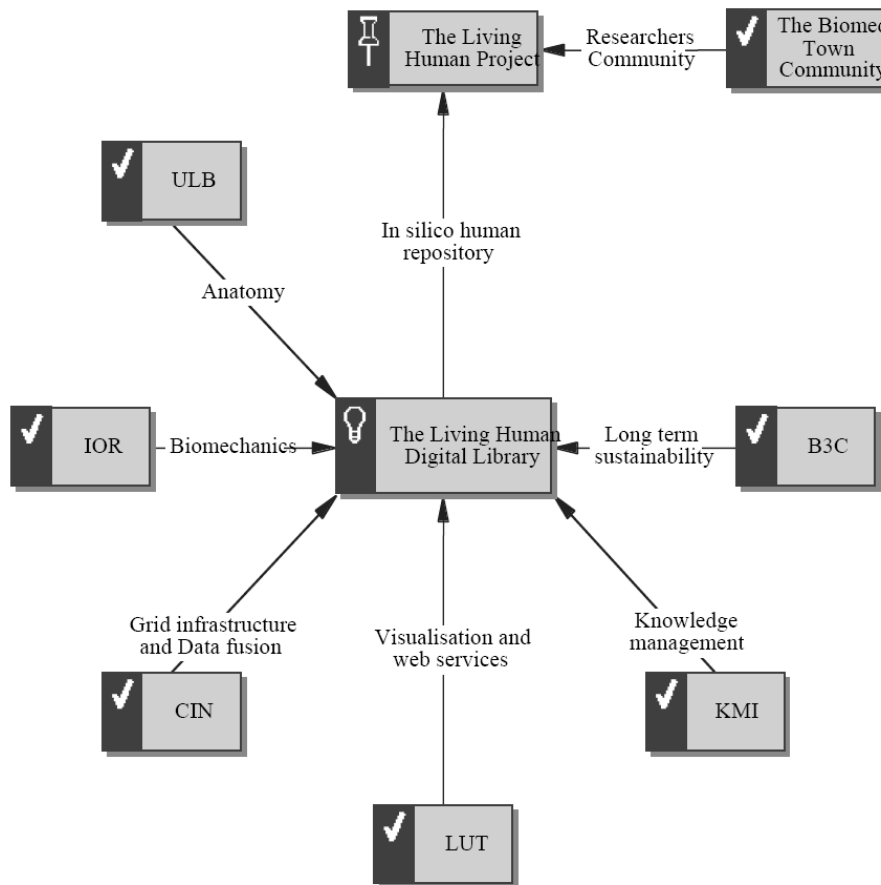


Fig. 1. The structure of the Living Human Project and the participant institutions

Dissectioned bone segments were shipped to IOR for biomechanical investigations.

The LTM laboratory consists of three subgroups: experimental, biological and computational which were subsequently investigating this same bone segments but at different levels. Once mechanically tested at the organ-level, bones were sectioned and the tissue-level biomechanical data were assessed, such as density, mineral content, micro hardness and Young's modules. At last part the bones sections underwent biological study. Collagen orientation and non mineral content were investigated. Simultaneously computational models, based on CT and experimental data, were created.

This thesis was dedicated to cover the organ-level experimental investigation part and its aims will be presented in the next chapter.

1.3 Scope of the thesis

The biomechanical *in vitro* investigation of human long bones was a general aim of this work. However this complex task consisted of well defined specific goals which shall be listed at this point. The partial scopes can be divided into:

Methodology related:

1. First scope was to create a marker system for different medical imaging techniques. The LHDL principal requirement was that all measurements acquired at different levels of the same cadavers become set together within univocal coordinate system. However, until now there wasn't a marker suitable for each of the visualisation techniques and preventing bones damaging from drilling holes for marker fixation in this same time (not magnetic- MRI, no artefacts-CT, not bone damaging- *in-vitro* testing).
2. The second scope within this thesis was to compare three anatomical coordinate systems for the tibia-fibula complex. The importance of this study lays at defending the most repeatable technique for tracing anatomical planes and subsequently to provide the best matching for multi level data testing.
3. Third scope was to create testing device able to accurately determine the position of the applied force during *in-vitro* tests. This is of great importance for subject-specific FE-models validation, which are extremely sensitive to their boundary conditions.
4. The forth scope of this thesis was to create a novel measuring technique to measure able to distinguish the crack initiation point on a bone surface when tested to fracture. This technique had to provide higher spatial resolution than high speed cameras techniques does.

Data collection related:

1. First of all, the LHDL project was aimed at collection of an enormous, encyclopaedic biomechanical dataset. A general biomechanical properties, such as whole bone stiffness strength and strain distribution of all major six human long

bones (radius, ulna, humerus, femur, tibia and fibula) had to be acquired. Moreover a loading direction and loading velocity influence had to be evaluated.

2. Secondary goals, the specific research questions, were related to the proximal portion of the femur. First study was aimed to provide a better understanding of the strain distribution, and of its correlation with the different directions of loading, and with bone quality. Where the second study, was aimed to investigate how to replicate *in-vitro* clinically relevant proximal femoral fractures.

1.4 Structure of the thesis

The present thesis consists of nine studies developed in the LTM during the LHDL project. Six of those studies have become articles. Three papers have been already published, two on the Journal of Biomechanics one on Strain, and three have been submitted.

Three other studies are not published, however they were technically essential to the development of the project and therefore have been presented here.

In the following paragraphs a path, created to guide through the present thesis and to bring forward the role of the author of this thesis has been presented.

Section **Methodology**, contains four chapters introducing technical requirements essential to compete experimental measurements.

Chapter 2.1, “**The marker system for different medical imaging techniques**”, describes development of tool able to assist data collection for different investigations at different levels: whole-body, body-segments and organs with this same univocal reference system. The entire study was developed by the author and partially carried out at the Department of Anatomy, Université Libre de Bruxelles, Belgium.

Chapter 2.2, “**Comparison of three anatomical coordinate systems for tibia-fibula complex**”. Whereas the procedure for defining of anatomical plans for femur has been well defined and validated, such verification was missing for tibia-fibula complex. Therefore the LTM group compared three different anatomical coordinate systems to define the most reproducible and the simplest for the experimental applications.

Once univocal reference system was ensured for both whole body and bone segment level, a testing setup had to be projected and developed. The experimental setup for whole bones testing had to provide all the FEM related constraints such as force, displacement, strain. However the load direction and fracture initiation point were difficult to assess.

Chapter 2.3 “**A Method to Improve Experimental Validation of Finite-Element Models of Long Bones**” presents development of a load cell (called FP-transducer) able to reproduce the position of the applied force during an *in vitro* test, where the

resultant joint force is one of boundary conditions crucial for accurate validation of FE-models.

Chapter 2.4 “**A new technique for bone crack propagation registration**” presents a novel technique for registration of fractures called the Crack-Grid. The main purpose of developing this technique was to distinguish crack initiation point, with the spatial resolution better than this given by the high speed camera. Providing accurate data for the FEM validation and delivering an extra information related to bone structure mechanics during bone fracture tests. Moreover thanks to its performances (700kHz sampling rate, 3mm spatial resolution, easy application onto irregular surfaces) and relatively low cost (<€100) this technique can find an application in other fields of materials science.

Section “General biomechanical characterization of long bones”, has been dedicated to present results related to general bone structural biomechanics such as whole bone strain distribution, whole bone stiffness, and whole bone strength.

Chapter 3.1, “**LHDL related data acquisition**”, summarises all tests executed within the LHDL project and related results, for both cadavers. The author was responsible for preparation and execution of all tests. A complete dataset contains: a strain-distribution, stiffness and strength information for each tested bone segment and has been already shared through the dedicated internet infrastructure www.biomedtown.org.

Basing on the LHDL data, collected by the author, a specific study has been carried out. Chapter 3.2, “**Structural behaviour of the long bones of the human lower limbs**”, deals with two experimental factors: loading direction and loading velocity. By comparing these factors, an insight has been given into the understanding of the bone-structure viscoelastic behaviour within physiological strain rates.

In the section “**Specific biomechanical characterization of long bones**” have been presented two studies concerning a human proximal femoral metaphysis. These studies were carried out on femoral bones which were not a part of the LHDL project and results were not directly related to the dataset requested for the LHDL. However results of these studies have been a support to the computational studies carried out at LTM

within the project. Moreover these same experimental setups and techniques developed within the LHDL project were applied here.

Chapter 4.1 **“Strain distribution in the proximal human femoral metaphysis”** describes a detailed, strain-gauge based, study. The strain distribution was correlated with the different directions of loading and with bone quality. To provide a better understanding of the proximal femur metaphysis stress/strain state has been of great interest because of its relevance for hip fractures and prosthetic replacements.

Spontaneous fractures are representing a significant percentage of proximal femur fractures. However this type of fracture has seldom been investigated and there is no evidence, nor consensus on the most relevant loading scenario. Chapter 4.2 **“In vitro replication of spontaneous fractures of the proximal human femur”** presents combined experimental/computational study aimed to develop and validate an experimental method to replicate spontaneous fractures *in vitro*, basing on clinically relevant loading scenario.

The know-how developed about testing the proximal femur was applied to testing and optimizing proximal epiphyseal replacement of the femur. In Appendix, the paper **“Stress-shielding and stress-concentration of contemporary epiphyseal hip prostheses”** has been presented.

2 METHODOLOGY

2.1. The marker for multi biomedical visualisation

Modeling of musculo-skeletal system is currently challenging due to the Inhomogeneity across the different multi-scale levels and the mis-match between the different data sets obtained. Thus, limiting the accuracy of the models in turn limiting the conclusions that can be drawn both in terms of basic scientific principle and within a more applied clinical context. The current state-of-the-art in the modeling field reports the use of data obtained from various sources (e.g. literature, colleagues, the Internet) without clear links between these sources and often lacking in validation (e.g. as done by Refs?). This LHDL project, however, aimed to obtain multi-scale data that was self-consistent, by obtaining all data from the same cadaver using the same univocal reference system. Thus, correcting the *ad-hoc* approach used so far for such data collection.

To provide this reference system dedicated markers were crafted. Suitable for each particular biomedical visualization technique (CT, MRI and stereophotogrammetry) and with respect to specific constraints. The entire study was carried out by the author and partially carried out at the Department of Anatomy, Université Libre de Bruxelles, Belgium.

During the designing process several constraints were considered:

- *Constraint 1.* Following recommendations from a feasibility study (performed before the LHDL project), the technical frames including reflective markers were mounted on customized pins allowing easy setting and removing. A special interface between the pin and the technical frame was required to maintain a constant position and orientation between the two components relative to each other. Technical frames were removed before storage in order to reduce (taking it out of the cooling room where it was kept between two dissection, setting the specimen on the experimental jig, dissection of the specimen, etc) reduce the likelihood of collisions with the technical frames which would displace them. This would have led to a loss of the relationship between the frame and the underlying bony structure.

Constraint 2. Latter stage of the LHDL data collection protocol included analysis of bone properties. These experiments required intact bones (i.e. with no holes). It was

therefore impossible to drill the pins used to support the above technical frames into some bones (mainly long bones: humerus, clavicles, femurs, tibias, ulnas, radiuses, and sternum). Therefore the basis of the technical frame included a hole. A plastic strap that was wrapped around the diaphysis of long bones, was present inside this hole, in such a way that the technical frame and its basis were “firmly” linked to the bone of interest (Fig1). Other bones (skull, jaw, scapula, iliac bones, metacarpal bones, metatarsal bones) were drilled to enable their attachment to the external frames.



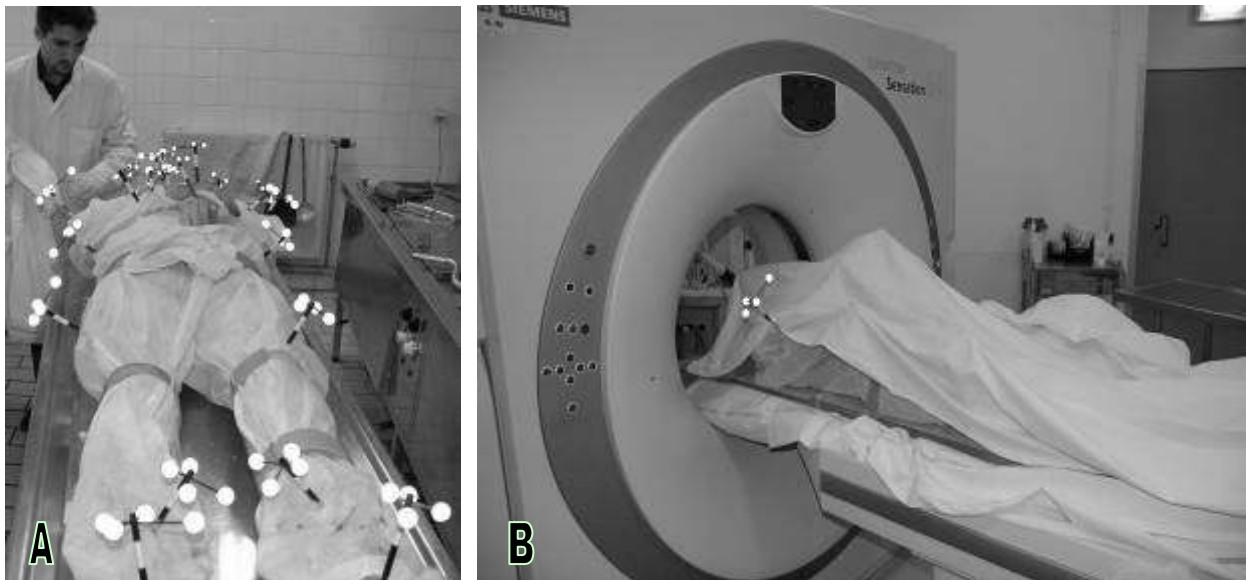
Figure 1 Model of the femur with the marker and close-up of the fastening strap

Constraint 3. In terms of the visualization techniques, the technical requirements for usage of each include:

- CT-scan is used not only for general skeleton morphology visualization. Material properties of bone are derived from image gray-scales, following calibration, for future subject specific FE-models. Therefore marker pins and supports were made of carbon-fiber and aluminum (materials less or equally dense as bone) in order to avoid imaging artifacts.

- MRI requires usage of non ferromagnetic materials. And carbon fiber and aluminum are suitable.

In summary, markers met considered requirements contributing to the multi level data collection. The data collection of both cadavers was as follows: The cadaver of a donor with average morphology from the ULB donation program was used. Each body



segment (thighs, shanks, feet, forearms, etc) was equipped with reflective markers to create technical frames linked to all major segment bones within 3 different visualization techniques. These reflective markers were visible within CT-scan datasets, stereophotogrammetry used to digitize dissection results, and stereophotogrammetry used for motion analysis.

Figure 2. The cadaver with reflective markers set on (A). The cadaver during CT-scan session (B).

2.2 Comparison of three standard anatomical reference frames for the tibia-fibula complex

Giorgia Conti, MEng^{1,2}, Luca Cristofolini, PhD^{1,2}, Mateusz Juszczuk, MEng^{1,2},
Alberto Leardini, PhD³, Marco Viceconti, PhD¹

¹Laboratorio di Tecnologia Medica, Istituto Ortopedico Rizzoli, Bologna, Italy

²Engineering Faculty, University of Bologna, Italy

³Laboratorio di Analisi del Movimento, Istituto Ortopedico Rizzoli, Bologna, Italy

The author contributed to this study at projecting experimental setup and executing measurements. This study was published on **Journal of Biomechanics**.

2.2.1 Abstract

Definition of anatomical reference frames is necessary both for *in vitro* biomechanical testing, and for *in vivo* human movement analyses. Different reference frames have been proposed in the literature for the lower limb, and in particular for the tibia-fibula complex. The scope of this work was to compare the three most commonly referred proposals (proposed by Ruff *et al* 1983, by Cappozzo *et al* 1995, and by the Standardization and Terminology Committee of the International Society of Biomechanics, Wu *et al.* 2002). These three frames were identified on six cadaveric tibia-fibula specimens based on the relevant anatomical landmarks, using a high-precision digitizer. The intra-operator (ten repetitions) and inter-operator (three operators) repeatability were investigated in terms of reference frame orientation. The three frames had similar intra-operator repeatability. The reference frame proposed by Ruff *et al* had a better inter-operator repeatability (this must be put in relation with the original context of interest, i.e. *in vitro* measurements on dissected bones). The reference frames proposed by Ruff *et al* and by ISB had a similar alignment; the frame proposed by Cappozzo *et al* was considerably externally rotated and flexed with respect to the other two. Thus, the reference frame proposed by Ruff *et al* is preferable when the full bone surface is accessible (typically during *in vitro* tests). Conversely, no advantage in terms of repeatability seems to exist between the reference frames proposed by Cappozzo *et al* and ISB.

Keywords:

Shank coordinate system, tibia-fibula complex, anatomical reference frames, *in vitro* landmarks, *in vivo* human movement analysis

2.2.2. INTRODUCTION

Univocal definition of reference frames is extremely important in musculoskeletal biomechanics (Fung, 1980; Currey, 1982; Van Sint Jan and Della Croce, 2005). In *in vivo* motion analysis, reference frames enable tracking segment and joint motion, and calculation of joint moments (Cappozzo et al., 1995; Wu et al., 2002). Reference frames *in vitro* enable aligning correctly the specimens and the test loads, and defining testing conditions so that these can be replicated (O'Connor, 1992; Cristofolini, 1997). This applies to all lower limb segments. Whereas a number of definitions have been discussed for the femur (Della Croce et al., 2003), little has been reported for the tibia-fibula complex.

One of the first reference frames for the lower limb bones was proposed by (Ruff, 1981; Ruff and Hayes, 1983). This frame was based on identification of landmarks and geometrical measurements that are possible only *in vitro* on dissected femur and tibia segments (further details in Materials and Methods). Although this method was originally intended for anatomical analyses, it was adopted successfully for *in vitro* biomechanical tests both on the femur (Cristofolini, 1997) and tibia (Cristofolini and Viceconti, 2000; Heiner and Brown, 2001; Gray et al., 2007; Gray et al., 2008). A different anatomical reference frame was proposed by (Cappozzo, et al., 1995) to provide consistent identification of landmarks for a more repeatable motion analysis. As it was intended for routine clinical use, it was based on palpation of those anatomical landmarks than can be accessed non-invasively *in vivo* (further details in Materials and Methods). Original identification of bony prominences rather than anatomical planes and axes lead to more repeatable measurements in gait analysis (Leardini et al., 2007). Later, the Standardization and Terminology Committee of the International Society of Biomechanics (ISB) proposed a slightly different reference frame (Wu, et al., 2002) (further details in Materials and Methods). Although such frame was mainly defined for movement analysis, this was the first time that the need for combining *in vitro* and *in vivo* reference frames was considered.

It is clear that an ideal reference frame should be based on landmarks that are easily and reproducibly identified in all subjects, also in case of severe bone deformity. Serious implications of incorrect identification of landmarks and reference frames have been reported both *in vitro* (Cristofolini and Viceconti, 2000; Gray, et al., 2007), and

in vivo (Della Croce et al., 2005; Thewlis et al., 2008). However, the repeatability in identifying these three reference frames (Ruff and Hayes, 1983; Cappozzo, et al., 1995; Wu, et al., 2002) for the tibia-fibula complex has never been reported. Also, as such reference frames were defined independently from each other, the relative orientation of one system respect to the other is unknown.

The scope of this work was to compare these three reference frames for the tibia-fibula complex (Ruff and Hayes, 1983; Cappozzo, et al., 1995; Wu, et al., 2002), with the following goals:

- Assess the intra-operator repeatability (i.e. when the same operator repeatedly identifies the reference frame on the same specimen);
- Assess the inter-operator repeatability (i.e. when the different operators identify the reference frame on the same specimen);
- Assess if the three reference frames overlap and, if not, to assess the relative poses.

2.2.3 MATERIALS AND METHODS

2.2.3.1 Specimens

Six specimens, consisting of intact tibia-fibula complexes were obtained through international donation programs from donors free of any musculoskeletal pathologies (Table 1). They were visually inspected and CT-scanned (HiSpeed, General Electric, USA) to document bone quality and lack of abnormality or defects. All soft tissues were removed, leaving only the articular cartilages and the interosseous membrane. The ligaments of the proximal and distal tibiofibular articulations (syndesmosis) were left intact to preserve the original relative position and orientation. To avoid errors due to bone shrinkage, tissue hydration was preserved by means of cloths soaked with saline solution during the measurement sessions.

Table 1 – Details of the sample analyzed (average, standard deviation and range over the 6 specimens). The ‘biomechanical length’ of the tibia (BL, see also Fig. 1) as in (Ruff and Hayes, 1983), is reported in the first column. Donors’ details are summarized in the last four columns.

| | Biomech length BL (mm) | Donor’s side | Age at death (years) | Donors’ height (cm) | Body Mass Index, BMI, (kg/m²) | Gender |
|--|-------------------------------|---------------------|-----------------------------|----------------------------|---|---------------|
| | | | | | | |

| | | | | | | |
|-------------------------------------|------------|-----------------------|-----------|------------|--------------|------------|
| Average ± standard deviation | 358 ± 12.6 | 50% right 50% left | 56 ± 23.6 | 173 ± 10.7 | 21 ± 3.7 | 50% male |
| Range | 341 to 379 | | 27 to 79 | 165 to 191 | 16.7 to 24.1 | 50% female |

2.2.2.3.2 Definition of the three reference frames

The reference frame *Ruff-coord* (Fig. 1) proposed by (Ruff, 1981; Ruff and Hayes, 1983) is based on the centers of the articulating cartilage areas at the proximal and distal tibia, with no landmarks on the fibula. Such centers must be measured using calipers. The *Ruff-coord* can only be identified *in vitro*, when the bone surface is visible. It must be noted that *Ruff-coord* only relies on the tibial anatomy, while the fibula is ignored. As (Ruff, 1981; Ruff and Hayes, 1983) did not suggest a separate reference for the fibula, we propose to use the same reference frame for the entire tibia-fibula complex.

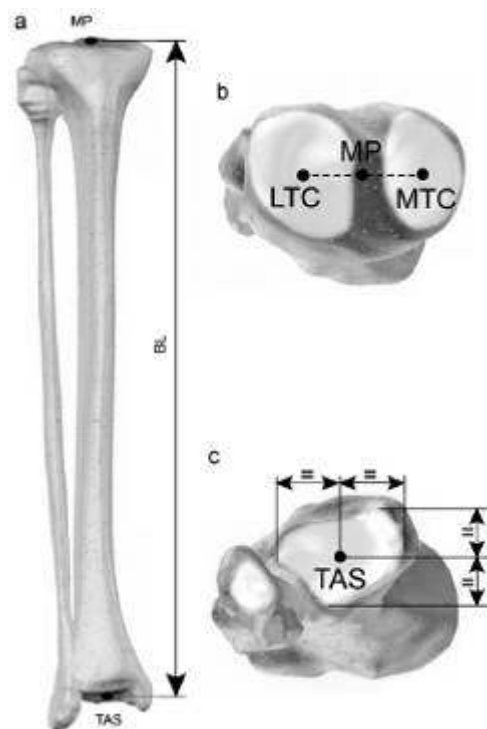


Fig. 1 – Reference frame *Ruff-coord* (Ruff, 1981; Ruff and Hayes, 1983) for a right tibia-fibula complex: anterior view (a), transverse view from above (b) and transverse view from below (c). The centers of the two tibial condyles (MTC, LTC) and of the surface articulating with top of the talus (TAS) are initially identified. This is performed by locating (with calipers) the mid-points in the antero-posterior and medio-lateral directions on each cartilage surface (as this procedure relies on an estimated

provisional alignment, the procedure must be iteratively repeated –typically twice- until no significant further correction is needed). As an example, the location of TAS is shown in (c). The midpoint (MP) between the two tibial condyles center points (MTC and LTC) is then calculated. The frontal plane is the one passing through MTC, LTC and TAS; the sagittal plane is perpendicular to the frontal plane and goes through points MP and TAS.

The reference frame *Cappozzo-coord* (Fig. 2) proposed by (Cappozzo, et al., 1995) is based on landmarks of the tibia and fibula that need to be palpable also *in vivo*. The reference frame *ISB-coord* (Fig. 3) recommended by the ISB (Wu, et al., 2002) is based on the same landmarks as *Cappozzo-coord* distally, but on different landmarks proximally (with landmarks over only the tibial plateau).



Fig. 2 – Reference frame *Cappozzo-coord* (Cappozzo, et al., 1995) for a right tibia-fibula complex (anterior view). First, the tibial tuberosity (TT), the apex of the head of the fibula (HF), the distal apex of the medial and lateral malleoli (MM, LM) are identified. The midpoint (MPM) of the line joining MM and LM is then calculated (this point coincides with IM of Fig. 3 (Wu, et al., 2002)). The frontal plane passes through HF, LM and MM; the sagittal plane is perpendicular to the frontal plane and goes through points MPM and TT



Fig. 3 – Reference frame *ISB-coord* proposed by the Standardization and Terminology Committee of the International Society of Biomechanics (Wu, et al., 2002) for a right tibia-fibula complex (anterior view). First, the most medial and lateral points on the edge of the relevant condyles (MC, LC), the tip of the medial and lateral malleoli (MM, LM) are identified. The inter-malleolar point (IM, which coincides with MPM of Fig. 2 (Cappozzo, et al., 1995)) located midway between MM and LM and the intercondylar point (IC) located midway between the MC and LC are calculated. The frontal plane passes through IM, MC and LC; the sagittal plane is perpendicular to the frontal plane and containing the points IC and IM.

Both *Cappozzo-coord* and *ISB-coord* rely on the anatomy of the entire tibia-fibula complex. It must be stressed that the *Cappozzo-reference* and the *ISB-reference* are designed for *in vivo* use, and the landmarks are identified with some approximation because of the interposition of soft tissues. In this study all the landmarks were accessed directly on the bone surfaces.

Relative orientation for each pair of reference frames was expressed using the same approach used by (Grood and Suntay, 1983) for referring one anatomical segment to the other. This entails defining flexion/extension as the relative orientation about the medio-lateral axis of a first frame, internal/external rotation as the relative orientation about the vertical axis of the second frame, and abduction/adduction as the relative orientation about a ‘floating’ axis orthogonal to the previous two.

2.2.3.3 *In vitro* acquisition

The landmarks described above were acquired with a 3D digitizer (Mod. Gage-Plus-V1.5, Faro-Europe, Stuttgart-Weilimdorf, Germany) with an accuracy of 10 micron.

The specimens were held in space by an adjustable vice. From these landmarks, the position and orientation of the three reference frames (*Ruff-coord*, *Cappozzo-coord*, *ISB-coord*) was obtained for each specimen. Reference frames belonging to left specimens were mirrored so as to treat them all as right.

To assess the intra-operator repeatability, each reference frame was identified ten times by the same operator on one randomly selected specimen, at a time distance of 10-20 minutes. To assess the inter-operator repeatability, three operators with a good knowledge of musculoskeletal biomechanics were asked to identify the landmarks of the three reference frames on each specimen. To avoid conditioning or biasing between replicates and between operators, each acquisition was blinded with respect to previous ones: the landmarks were only temporarily marked on the bone, and erased before each new acquisition.

2.2.3.4 Statistical analysis

The orientation of each reference frame and of each repetition was expressed using the angles defined by (Grood and Suntay, 1983), using custom-written code in Matlab (Matlab inc, Natick, MA, USA).

To estimate the intra-operator repeatability (ten repetitions, one operator, one specimen):

- The average coordinates of each landmark (with respect to the digitizer coordinate system) was computed over the ten repetitions by the same operator;
- An average reference frame was identified based on such average landmarks;
- The pose (i.e. of the angles defined by (Grood and Suntay, 1983)) of each of the ten repetitions was computed with respect to such average reference frame;
- The variance and standard deviation of the ten poses (i.e. of the angles defined by (Grood and Suntay, 1983)) was computed;
- To compare the intra-operator repeatability of the three reference frames, an F-test was applied to the ratio of the respective variances.

To estimate the inter-operator repeatability (three operators, six specimens):

- For each specimen, the average coordinates of each landmark (with respect to the digitizer coordinate system) was computed between the three operators;

- For each specimen, an average reference frame was identified based on such average landmarks;
- For each operator, the pose (i.e. of the angles defined by (Grood and Suntay, 1983)) was computed with respect to such average reference frame, for each specimen;
- The variance and standard deviation of the ten poses (i.e. of the angles defined by (Grood and Suntay, 1983)) was computed, for each specimen;
- The Root Mean Square Error (RMSE) was computed between specimens;
- To compare the inter-operator repeatability of the three reference frames, an F-test was applied to the ratio of the respective variances.

To estimate the relative orientation of the three reference frames using a pairwise comparison of each reference frame with respect to the other:

- For each specimen, the average coordinates of each landmark (with respect to the digitizer coordinate system) was computed between the three operators, for each reference frame (*Ruff-coord*, *Cappozzo-coord*, *ISB-coord*);
- For each specimen, an average reference frame was identified based on such average landmarks, for each reference frame (*Ruff-coord*, *Cappozzo-coord*, *ISB-coord*);
- The relative orientation of each reference frame respect to the each of the other two frames was computed, for each specimen: *Cappozzo-coord* with respect to *Ruff-coord*, *Ruff-coord* with respect to *ISB-coord*, *ISB-coord* with respect to *Cappozzo-coord*;
- The average and standard deviation of such relative orientations was computed between specimens;
- The significance of such relative orientations (*Cappozzo-coord* with respect to *Ruff-coord*, *Ruff-coord* with respect to *ISB-coord*, *ISB-coord* with respect to *Cappozzo-coord*) was assessed with two-tailed paired t-tests.

2.2.4 RESULTS

2.2.4.1 Repeatability of the landmarks

For *Ruff-coord* the intra-operator repeatability in identifying the individual landmarks was 0.58-0.98 mm (the error was largest for the center of the tibial condyles, MTC and LTC, Table 2); the inter-operator repeatability was 1.64-2.34 mm (the error was largest for the center of the tibial condyles, MTC and LTC). For *Cappozzo-coord* the intra-operator repeatability for the landmarks was 1.17-2.19 mm (the error was largest for the head of the fibula, HF, Table 2); the inter-operator repeatability was 3.18-6.96 mm (the error was largest for MM, LM and HF). For *ISB-coord* the intra-operator repeatability for the landmarks was 0.94-1.42 mm (the error was similar for all landmarks, Table 2); the inter-operator repeatability was 3.18-7.07 mm (the error was largest for the most medial point on the tibial condyles, MC, and for the medial malleolus, MM).

Table 2 – Repeatability (vector error) of the identification of the landmarks defined for the three reference frames examined. Landmarks are defined as in Fig. 1 (*Ruff-coord*), Fig. 2 (*Cappozzo-coord*) and Fig. 3 (*ISB-coord*).

| | | <i>Proximal landmarks</i> | <i>Distal landmarks</i> |
|---|--|---------------------------|-------------------------|
| Intra-operator repeatability (10 repetitions, 1 operator, 1 specimen) | <i>Ruff-coord</i> (Ruff and Hayes, 1983) | LTC: ± 0.98 mm | |
| | | MTC: ± 0.87 mm | TAS: ± 0.58 mm |
| | | MP: ± 0.75 mm | |
| | <i>Cappozzo-coord</i> (Cappozzo, et al., 1995) | HF: ± 2.19 mm | LM: ± 1.33 mm |
| | | TT: ± 1.17 mm | MM: ± 1.42 mm |
| | | | MPM: ± 1.17 mm |
| | <i>ISB-coord</i> (Wu, et al., 2002) | LC: ± 1.06 mm | LM: ± 1.33 mm |
| | | MC: ± 1.37 mm | MM: ± 1.42 mm |
| | | IC: ± 0.94 mm | IM: ± 1.17 mm |
| Inter-operator repeatability (3 operators, 6 specimens) | <i>Ruff-coord</i> (Ruff and Hayes, 1983) | LTC: ± 1.97 mm | |
| | | MTC: ± 2.34 mm | TAS: ± 1.81 mm |
| | | MP: ± 1.64 mm | |
| | <i>Cappozzo-coord</i> (Cappozzo, et al., 1995) | HF: ± 6.17 mm | LM: ± 5.88 mm |
| | | TT: ± 4.53 mm | MM: ± 6.96 mm |
| | | | MPM: ± 3.18 mm |

| | | |
|---|---------------|---------------|
| <i>ISB-coord</i> (Wu, et al., 2002) | LC: ± 5.62 mm | LM: ± 5.88 mm |
| | MC: ± 7.07 mm | MM: ± 6.96 mm |
| | IC: ± 3.70 mm | IM: ± 3.18 mm |

2.2.4.2 Repeatability of the reference frames

The intra-operator repeatability was of the same order of magnitude for the three reference frames (Table 3).

Table 3 – Repeatability of the definition of the three reference frames examined for the tibia-fibula complex.

| | | <i>Ruff-coord</i> (Ruff and Hayes, 1983) | <i>Cappozzo-coord</i> (Cappozzo, et al., 1995) | <i>ISB-coord</i> (Wu, et al., 2002) |
|---|-----------------------------------|---|---|---|
| Intra-operator repeatability (10 repetitions, 1 operator, 1 specimen) | abduction/ adduction | 0.06° | 0.39° | 0.07° |
| | flexion/ extension | 0.16° | 0.27° | 0.15° |
| | internal/ external rotation | 0.88° | 0.30° | 1.11° |
| | abduction/ adduction | 0.25° | 1.55° | 0.29° |
| Inter-operator repeatability (3 operators, 6 specimens) | flexion/ extension | 0.27° | 0.68° | 0.54° |
| | internal/ external rotation | 2.78° | 3.51° | 5.71° |

In abduction/adduction *Cappozzo-coord* was significantly less repeatable than *Ruff-coord* and *ISB-coord* (F-test, $p < 0.00005$); the difference between the repeatability of *Ruff-coord* and *ISB-coord* was not significant (F-test, $p = 0.7$). The repeatability was similar (F-test, $p > 0.1$) for the three reference frames in flexion/extension. In internal/external rotation *Cappozzo-coord* was more repeatable than *Ruff-coord* and

ISB-coord (F-test, $p<0.005$); the difference between the repeatability of *Ruff-coord* and *ISB-coord* was not significant (F-test, $p=0.5$).

The inter-operator repeatability of the reference frames was worse than the intra-operator repeatability (Table 3). In the frontal plane (abduction/adduction) *Cappozzo-coord* was one order of magnitude less repeatable than *Ruff-coord* and *ISB-coord* (F-test, $p<0.0001$); the difference between *Ruff-coord* and *ISB-coord* was not significant (F-test, $p=0.3$). In the sagittal plane (flexion/extension) *Ruff-coord* was more repeatable than *Cappozzo-coord* and *ISB-coord* (F-test, $p<0.01$); the difference between *Cappozzo-coord* and *ISB-coord* was not significant (F-test, $p=0.3$). In the transverse plane (internal/external rotation) the only significant difference was that *Ruff-coord* was more repeatable than *ISB-coord* (F-test, $p<0.01$); all other differences were not significant (F-test, $p>0.05$).

2.2.4.3 Different orientation of the reference frames

The most obvious difference was the external rotation of *Cappozzo-coord* with respect to the other two reference frames (Fig. 4 and Table 4).

Table 4 – Relative orientation of the three reference frames using a pairwise comparison of each reference frame with respect to the other (see also Fig. 4). (*) two-tailed paired t-test: $p<0.05$, (**) two-tailed paired t-test: $p<0.005$

| Pairs of reference frames being compared | Rotations of <i>Cappozzo-coord</i> (Cappozzo, et al., 1995) respect to <i>Ruff-coord</i> (Ruff and Hayes, 1983) | Rotations of <i>Ruff-coord</i> (Ruff and Hayes, 1983) respect to <i>ISB-coord</i> (Wu, et al., 2002) | Rotations of <i>ISB-coord</i> (Wu, et al., 2002) respect to <i>Cappozzo-coord</i> (Cappozzo, et al., 1995) |
|---|--|---|---|
| abduction/adduction | abducted by <1° | adducted by <1° | abducted by <1° |
| flexion/extension | flexed by 4° (*) | flexed by <1° | extended by 3° (*) |
| internal/external rotation | externally rotated by 39° (**) | externally rotated by 4° | internally rotated by 34° (**) |

This is accounted for by the definition of the frontal plane of *Cappozzo-coord*, which includes the two apexes of the malleoli, being the lateral malleolus much more posterior than the medial one. No significant difference (paired t-test, $p>0.2$) existed between the pose of *Ruff-coord* and *ISB-coord* (Fig. 4 and Table 4). *Cappozzo-coord*

was significantly flexed (paired t-test, $p=0.006$) and externally rotated (paired t-test, $p=0.002$) with respect to *ISB-coord*. *Cappozzo-coord* was significantly flexed (paired t-test, $p=0.02$) and externally rotated (paired t-test, $p=0.002$) with respect to *Ruff-coord*. The fact that the two malleoli (used in *Cappozzo-coord*) are more posterior than the points on the tibial tray identified by *Ruff-coord* and *ISB-coord* explains such differences.

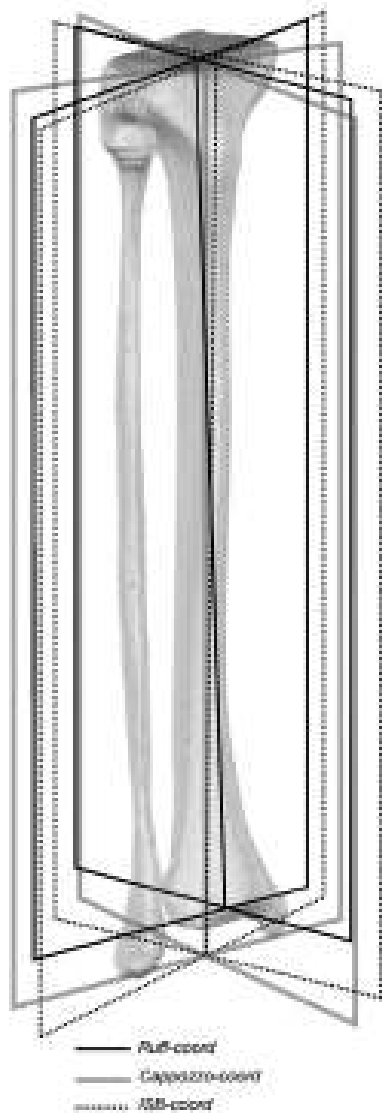


Fig. 4 – Alignments of the three reference frames on a right tibia-fibula complex in an antero-lateral view. The three frames had similar alignments in the sagittal and transverse planes. However, *Cappozzo-coord* was translated laterally and externally rotated with respect to *Ruff-coord* in the frontal plane. No significant rotation existed between *Ruff-coord* and *ISB-coord*. Relative orientations are detailed in Table 4.

2.2.5 DISCUSSION

Three reference frames for the tibia-fibula complex (Ruff and Hayes, 1983; Cappozzo, et al., 1995; Wu, et al., 2002), were experimentally compared on the same specimens. Small differences existed between the three reference frames in terms of intra-operator repeatability. *Ruff-coord* had a better inter-operator repeatability than *Cappozzo-coord* and *ISB-coord*. The three frames had similar alignments in the sagittal and frontal planes. However, *Cappozzo-coord* was significantly externally rotated and flexed with respect to *Ruff-coord* and *ISB-coord*. No significant rotation existed between *Ruff-coord* and *ISB-coord*.

All operators reported the impression that *Ruff-coord* was more repeatable because it relied on landmarks that could be accurately measured (i.e. by calipers) on the bone surface. In fact, *Ruff-coord* (Ruff and Hayes, 1983) is intended for *in vitro* use, where the bone surface can be easily accessed and measured. The main problem reported with *Cappozzo-coord* (Cappozzo, et al., 1995) was with point TT on the tibial tuberosity (Fig. 2). Conversely, identification of the other landmarks (apex of the head of the fibula and of the malleoli, Fig. 2) was less critical because these are pronounced bony prominences. The main problem reported with *ISB-coord* (Wu, et al., 2002) was the identification of the most medial and lateral points on tibial condyles (MC, LC, Fig. 3), which was quite subjective because of the large and nearly linear crest; this affects the repeatability in identifying internal/external rotation.

It must be noted that the repeatability reported here for *Cappozzo-coord* and *ISB-coord* represents the lower bound of the error that can be expected in clinical practice. In fact, during this study the bone surface could be accessed directly, while in clinical use the interposition of soft tissues makes the identification of anatomical landmarks less accurate (Van Sint Jan and Della Croce, 2005).

Human movement analysis using commercial systems (e.g. Vicon, Motion Analysis, BTS) can rely in principle on any anatomical based reference frame (Cappozzo, et al., 1995; Della Croce, et al., 2005). However, *Ruff-coord* is clearly not applicable *in vivo*, and *ISB-coord* was rarely reported, likely because of the difficult identification and tracking of the tibial condyles in living subjects. The *Cappozzo-coord* was proposed in the original CAST protocol (Cappozzo, et al., 1995), and recently in a new protocol by (Leardini, et al., 2007), apparently achieving the best inter-operator *in vivo* repeatability just because of the easily identifiable landmarks.

Thus, the reference frame proposed by (Ruff and Hayes, 1983) is preferable when the full bone surface is accessible, typically during *in vitro* tests. No clear advantage of one system over the others appeared for mixed conditions, where the proximal part of the shank bones is accessible directly and the distal part is covered by soft tissue (surgical navigation of total knee replacement), or vice versa (surgical navigation of total ankle replacement). No advantage in terms of *in vitro* repeatability seems to exist between *Cappozzo-coord* (Cappozzo, et al., 1995) and *ISB-coord* (Wu, et al., 2002).

Acknowledgments

The Authors wish to thank Caroline Öhman and Andrea Malandrino for their support in digitizing the landmarks, and Luigi Lena for the artwork. This work was partially supported by the European Community (project number: IST-2004-026932; title: Living Human Digital Library; acronym: LHDL)

2.2.6 REFERENCES

- Cappozzo, A., Catani, F., Della Croce, U., Leardini, A., 1995. Position and orientation in space of bones during movement: anatomical frame definition and determination. *Clin Biomech (Bristol, Avon)* 10, 171-178.
- Cristofolini, L., 1997. A critical analysis of stress shielding evaluation of hip prostheses. *Critical Reviews in Biomedical Engineering* 25, 409-483.
- Cristofolini, L., Viceconti, M., 2000. Mechanical validation of whole bone composite tibia models. *J Biomech* 33, 279-288.
- Currey, J.D., 1982. Bone as a mechanical structure. In: *Biomechanics - Principles and applications*. Huiskes, R., van Campen, D.H., de Wijn, J.R. (Eds). Martinus Nijhoff Publishers, pp. 75-85.
- Della Croce, U., Camomilla, V., Leardini, A., Cappozzo, A., 2003. Femoral anatomical frame: assessment of various definitions. *Med Eng Phys* 25, 425-431.
- Della Croce, U., Leardini, A., Chiari, L., Cappozzo, A., 2005. Human movement analysis using stereophotogrammetry. Part 4: assessment of anatomical landmark misplacement and its effects on joint kinematics. *Gait Posture* 21, 226-237.
- Fung, Y.C., 1980. Bone and cartilage. In: *Biomechanics - Mechanical properties of living tissues*. (Eds). Springer Verlag, New York, pp. 383-415.
- Gray, H.A., Taddei, F., Zavatsky, A.B., Cristofolini, L., Gill, H.S., 2008. Experimental validation of a finite element model of a human cadaveric tibia. *J. Biomech. Engineering* 130, 031016-031011 (031019 pages).
- Gray, H.A., Zavatsky, A.B., Taddei, F., Cristofolini, L., Gill, H.S., 2007. Experimental validation of a finite element model of a composite tibia. *Proc Inst Mech Eng [H]* 221, 315-324.
- Grood, E.S., Suntay, W.J., 1983. A joint coordinate system for the clinical description of three-dimensional motions: application to the knee. *Journal of Biomechanical Engineering* 105, 136-144.
- Heiner, A.D., Brown, T.D., 2001. Structural properties of a new design composite replicate femurs and tibias. *J Biomech.* 34, 773-781.
- Leardini, A., Sawacha, Z., Paolini, G., Ingrosso, S., Nativo, R., Benedetti, M.G., 2007. A new anatomically based protocol for gait analysis in children. *Gait Posture* 26, 560-571.

- O'Connor, J.J., 1992. Load simulation problems in model testing. In: Strain measurement biomechanics. Miles, A.W., Tanner, K.E. (Eds). Chapman & Hall, London, pp. 14-38.
- Ruff, C.B. (1981) Structural changes in the lower limb bones with aging at Pecos Pueblo. Thesis, Dissertation in Anthropology Presented to the Graduate Faculties, University of Pennsylvania,
- Ruff, C.B., Hayes, W.C., 1983. Cross-sectional geometry at Pecos Pueblo femora and tibiae - A biomechanical investigation: I. method and general patterns of variation. *American Journal of Physical Anthropology* 60, 359-381.
- Thewlis, D., Richards, J., Bower, J., 2008. Discrepancies in knee joint moments using common anatomical frames. *J. Applied Biomechanics* 24, 185-190.
- Van Sint Jan, S., Della Croce, U., 2005. Identifying the location of human skeletal landmarks: why standardized definitions are necessary--a proposal. *Clin Biomech (Bristol, Avon)* 20, 659-660.
- Wu, G., Siegler, S., Allard, P., Kirtley, C., Leardini, A., Rosenbaum, D., Whittle, M., D'Lima, D.D., Cristofolini, L., Witte, H., Schmid, O., Stokes, I., 2002. ISB recommendation on definitions of joint coordinate system of various joints for the reporting of human joint motion--part I: ankle, hip, and spine. *International Society of Biomechanics. J Biomech* 35, 543-548.

2.3 A method to improve experimental validation of Finite-Element models of long bones

Mateusz Juszczuk^{a,b}, Enrico Schileo^a, Saulo Martelli^{a,b},
Luca Cristofolini^{a,b}, Marco Viceconti^a

^a *Laboratorio di Tecnologia Medica, Istituti Ortopedici Rizzoli, Bologna, Italy*

^b *Engineering Faculty, University of Bologna, Bologna, Italy*

Presented FP-transducer was designed, made and calibrated by the author of the thesis.
This study has been published on Strain.

2.3.1 ABSTRACT

Finite element (FE) simulations are extremely sensitive to boundary conditions, including the position of applied forces. This is particularly critical for FE models of bones, where the lack of a univocal reference system makes identifying the boundary conditions difficult. The aims of this work were to design a transducer (*FP-transducer*) to accurately determine the position of the resultant joint force during in vitro tests, and to assess its accuracy for future application in validating numerical models of long bones. A strain gauge-based transducer was designed to indirectly measure the position of the force applied to the long bones during in vitro tests, by measuring the reaction moments about two perpendicular axes, generated by the force applied. Validation tests were performed to quantify the intrinsic precision of the *FP-transducer* (by applying calibrated forces at known locations), and the overall accuracy when the *FP-transducer* was included in a typical setup for long bone testing. The intrinsic accuracy of the *FP-transducer* when used to calculate the position of an offset force was satisfactory (0.66 mm). The overall accuracy of the *FP-transducer* in measuring the position of the applied force, when included in a typical setup for long bone testing was 0.85mm. In-vitro validation of FE models of long bones may, therefore, be improved thanks to a more accurate determination of the force application point.

KEYWORDS

Orthopaedic biomechanics; long bones; femur; in vitro validation; finite element models; determination of boundary conditions; biaxial load cell; calibration; force application point

2.3.2 INTRODUCTION

The validation of finite element (FE) models using experimentally derived data is a fundamental step to ensure model accuracy and adequacy (Roarche 1998). Because of the complexity of geometry and materials involved (Keyak, Fourkas et al. 1993; Les, Keyak et al. 1997; Keyak, Rossi et al. 1998; Lengsfeld, Schmitt et al. 1998; Ota, Yamamoto et al. 1999; Couteau, Mansat et al. 2001; Gupta, van der Helm et al. 2004), validation becomes particularly important when FE models of intact and implanted bones are used to predict mechanical stress, risk of failure, load transfer and micromotions between bone and implant. Validation is a fundamental step when FE models are used to gain clinically relevant information (Viceconti, Olsen et al. 2005). Validation can be achieved by means of dedicated *in vitro* experiments and purpose-designed transducers to enhance comparisons of the numerical results with the experimental measurements (Viceconti, Olsen et al. 2005). To quantitatively validate an FE model of a long bone (e.g. a femur), reliable data, especially concerning boundary conditions, need to be transferred from the experimental field to the computational model (Keyak, Skinner et al. 2001; Taddei, Cristofolini et al. 2006). Thus, it is necessary to design an experiment in which precise boundary conditions can be determined and transferred to the model, so as to enable applying to the FE model identical loading conditions as in the physical specimen. It must be stressed that experimental validation of FE models is necessary, but is not sufficient by itself to prove the clinical relevance of the simulation.

One of the most critical factors determining the output of an FE model of a long bone is the position of the applied force relative to the bone. For instance, when the hip joint force is applied to the femoral head *in-vitro* (Cristofolini, Cappello et al. 1994; Cody, Gross et al. 1999; Ota, Yamamoto et al. 1999; Keyak, Kaneko et al. 2005; Cristofolini, Juszczuk et al. 2006; Taddei, Cristofolini et al. 2006; Cristofolini, Juszczuk et al. 2007), it is not possible *a priori* to determine accurately the position of the resultant force, as: (i) the contact area between the bone surface and the loading device is difficult to measure accurately due to the large deformation of the bone surface; (ii) even if the contact area was accurately measured, the distribution of the contact pressure (and its resultant) cannot be easily measured experimentally. Additionally, long bones undergo significant deflection when loaded (of the order of 10 mm (Cristofolini and Viceconti 1999; Cristofolini and Viceconti 1999; Cristofolini,

Juszczyk et al. 2006)). It is not possible to predict *a priori* the changing position of the applied force while the bone specimen is deflecting due to the material deformation as load is applied. In previous *in vitro* studies (Cristofolini and Viceconti 1999; Cristofolini and Viceconti 1999) the point of application of the force was intentionally displaced by known amounts, so as to estimate the effect of such uncertainty on the strain distribution. Such experiments showed that an error of only a few millimeters in positioning the hip joint force onto the femur can result in extremely high errors in the estimated stress (as high as 50%). Thus, accurate identification of the force position is a major issue when investigating the biomechanics of long bones, such as femurs, using FE models.

Therefore, even assuming that when designing an experiment or an FE model the position of the applied force is defined in principle, based on biomechanical and anatomical considerations, the problem remains about how to accurately measure the actual position of force application in the real *in vitro* experiment (the actual position of the applied force is determined not only by the testing setup, but also by the bone deformations, see above). Inaccurate identification of such position would undermine the accuracy of the comparison between *in vitro* experiment and FE model, thus compromising the validation of the FE model.

To the authors' best knowledge, the actual position of the applied force has never been measured during mechanical *in vitro* tests of long bones, such as femurs (nor tracked while the bone deflects). As a consequence, this information has never been incorporated into FE models simulating the same bone. In some studies it has been assumed that the position of the force to be applied to the FE model should be the one theoretically identified on an ideal physical bone specimen (i.e. ignoring the local and global bone deformation, and postulating an idealized contact between the physical specimen and the constraints) (Keyak, Rossi et al. 1998; Cody, Gross et al. 1999; Taddei, Cristofolini et al. 2006). In other cases no information has been provided on the location of the applied force that was used to replicate the experimental forces on the FE models (e.g. (Ota, Yamamoto et al. 1999)).

One such means of measuring the position of an applied force is a multiaxial load cell such as those designed for indirectly measuring the application point of an applied force in milling machines (Saglam 2001). Such load cells are normally designed to

measure forces or moments. In fact, the actual position of a given force can be calculated using load cells to measure the applied force and the reaction moment that the force generates.

To locate the actual position of the force applied to the femoral head, the bending moment applied to a femur has been measured using strain gauges directly attached to the femur diaphysis (Villa, Pietrabissa et al. 2000). However, determining the position of the applied force with such an arrangement depends on the pre-identification of the centre of the diaphysis, which cannot be achieved without a means to calculate the neutral axis of complex geometries, because of the irregular shape of bones.

In order to improve validation of FE models of long bones, we developed a method, based on a dedicated transducer, to measure the position of the force applied to the modelled bone specimen when tested *in vitro*. In the research reported here, we:

- 1) Modified an existing *in vitro* testing protocol so as to include a custom-made force-position transducer (*FP-transducer*), in order to determine the position of the force and to incorporate this information into the corresponding FE model. The *FP-transducer* consisted of a strain gauge-based load cell that measured the reaction moment generated by the position of the force applied to the bone in order to determine the coordinates of the applied force in relation to the bone specimen.
- 2) Calibrated the *FP-transducer*, determined its intrinsic repeatability and also its accuracy independently of its specific application
- 3) Tested the applicability of the modified *in vitro* testing protocol, and determined the overall repeatability and accuracy the *FP-transducer* when incorporated in a mechanical testing setup typically used for testing long bones.

2.3.3 MATERIALS AND METHODS

Overview of the test setup for *in vitro* validation

An experimental setup used for investigating the strain distribution and the strength of the proximal femur (Cristofolini and Viceconti 1999; Cristofolini, Juszczuk et al. 2006; Taddei, Cristofolini et al. 2006) was modified to provide more accurate validation for FE models. A sketch of the setup in exercise, when testing a femoral

bone, is shown in Fig. 1. The setup consists of the load cell forming the base of the testing machine, with the *FP-transducer* mounted on top of the load cell. The bone specimen is potted on top of the *FP-transducer*; to allow application of the force in the desired directions(Cristofolini, Juszcyk et al. 2006; Cristofolini, Juszcyk et al. 2007), interchangeable wedges are used to tilt the bone by given angles. A vertical force is applied to the proximal end of the specimen by the actuator of the testing machine, through a system of low-friction cross-rails that eliminated any horizontal force component.

The *FP-transducer* was calibrated so as to track the horizontal position of the force applied vertically to the bone specimen, by measuring the reaction moments about two perpendicular axes. This layout allowed the coordinates of the applied force (ΔA and ΔB in Fig. 1) to be measured by the *FP-transducer* with respect to a known reference system.

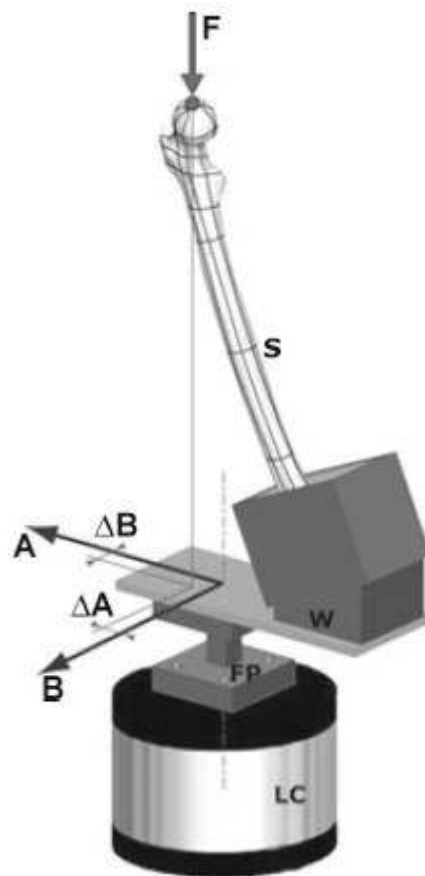


Fig. 1 - Schematic of the loading setup for the biomechanical testing of long bones (a femur in this instance) in different anatomical positions. The bone specimen (S: a femur, in this instance) is mounted on top of interchangeable wedges (W) that are attached to the transducer and allow tilting the specimen

at prescribed angles (24° in the coronal plane with respect to the vertical axis in this instance). The *FP-transducer* (FP) measuring the force position is mounted below the specimen. Its reference axes (A and B) are indicated, as well as the coordinates (ΔA and ΔB) of the applied force F relative to the transducer reference. The entire system is mounted on top of the load cell (LC) of the testing machine, which is measuring the force (F) applied by the actuator of the testing machine.

Design of the *FP-transducer*

Although multiaxial load cells are commercially available, none was found that met all technical requirements:

- Capable of measuring two moment components (to measure the coordinates of the applied force in two directions).
- With a test capacity suitable for the *in vitro* tests on long bones (details below).
- Waterproof (to be applied also when testing tissue specimens in wet environment).

Therefore, a dedicated load cell (the *FP-transducer*) was designed for the geometry and the loads of human femurs.

The *FP-transducer* measured the reaction moment about two orthogonal directions generated by a force applied to the bone specimen. The load cell of the testing machine (Mod. 5kN-UK143, Instron Ltd., Canton, MA, USA) measured the force value (Fig. 1). Thus, the coordinates of the applied force with respect to the *FP-transducer* coordinate system (i.e., the lever arms) could be easily obtained if the transfer functions (between output voltages and bending moments) of the *FP-transducer* is known.

As shown in Fig. 2, the *FP-transducer* consisted of two plates and a connecting beam, which was the sensing element measuring the reaction moments. The connecting beam, which was the transducer core, had a square section.

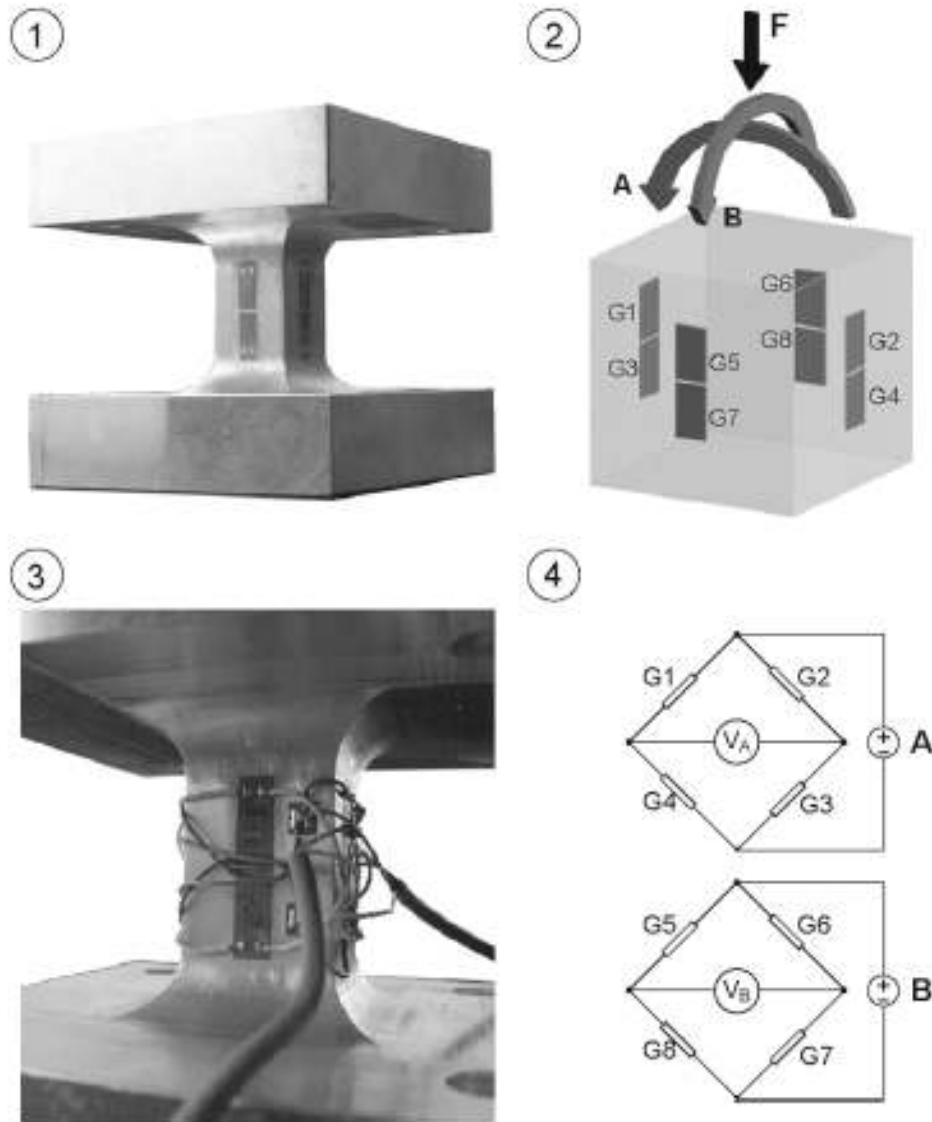


Fig. 2 - The *FP-transducer* in construction: (1) Instrumented *FP-transducer* core, with two strain gauges mounted one adjacent to the other on each side of the sensing beam. (2) Schematic of the strain gauge (G1 to G8) positions on the transducer core; also indicated is the applied force F and the two directions (A and B) of the measured reaction moments. (3) Photo of the wired strain gauges. (4) Schematic of the wiring of the strain gauges showing the grids connected to the two Wheatstone bridges. Two full Wheatstone bridges were built so as to measure the reaction moments A and B separately, while eliminating the effect of the axial force F (which was measured by the load cell of the testing machine, see Fig. 1 and 4).

The test capacity of the transducer was defined based on the forces and moments generated during *in vitro* tests of the proximal femur. The testing protocol adopted by these authors (Cristofolini, Juszczak et al. 2006; Taddei, Cristofolini et al. 2006) involved positioning the femur at different prescribed angles to cover the range of physiological loads during daily motor tasks (Bergmann, Graichen et al. 1993; Bergmann, Deuretzbacher et al. 2001). The dimensions of the transducer were chosen based on the anatomical variability and different loading directions of the femur

specimen. In order to reduce the range of reaction moments to be measured by the *FP-transducer*, the interchangeable wedges above the *FP-transducer* were designed to keep the force application point (i.e.: the femoral head) close to the axis of the *FP-transducer*. In order to estimate the range of possible positions of the femoral head (i.e. of the resultant force), a CAD simulation was carried out exploring the effect of three anatomical parameters (diaphyseal length, neck anteversion, and neck length), and including the different possible alignments of the femur under the testing machine (Cristofolini, Juszczuk et al. 2006; Taddei, Cristofolini et al. 2006). Such simulation indicated that the force application point (i.e.: the femoral head) always fell within 55 mm from the axis of the *FP-transducer*. Based on previous experience (Cristofolini and Viceconti 1999; Cristofolini, Juszczuk et al. 2006), the maximum force to be applied to the femur in a non-destructive test was estimated (1500 N). However, to take into account possible overloads and future tests with larger loads, the *FP-transducer* was designed to withstand a larger force (2500 N). Thus, the maximum resultant moment during testing could be estimated, which provided an indication of the required test capacity of the *FP-transducer* (maximum bending moment = 140 Nm).

The *FP-transducer* was machined out of a single block of Al2011-T6 aluminum alloy (UNS-A92011). This alloy was chosen because of its high elastic range, low Young's modulus, and ease of manufacture. The cross section of the instrumented beam measured 24x24 mm², to ensure that maximum stress due to bending was 60 MPa when the test capacity was applied (safely lower than the yield stress of the selected alloy, which is 270 MPa (ISO3522:2007)). The transducer was sufficiently stiff to avoid excessive deflection when loaded (less than 0.2° with the maximum load).

Eight uniaxial strain gauges (1-LY41- 6/350, HBM, Darmstadt, Germany) were bonded on the connecting beam with cyanoacrylate adhesive (Z70, HBM). They were placed two on each face of the connecting beam, parallel to the long axis of the beam (Fig. 2). The strain gauges were connected in groups of four to form two Wheatstone bridges (Fig. 2). A full Wheatstone bridge configuration was used for each direction of bending to amplify the output signal of the *FP-transducer* (bending strain was amplified four-fold, while the axial component was eliminated). Thus, the *FP-transducer* provided two independent measurements (Bridges A and B) related to bending in two orthogonal directions. In order to reduce thermal drift and maximize

signal, a bridge excitation of 5 V was chosen based on the strain gauge size. Because testing of real bones often necessarily involves wet test environment, the instrumented transducer core, was covered with two layers of polyurethane (PU-120, HBM) for insulation and a layer of silicone rubber (SG-250, HBM) for mechanical protection. An external copper shell was provided over the *FP-transducer* core to shield from electrical noise.

Electrical testing of the *FP-transducer*

Electrical tests were performed to assess the quality of the signal provided by the *FP-transducer*, to ensure that baseline noise would not compromise signal quality. To cover different possible applications (which can include creep, quasi-static loading and impact loading), signal high-frequency noise and long-term drift were checked at different sampling rates (1 to 5000 Hz) and on different time intervals (up to 12 hours of monitoring), with a high-speed data logger (System 6000, Vishay, Malvern, USA), when the transducer was unloaded. Tests were carried out at different temperatures ranging from 18°C to 38°C.

Calibration of the *FP-transducer* and assessment of its accuracy

We devised a calibration procedure to measure the intrinsic repeatability and accuracy of the *FP-transducer* in calculating the position of the applied force. Calibration forces were applied at a set of known positions on the *FP-transducer* to determine the parameters of the transfer functions. using the hydraulic testing machine (Mod. 8502, Instron). A jig was designed to control the position of the force applied during calibration. Twenty-five holes were grid-wise machined (five in five lines, each 20 mm from each other) on a calibration plate, which was mounted on top of the *FP-transducer*, collinearly with the main bending axes (Fig. 3). Twenty-five holes (in a 5 x 5 grid pattern with regular spacing of 20 mm) were machined on a calibration plate, which was mounted on top of the *FP-transducer* (Fig. 3). The calibration forces were applied by the actuator of the testing machine and transmitted by a steel ball placed in each hole of the calibration plate. Low-friction cross-rails were used to ensure a frictionless transmission of the calibration forces.

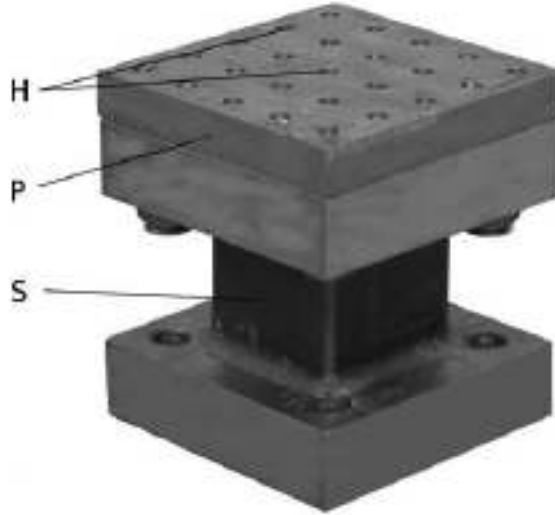


Fig. 3 - The fully assembled *FP-transducer* (including the external shielding (S)) is visible, with the loading plate used for calibration mounted on the top face (P). Twenty-five holes were grid-wise machined on the calibration plate to accurately locate the calibration force by means of a steel ball (H).

Each calibration point was tested three times applying a load ramp from 0 to 1500N. Signals from the *FP-transducer* and from the load cell of the testing machine were acquired synchronously by the data logger (System 6000).

Automatic data-processing procedures were custom-written in MatLab (MatLab 6.1, MathWorks, Natick, MA, US). The voltage signal outputs from the two Wheatstone bridges of the *FP-transducer* (which correspond to the reaction moment about two directions A and B, Fig. 2) were normalized by dividing them by the corresponding force value (measured by the load cell of the testing machine). A “black-box” approach (Draper 1966) was used to define the correlation between collected readouts of the *FP-transducer* and known positions of the applied calibration forces. First-order equations, both without (Eq. 1) and with interaction between the two Wheatstone bridges (Eq. 2), were tested, using least squares fitting:

$$\begin{cases} \Delta\mathbf{A} = (\mathbf{V}_A \times k_{AA})/\mathbf{F} \\ \Delta\mathbf{B} = (\mathbf{V}_B \times k_{BB})/\mathbf{F} \end{cases} \quad (\text{Eq. 1})$$

$$\begin{cases} \Delta\mathbf{A} = (\mathbf{V}_A \times k_{AA} + \mathbf{V}_B \times k_{AB})/\mathbf{F} \\ \Delta\mathbf{B} = (\mathbf{V}_B \times k_{BB} + \mathbf{V}_A \times k_{BA})/\mathbf{F} \end{cases} \quad (\text{Eq. 2})$$

where: \mathbf{F} is the force applied (measured by the load cell of the testing machine); $\Delta\mathbf{A}$ and $\Delta\mathbf{B}$ are the coordinates of the force \mathbf{F} with respect to the reference system of the *FP-transducer* (Fig. 1); \mathbf{V}_A and \mathbf{V}_B are respectively the signals from Wheatstone

bridges A and B (Fig. 2); k_{AA} , k_{BB} , k_{AB} , k_{BA} are the calibration constants (due to the construction of the transducer, k_{AB} and k_{BA} are expected to be significantly smaller than k_{AA} and k_{BB}).

It must be noticed that determination of moment arms using the *FP-transducer* is dependent on accurate measurement of the vertical component of applied force using the load cell of the testing machine (Mod. 5kN-UK143, Instron Ltd., Canton, MA, USA). The *FP-transducer* and loading fixtures were designed so that the resultant force always fell within 55 mm from the axis of the FP-transducer (which was aligned with the load cell of the testing machine). For such an offset, the error indicated by the manufacturer of the load cell of the testing machine is smaller than 0.5% of the force readout. When this force is used to estimate the position of the applied force (Eq. 1 or 2, see above), this propagates to an error of 0.5% on the estimated position. In the worst case, this corresponds to an error of 0.25mm. Such an error is smaller than the other sources of error reported below. Measurement repeatability was computed for each of the 25 points of application of the calibration force. The standard deviation among the three repetitions of estimation of the coordinates of the applied force when the force was applied in the same position. To estimate the average repeatability of the *FP-transducer*, the average error and the Root Mean Squared Error (RMSE) were computed (for direction A, B and for the error vector) based on the repeatability at each point of application of the calibration force.

The accuracy (closeness to target value) of the *FP-transducer* was estimated for each of the 25 points of application of the calibration force, based on the difference between the actual coordinates of the applied force (pre-determined by the position of the machined holes of the calibration plate), and the ones calculated based on the calibrated *FP-transducer*. To estimate the average accuracy of the *FP-transducer*, the average error and the Root Mean Squared Error (RMSE) was computed (for direction A, B and for the error vector) based on the error at each point of application of the calibration force.

Assessment of the performance of the *FP-transducer* in a setup for biomechanical testing of long bones

To assess the behaviour and the applicability of the *FP-transducer* to measure the position of the force applied to a long bone, a setup for biomechanical testing of long bones was built where the *FP-transducer* was included. To avoid the additional variability and non-linearity associated with the use of cadaveric bone in this test, a dummy artificial bone model was built. As in the present application the *FP-transducer* was designed for testing a femur specimen, a dummy femur was used. This femur was made of a steel T-profile 500 mm long and was welded to a flat plate at a 70° inclination (Fig. 4), replicating a typical testing setup for a femur (Cristofolini and Viceconti 1999; Cristofolini, Juszczuk et al. 2006; Taddei, Cristofolini et al. 2006). The dummy femur was designed so as to have a comparable stiffness to human femurs (Cristofolini, Viceconti et al. 1996; Cristofolini, Juszczuk et al. 2006). This enabled to use this simplified test specimen to reproduce relevant deflections of the proximal extremity of femur under load.

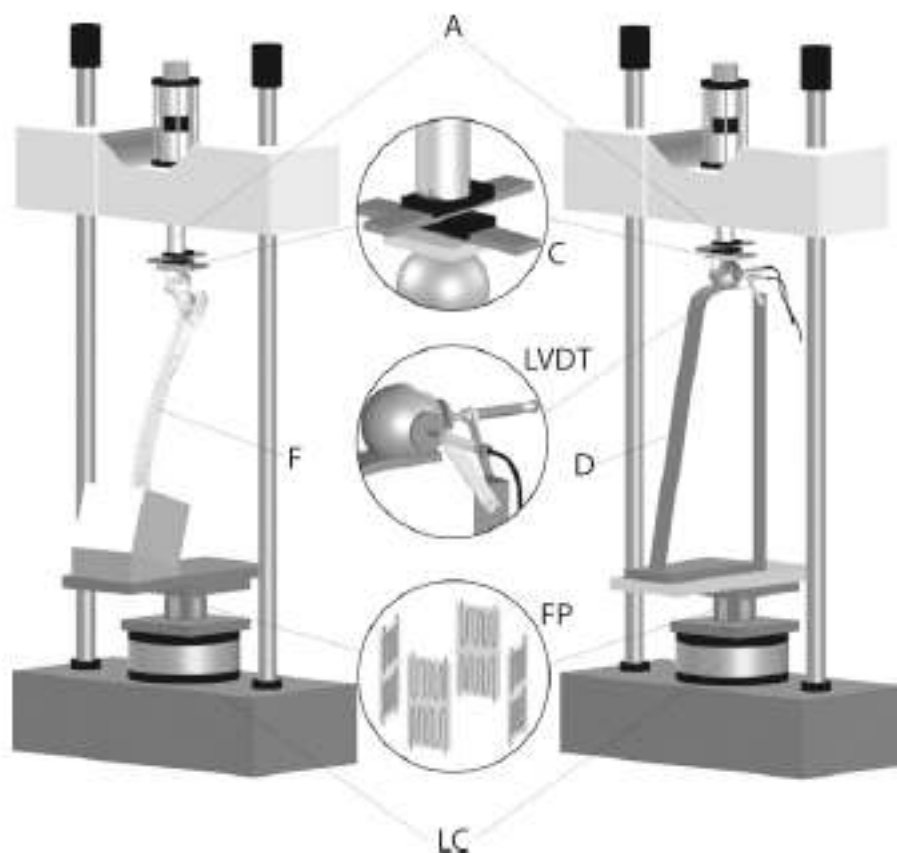


Fig. 4 – Testing setup for a long bone, including the *FP-transducer*: setup for testing a real femur (left); simplified setup for validating the force-position transducer using a dummy femur (right). The actuator

of the testing machine (A) applies the force from top, through a system of cross-rails (C), which eliminate the horizontal force components. The femur (F) and the dummy specimen (D) are mounted in the same respective position and inclination. The *FP-transducer* (FP) is mounted just below the fixture to hold the specimen at prescribed angles. The load cell of the testing machine (LC) measures the applied vertical force. In addition, two LVDTs (detail LVDT) measure the deflection of the dummy femur, to validate the readout from the *FP-transducer*.

The dummy femur specimen was fixed to the top of the *FP-transducer* and mounted on the testing machine. Force was applied from the actuator of the testing machine using low-friction cross-rails to avoid transmission of horizontal force components. The dummy femur was provided with a steel ball to ensure point-wise force application. A force ramp was applied up to 1500 N. Readouts from the *FP-transducer* were collected and converted to position coordinates.

To independently validate the force position estimated by the *FP-transducer*, the actual horizontal deflection of the dummy femur head was measured in two directions by means of two spring-preloaded LVDTs (Mod. GHSA750-500, with Mod. LVDT-A amplifier, Macro Sensors, Pennsauken, NJ, USA; precision: 0.01 mm, range 12.5 mm; Fig. 4). The LVDTs were provided with a flat probe, which was touching the steel ball on top of the dummy femur. Signals from the LVDTs were recorded by the scanner (System 6000, Vishay), synchronously with the signals from the *FP-transducer*. The test was repeated five times, with the entire testing setup being dismantled and reassembled each time.

Correlation between the actual deflection of the test specimen when the force was applied (measured by the LVDTs), and the estimated deflection (by the *FP-transducer*) was estimated by linear regression. Additionally, the difference between measured and estimated position of the applied force was computed (for direction A, B and for the error vector), and the RMSE will be reported. The average error and the Root Mean Squared Error (RMSE) were computed.

Use of the *FP-transducer* to determine the force position and to transfer the force position to an FE model

Details of the procedure for transferring experimentally measured coordinates of the applied force to the FE model are reported elsewhere (Cristofolini, Juszczuk et al. 2006). The procedure can be summarized as follows:

- First of all, reaction moments are recorded by the *FP-transducer* (synchronously with the value of the applied force from the testing machine) as the physical bone specimen is tested.
- This data are later converted to coordinates of the applied force (using the calibration equation of the *FP-transducer*, see below). This is not a single set of coordinates, but a series of coordinates that changes as the bone deflects when force is applied.
- A digitizer (Micro Scribe 3DX, Immersion Corporation, USA) is used to measure coordinates on the experimental testing setup: (i) a cloud of points on the surface of the physical bone specimen and (ii) a number of reference points on the *FP-transducer*.
- An iterative-closest-point algorithm (Taddei, Cristofolini et al. 2006) is applied, to identify the spatial transformation that registers the surface of the FE model of the bone with respect to the physical bone specimen.
- Finally, the position of the force applied in the *in vitro* test can be replicated on the FE model based on the coordinates obtained from the *FP-transducer* readouts.

It is clear that this approach is applicable only if the FE model is specimen-specific.

2.3.4 RESULTS AND DISCUSSION

Electrical testing

In the preliminary electrical tests, total signal noise (including long-term drift and high-frequency noise) was within ± 0.30 microstrain. Based on the calibration equation used to convert strain readout to the position of the applied force, it can be estimated that such error corresponds to an error of ± 0.07 mm on the estimated force position when a force of 1500 N is applied. Thus, the error caused by electrical noise was almost two orders of magnitude lower than any other source of error (see below), and was negligible with respect to the measurement range (± 55 mm).

Calibration

Based on the data recorded, the coefficients of the first-order calibration functions (Eq. 1 and 2 above) were obtained, both incorporating and neglecting an interaction between the two Wheatstone bridges (corresponding to the two directions of bending moment axes A and B, Fig. 2). It was found that including the interaction between the two Wheatstone bridges improved calibration accuracy (Table 1):

- The errors of the estimated force position were similar in both directions.
- Errors on the estimated position slightly decreased as applied force increased. The values in Table 1 are the largest errors found on the whole range of calibration force.
- The measurement repeatability when the calibration force was applied to the same assigned position three times was better than 0.39 mm as a resultant (Table 1, first row).
- The accuracy of the *FP-transducer*, expressed as a vector distance between the estimated and the actual position of the applied calibration force, was 0.66 mm (RMSE of the error vector; Table 1, last row).

Table 1 – Calibration of the *FP-transducer*. The first section reports the measurement repeatability on the same assigned position of the calibration force, computed as standard deviation among three measurement repetitions. The last row reports the accuracy (closeness to target value) of the *FP-transducer* as the difference between the actual coordinates of the applied force, and the coordinates estimated by the *FP-transducer*. Errors are reported for both measurement directions (A and B); the last column reports the error vector computed as vector sum of the errors in the two directions A and B. The average error and the Root Mean Squared Error (RMSE) are reported for direction A, B and for the vector error.

| | A DIRECTION | B DIRECTION | RESULTANT VECTOR |
|---|-----------------------------------|-----------------------------------|-----------------------------------|
| REPEATABILITY (variation btw 3 replicates) | Average: 0.22 mm RMSE: 0.29 mm | Average: 0.20 mm RMSE: 0.26 mm | Average: 0.34 mm RMSE: 0.39 mm |
| ACCURACY (difference btw assigned position of the calibration force position and position measured by the <i>FP-transducer</i>) | Average: 0.36 mm RMSE: 0.43 mm | Average: 0.38mm RMSE: 0.48 mm | Average: 0.58 mm RMSE: 0.66 mm |

Performance of the *FP-transducer* in a biomechanical testing setup

In the preliminary application with the dummy femur, a maximum horizontal deflection of 15 mm was measured by the LVDTs, which is of the same order of magnitude of the deflection found with human femurs when similar forces are applied

(Cristofolini, Juszczuk et al. 2006). A comparison between the horizontal deflection measured by the LVDTs and the deflection estimated from the *FP-transducer* provided an indication of the overall error when the *FP-transducer* was applied to long bone testing (Fig. 5):

- The position and displacement of the applied force measured by the *FP-transducer* as force was increased correlated well with that measured by the LVDTs ($R^2 = 0.988$, slope = 0.95).
- The RMSE in the force position was 0.60 mm for direction A and B, and 0.85 mm for the vector error.

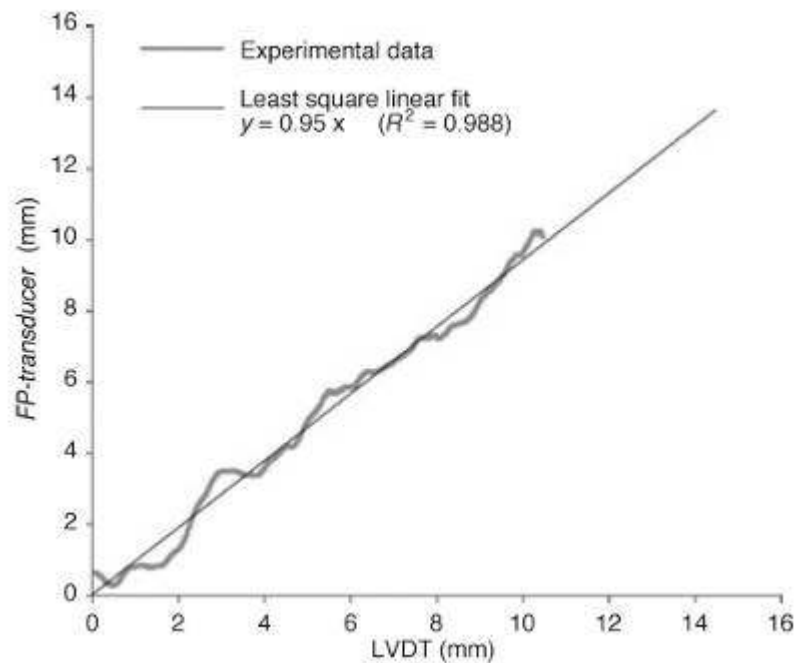


Fig. 5 – Performance of the *FP-transducer* in a testing setup simulating force application on a long bone (Fig. 4): correlation between the actual position of the vertical applied force (measured by the LVDTs) and the position estimated by the *FP-transducer* (similar results were obtained for direction A and B).

Thus, it can be assumed that, when the *FP-transducer* is used, the position of the force applied to a long bone can be measured with an accuracy of better than 0.85 mm. Therefore, the proposed method allows reporting the position of the applied force onto an FE model with an RMS accuracy of 0.85 mm. FE models of long bones are very sensitive to changes in the position of the force (Roarche 1998; Cody, Gross et al. 1999; Viceconti, Olsen et al. 2005; Taddei, Cristofolini et al. 2006), which is usually applied to nodal points. The accuracy of the *FP-transducer* is smaller or comparable to the average inter-nodal distance of converged state-of-the-art FE meshes of long bones

(2-5 mm) (Perillo-Marcone, Alonso-Vazquez et al. 2003; Helgason, Taddei et al. 2007). A previous FE analysis (Cristofolini, Juszczuk et al. 2006) with the methods described and verified in (Taddei, Martelli et al. 2006) showed that shifting by 2 mm the position of the resultant force applied to an FE model can induce a 5% change in the overall model accuracy when compared to experimental strain measurements. Therefore, use of the *FP-transducer* will likely help reducing the current bias.

Limitations

One limitation is that the *FP-transducer* not only measures the reaction moments generated by the lever arm of the applied vertical force, but it is also affected by the reaction moment generated by horizontal forces (if present). In fact, undesirable horizontal force may exist because of friction: when the vertical force is applied, the bone specimen tends to deflect, so that the unconstrained proximal extremity moves in a horizontal direction. The cross-rails used to allow for horizontal displacements of the proximal extremity (Fig. 4) reduce friction, but cannot eliminate it completely. Such passive horizontal force component generates an additional reaction moment, that adds to the one generated by the offset of the vertical force component. The effect of such passive horizontal force tends to be significantly amplified because of the large lever arm (the bone length).

In order to estimate an acceptable magnitude of such friction, we should consider a typical femur having a biomechanical length (Ruff and Hayes 1983) of 500 mm, loaded with a force of 1500 N. If the horizontal force component (caused by friction) is 6 N, it causes an additional (artifactual) bending moment (3 Nm). Such artifactual bending moment is equivalent to the moment caused by a displacement of 2 mm of the vertical force (1500 N). Hence, the position of the vertical force is affected by an error of 2 mm. This can be obtained only if the vertical force is applied with a low-friction system (coefficient of friction ≤ 0.004) that ensures extremely low horizontal forces. Thus, care should be taken in evaluating each possible source of friction, such as worn or badly mounted cross-rails.

Finally, the *FP-transducer* was designed and optimized for the geometry and the loads of human femurs. However, a transducer based on this concept can be tuned to test other long bones, such as the tibia or the humerus.

Comparison with previous similar works

The error affecting the estimated position of the applied force in previous cross-validation experiments where the *FP-transducer* was not present was more than 10 mm (Cristofolini, Juszczuk et al. 2006), due to uncertainty and variability in identifying the contact area under load. This error may seriously affect the stress predicted by an FE model (Cristofolini and Viceconti 1999; Cristofolini and Viceconti 1999). An FE analysis (Cristofolini, Juszczuk et al. 2006) using validated methods (Cristofolini, Juszczuk et al. 2006; Taddei, Martelli et al. 2006) showed that an uncertainty of 2 mm affecting the position of the resultant force applied to an FE model can affect the predicted strain by 5%. It has been experimentally shown (Cristofolini and Viceconti 1999; Cristofolini and Viceconti 1999) that an error of a few millimeters in positioning the hip force onto the femur can result in high (up to 50%) errors in the estimated stress.

2.3.5 CONCLUSIONS

The aim of the research reported here was to provide a method to improve validation of FE models of long bones. It must be pointed out that, while the proposed method can strengthen the comparison between *in vitro* experiments and FE models, it cannot contribute to assessing the clinical relevance of the FE simulation.

We designed a transducer that was incorporated into a standard testing setup for long bones, so as to measure the reaction moments. The *FP-transducer* successfully estimated the position of the force applied to the proximal extremity of the femur. The intrinsic accuracy of the *FP-transducer* was 0.66 mm (RMSE) when tested alone, and better than 0.85 mm (RMSE) when incorporated in a setup for testing a femur.

To the authors' knowledge, measurement of the force position relative to the bone in similar experiments has never been reported. The spatial accuracy at which the *FP-transducer* estimates the force position is significant for validating an FE model. In fact, such accuracy is smaller or comparable to the inter-nodal distance in converged FE meshes of long bones (Perillo-Marccone, Alonso-Vazquez et al. 2003; Taddei, Cristofolini et al. 2006; Helgason, Taddei et al. 2007).

Moreover, the proposed method was able to account for the changing position of the applied force throughout the load application. This possibility is extremely important because long bones undergo significant deflection when loaded (of the order of 10 mm (Cristofolini and Viceconti 1999; Cristofolini and Viceconti 1999; Cristofolini, Juszczak et al. 2006; Taddei, Cristofolini et al. 2006)). Thus, the accuracy of FE analyses of long bones may be improved with a better definition of boundary conditions (the actual position of the applied force).

ACKNOWLEDGEMENTS

The authors wish to thank Luigi Lena for the artwork, and Sandra Oster for the careful revision of the manuscript. This work was partially supported by the European Community (project number: IST-2004-026932; title: Living Human Digital Library; acronym: LHDL)

2.3.6 REFERENCES

- Bergmann, G., G. Deuretzbacher, et al. (2001). "Hip contact forces and gait patterns from routine activities." J Biomech 34(7): 859-71.
- Bergmann, G., F. Graichen, et al. (1993). "Hip joint loading during walking and running, measured in two patients." Journal of Biomechanics. 26(8): 969-90.
- Cody, D. D., G. J. Gross, et al. (1999). "Femoral strength is better predicted by finite element models than QCT and DXA." J Biomech 32(10): 1013-20.
- Couteau, B., P. Mansat, et al. (2001). "Finite element analysis of the mechanical behavior of a scapula implanted with a glenoid prosthesis." Clinical biomechanics (Bristol, Avon) 16(7): 566-75.
- Cristofolini, L., A. Cappello, et al. (1994). "Experimental errors in the application of photoelastic coatings on human femurs with uncemented hip stems." Strain 30(3): 95-103.
- Cristofolini, L., M. Juszczak, et al. (2007). "In vitro replication of spontaneous fractures of the proximal human femur." J. Biomechanics 40(13): 2837-2845.
- Cristofolini, L., M. Juszczak, et al. (2006). Biomechanical testing of the proximal femoral epiphysis: intact and implanted condition. 8th Biennial Conference on Engineering Systems Design and Analysis ASME-ESDA 2006, Turin, ASME.
- Cristofolini, L. and M. Viceconti (1999). "In vitro stress shielding measurements can be affected by large errors." Journal of Arthroplasty 14(2): 215-9.
- Cristofolini, L. and M. Viceconti (1999). "Towards the standardization of in vitro load transfer investigations of hip prostheses." Journal of Strain Analysis for Engineering Design 34(1): 1-15.
- Cristofolini, L., M. Viceconti, et al. (1996). "Mechanical validation of whole bone composite femur models." Journal of biomechanics 29(4): 525-535.
- Draper, N. R., Smith, H. (1966). Applied Regression Analysis. New York, John Wiley & Sons.
- Gupta, S., F. C. van der Helm, et al. (2004). "Development and experimental validation of a three-dimensional finite element model of the human scapula." Proceedings of the Institution of Mechanical Engineers. Part H, Journal of engineering in medicine. 218(2): 127-42.
- Helgason, B., F. Taddei, et al. (2007). "A modified method for assigning material properties to FE models of bones." Med Eng Phys.
- Keyak, J. H., M. G. Fourkas, et al. (1993). "Validation of an automated method of three-dimensional finite element modelling of bone." Journal of biomedical engineering 15(6): 505-9.
- Keyak, J. H., T. S. Kaneko, et al. (2005). "Predicting proximal femoral strength using structural engineering models." Clin Orthop Relat Res(437): 219-28.
- Keyak, J. H., S. A. Rossi, et al. (1998). "Prediction of femoral fracture load using automated finite element modeling." Journal of Biomechanics 31(2): 125-33.
- Keyak, J. H., H. B. Skinner, et al. (2001). "Effect of force direction on femoral fracture load for two types of loading conditions." J Orthop Res 19(4): 539-44.

- Lengsfeld, M., J. Schmitt, et al. (1998). "Comparison of geometry-based and CT voxel-based finite element modelling and experimental validation." Medical engineering & physics 20(7): 515-22.
- Les, C. M., J. H. Keyak, et al. (1997). "Development and validation of a series of three-dimensional finite element models of the equine metacarpus." Journal of biomechanics 30(7): 737-42.
- Ota, T., I. Yamamoto, et al. (1999). "Fracture simulation of the femoral bone using the finite-element method: how a fracture initiates and proceeds." J Bone Miner Metab 17(2): 108-12.
- Perillo-Marcone, A., A. Alonso-Vazquez, et al. (2003). "Assessment of the effect of mesh density on the material property discretisation within QCT based FE models: a practical example using the implanted proximal tibia." Comput Methods Biomech Biomed Engin 6(1): 17-26.
- Roache, P. (1998). Verification and Validation in Computational Science and Engineering. Albuquerque, Herrmosa Publisher.
- Ruff, C. B. and W. C. Hayes (1983). "Cross-sectional geometry at Pecos Pueblo femora and tibiae - A biomechanical investigation: I. method and general patterns of variation." American Journal of Physical Anthropology 60: 359-381.
- Saglam, H., Unuvar, A. (2001). "Three-component, strain gage based milling dynamometer design and manufacturing." Journal of Integrated Design and Process Science 5(2): 95-109.
- Taddei, F., L. Cristofolini, et al. (2006). "Subject-specific finite element models of long bones: An in vitro evaluation of the overall accuracy." J Biomech 39(13): 2457-67.
- Taddei, F., S. Martelli, et al. (2006). "Finite-element modeling of bones from CT data: sensitivity to geometry and material uncertainties." IEEE Trans Biomed Eng 53(11): 2194-200.
- Viceconti, M., S. Olsen, et al. (2005). "Extracting clinically relevant data from finite element simulations." Clin Biomech (Bristol, Avon) 20(5): 451-4.
- Villa, T., R. Pietrabissa, et al. (2000). Testing procedure for biomechanical evaluation for nailed femur. Proceedings of the 12th Conference of the European Society of Biomechanics, Dublin, Royal Academy of Medicine in Ireland.

2.4 In vitro technique to determine time and location of fracture initiation in bones

Mateusz Juszczak, Ph.D.^{1,2}, Luca Cristofolini, Ph.D.^{1,2}, Jacek Kaniuk,
Enrico Schileo, Ph.D.¹, Marco Viceconti, Ph.D.¹

¹Laboratorio di Tecnologia Medica, Istituto Ortopedico Rizzoli, Bologna, Italy

²Facoltà di Ingegneria, Università di Bologna, Italy

Submitted to Journal of Biomechanics

2.4.1 Introduction

Bone fractures represent a severe clinical condition. In addition to those consequent to high energy trauma, there is a growing number of fragility fractures in the elderly population, often regarded as a pandemic disease (Kanis, Oden et al. 2007) for which current risk assessment methods are inadequate (Wilkin and Devendra 2001). Bone fracture is a complex process because inherently multiscale in space and time: at physiological loading rates, the macroscopic failure of a bone segment occurs abruptly through the disruptive propagation of cracks which are microscopic (Hansen, Zioupos et al. 2008); however, the unavoidable presence of cracks in bone tissue (Lee, Mohsin et al. 2003) is not necessarily detrimental to the health of a bone (e.g. it may trigger bone apposition (Prendergast and Taylor 1994)), and the evolution of the cracking process may be slow and discontinuous (Malik, Stover et al. 2003). This paper will focus on the characterization of the disruptive phase of crack propagation in bones. In fact, predictive numerical models of bone at the organ level seem to be the most promising approach to reliably assess skeletal fracture risk (Crawford, Cann et al. 2003; Schileo, Taddei et al. 2008) and evaluate preventive therapies (Cody, Hou et al. 2000; Keaveny, Hoffmann et al. 2008). To develop and validate such models, a thorough characterization of the bone fracture process is necessary.

The biggest quantitative contribution to bone fracture characterization comes from *in-vitro* experiments. So far, a consistent number of tests have been conducted at the macro scale on whole bones, loading them to fracture in a given configuration, and measuring their ultimate load. They managed, when accurately devised, to replicate clinically relevant fracture scenarios (Cristofolini, Juszczuk et al. 2007). Therefore, they established as the gold standard for the validation of models aimed at predicting

bone fracture (Bessho, Ohnishi et al. 2007; Schileo, Taddei et al. 2007); however, a major limitation is the impossibility of identifying the point of fracture onset, which is key information for models validation. An attempt to overcome this limitation was made using high speed videos (Schileo, Taddei et al. 2008), but often frame rates as high as 15000fps are not sufficient to discriminate the point of fracture onset, and a trade-off is necessary between frame rate and spatial resolution. A relevant number of studies have been conducted at the micro-scale, too, producing impressive descriptions of how toughness of bone tissue is achieved (Vashishth, Behiri et al. 1997; Nalla, Stölken et al. 2005; Yang, Cox et al. 2006). However, most of those experiments focused on crack nucleation and crack-growth resistance mechanisms that happen in fatigue conditions and in any case before the development of macroscopic fracture. In addition, those tests were usually conducted in controlled energy release conditions on standardized shape specimens, while real fractures happen on bones of complex geometries, with no bounds on energy release.

In other engineering fields, several techniques have been developed to detect and measure propagating cracks in different engineering fields, but seem not suitable for the characterization of bone fracture. Acoustic sensors were applied to bone to have a gross estimate of thickness and density (Hatakeyama, Yoshizawa et al.) and to crack propagation detection in crystalline materials (Boudet, Ciliberto et al. 1996) but seems unsuitable to detect fracture in an inhomogeneous and irregularly structured material such as bone. Optical sensors performance has been notably increasing for the past few years, and applied to bone (Turner, Erickson et al. 2006) thanks also to the development of digital image correlation techniques (Yao, Wang et al. 2008), but their use in the detection of bone fracture suffers from the same frame rate/resolution limitations above reported for generic high-speed camera. Crack Propagation Sensors (CPS) (Boudet, Ciliberto et al. 1996), that consist of parallel-connected resistor strands mounted on a resin base, and monitor the increase in total resistance as a crack propagates through the underlying structure, present some limitations, too: they are applicable only on flat surfaces (as strain gauges), and are currently available only for a maximum of 20 strands for a length of 40mm (Vishay Crack propagation patterns, Doc.Nr: 11521, www.vishaymg.com). Crack Gauges (CG), whose signal is based on the change in the electrical resistance of a foil when cracking (Boudet, Ciliberto et al. 1996; Guyer and Dauskardt 2004), have been developed mostly for investigating fatigue crack propagation on C(T) specimens defined by ISO. The CG concept seems

adaptable to characterization of bone fracture, but currently CG are applicable only on flat surfaces of regularly shaped specimens, with controlled fracture direction, and at a low sampling rate (i.e. not applicable to brittle materials such as rock (Smirnov 1968)).

Aims of the present study were:

- to develop a crack grid system capable of detecting and measuring crack propagation combining meso-scale spatial resolution (in the order of 1mm) with a very high sampling rate (in the order of 1MHz);
- to preliminarily assess the system performance in the detection of disruptive crack propagation in bone tissue during tissue level (meso-scale) and organ level tests.

2.4.2. Materials

In order to detect initiation of bone fracture, the relevant region of the bone surface was covered with a series of parallel lines of electro-conductive dye (ECD) forming a crack-grid (CG). Such CG-lines must intersect the plane where fracture is expected to occur (however, they do not necessarily need to be perpendicular to the plane of fracture). Disruption of a CG-line indicates that the bone surface was locally fractured. Each line was connected to a custom-designed data-logger capable of detecting loss of conductivity of the line. Accurate identification of the time of disruption of each line enabled detecting the point of fracture initiation.

2.4.2.1 Crack-grid application

The regions of the tested bone, where crack propagation was expected, were prepared with CG-lines. Preliminarily, the bone surface was cleaned (Cristofolini, Juszczak et al. IN PRESS 2009) and spread with cyanoacrylate glue (Super Attak Easy Brush, Henkel Loctite, Zingonia, Italy) to provide a brittle electrically insulating support layer, and enhance adhesion of the ECD dye. A layer of electro conductive dye (EMI35, CRC Industries Europe BVBA, Zele, Belgium) was sprayed on the bone surface. Two applications usually suffice to generate an electro-conductive layer approximately 50 micron thick. To obtain a fine crack-grid (1-mm lines at 1-mm interval), a mask was prepared with masking tape. This procedure enabled depositing the CG also on double-curvature surfaces such as the proximal femur (Fig. 1).

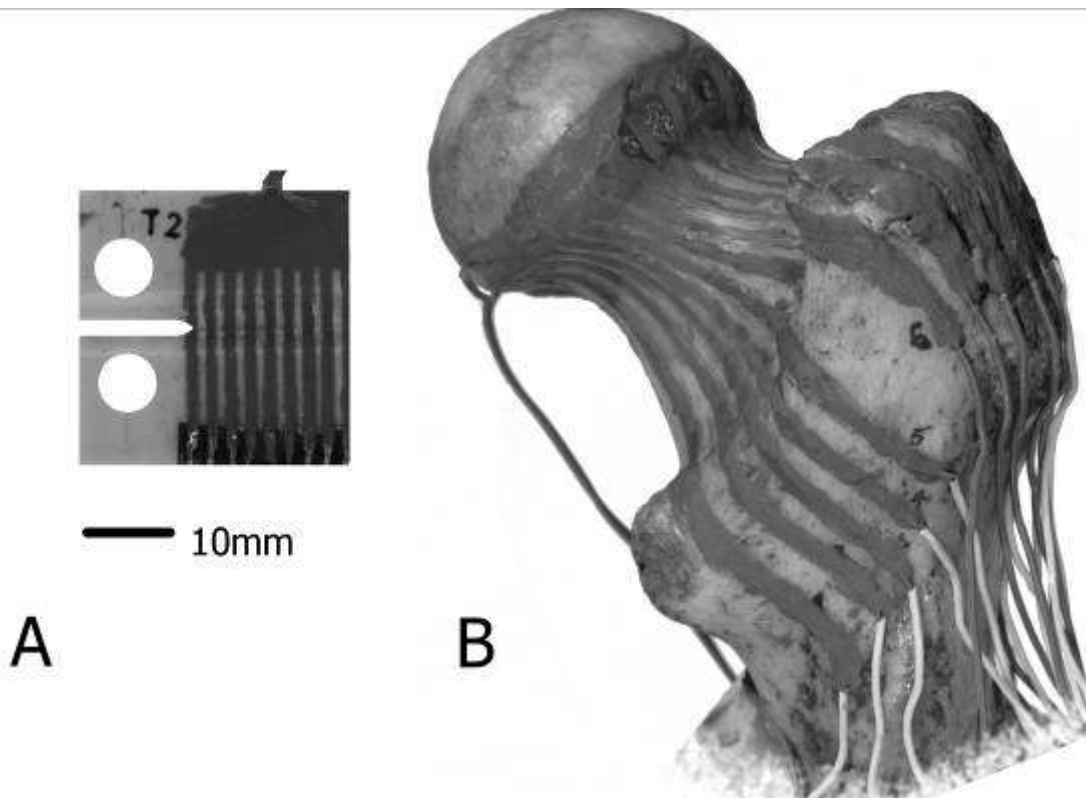


Fig. 1 – (a) Flat compact-tension bone specimen with a fine crack-grid (CG): the lines were 1mm thin, and spaced 1 mm each other. (b) Proximal human femoral metaphysis (lateral-proximal view) with the crack-grid: the lines in the expected region of fracture were approximately 1mm thin, and spaced 1-5 mm each other. The lead wires connecting each line to the data logger are bonded to the two extremities of the CG.

To provide an electrical connection between the CG-lines and the data logger, leadwires were attached to the bone surface and electrically connected using additional ECD.

2.4.2.2 Data logging

To record the time of disruption of each CG-line, a dedicated data logger (Break'O'Meter, BOM) was developed (Fig. 2). It consisted of a self-contained board (MB-128-MAX, MikroBit, Jaworzno, Poland) based on a microcontroller (Atmega-128, Atmel Corporation, San Jose, CA USA), with a 16MHz clock. The BOM included an LCD display, and pushbuttons to trigger the acquisition. To enable synchronization of load-displacement data (from the testing machine) and fracture events, the BOM can be triggered by the digital signal of a testing machine. Recorded data (time of disruption of a CG-line) were stored in non-volatile memory, and were transferred to a PC with the RS232 port of a PC through the TTL/RS232converter included in the board. Alternatively, results stored in the BOM memory can be browsed and displayed without a PC.

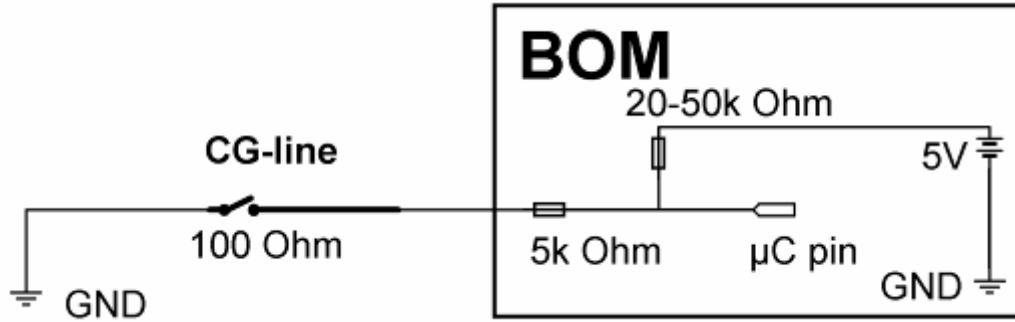


Fig. 2 – Schematic of the Break'O'Meter (BOM) electronics for a single line of the crack-gauge (CG-line).

The BOM was capable of sampling up to 32 CG-lines at a frequency of 700kHz for 8seconds. It detected a line disruption when the resistance exceeded 5kOhm (typical resistance of an intact CG-line: 50-300Ohm, see below).

2.4.3 Electrical testing of the crack-grid

To ensure that a thin CG-line provides adequate (and repeatable) electrical resistance, CG-lines were tested. CG-lines were created on a high-insulation flat surface (polytetrafluoroethylene, PTFE) having a length of 100mm, with different width (1 mm, 3 mm, 5 mm, 3 specimens for each width).

Table 1 – Resistance of crack-gauge lines of different width, and of a 1-mm line at different levels of strain

| CG-line width | Resistance (Ohm) |
|--------------------------|------------------|
| 5 mm - unstretched | 32 ± 1 |
| 3 mm - unstretched | 60 ± 1 |
| 1 mm - unstretched | 120 ± 4 |
| 1 mm - 20000 microstrain | 150 ± 5 |
| 1 mm - 50000 microstrain | 200 ± 10 |

Resistance varied with width (150 Ohm for 1mm width to 40 Ohm for 5mm), but was quite repeatable between specimens (better than 3%, Table 1). Thus, the resistance of the 1mm line was adequate for the specifications of the BOM (disruption detected at 5 kOhm).

2.4.4. Mechanical testing of the crack-grid

2.4.4.1 Methods

As the ECD material is not specifically designed for this purpose, before using the CG to investigate bone fracture, it was necessary ensure that: (i) the ECD does not fail nor significantly alter its conductivity in the strain range spanned by bone tissue; (ii) it will develops a brittle fracture, following the bone surface crack, creating a gap immediately

Healthy human bone fails in a brittle way when principal tensile strain exceeds 7000-12000microstrain (Currey 2001; Bayraktar, Morgan et al. 2004). To assess the maximum strain supported by the CG material without failure, dog-bone shaped specimens were machined out of PTFE (5 mm x 5 mm cross-section; 40mm gauge length). A CG-line (1mm wide) was created along the gauge length of each specimen. The specimens were stretched with a monotonic ramp of 1mm/sec on a material testing machine (Mod.8502, Instron-Corp., Canton, MA, USA) with an extensometer (Mod. 2620-601, Instron Corp., Canton, MA, USA) up to 50000microstrain (Fig. 3). Six such specimens were prepared and tested.

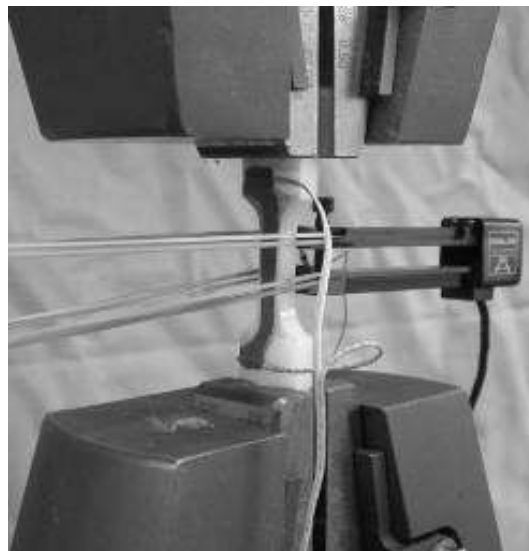


Fig. 3 – PTFE dog-bone specimen with a single CG-line (dark) along the gauge length. The specimen is clamped on the material testing machine. The extensometer (with rubber bands to hold it in position) monitoring the specimen strain is visible on the right.

To verify that the CG material fails in a brittle way when a crack opens in the underlying material, a setup was created to create a controlled gap opening. This enabled measuring the minimal gap needed to disrupt a CG-line. The setup consisted of a glass plate (microscope slide) fractured along a straight line: the two fragments

were brought in contact so that the edges matched perfectly. One half of the broken glass plate was fixed to the load cell of the testing machine, the counterpart to the actuator of the testing machine in a way that the broken parts matched one another, and the line of fracture was perpendicular to the actuator. The reassembled glass was preloaded with 10N to provide end-to-end contact. Three CG-lines were created on the glass construct once reassembled and preloaded. The extensometer was mounted across the reassembled crack on the glass plate, so as to measure the gap aperture (Fig. 4). A relatively slow (0.2mm/sec) monotonic ramp of was applied to ensure clear data acquisition. Four such specimens were prepared and tested.

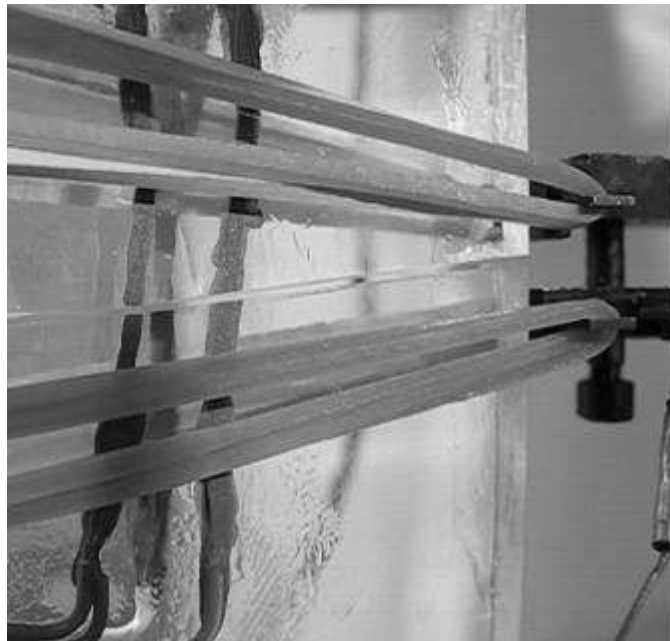


Fig. 4 – Glass plate used to measure the minimal gap to cause a disruption of the CG lines. The horizontal fracture is visible in the centre, after the two fragments were pulled 0.5 mm apart. Three CG-lines (dark, two on the front side of the glass, one on the opposite side) were prepared vertically crossing the pre-fracture interface. The specimen is clamped on the material testing machine. The arms of the extensometer (with rubber bands to hold it in position) monitoring gap opening is visible on the right. To continuously monitor the variation of resistance of the CG, the CG-lines were connected to a scanner (System 6000, Vishay Intertechnology Inc., Malvern, PA USA) acquiring synchronously (10 kHz) the CG-signals as well as the signals from the transducers of the Instron.

2.4.4.2 Results

The CG-lines applied to the PTFE dog-bone specimens kept conducting up to 50000 microstrain. The resistance increased by <20% at 10000 microstrain (typical bone-

breaking strain), and by <60% at 50000 microstrain (Table 1). Such values are below the threshold where the BOM detects a line disruption (5 kOhm). Therefore, there is no risk that a false disruption is recorded while the bone strains before failure.

The gap opening at which the CG-lines were disrupted was 30 micron. It is possible that the CG-line actually was disrupted at a narrower gap, but the resolution of the system used did not enable a more accurate estimate.

2.4.5 Testing of the crack-gauge on simplified bone specimens

2.4.5.1 Methods

To test the applicability of the crack-gauge method on real bone, first simplified bone specimens were prepared. This enabled checking:

- Whether the CG material could be applied on bone tissue;
- Whether the CG-lines suffer any damage by being submerged into saline solution (this is necessary to correctly preserve bone tissue);
- The ability of this method to monitor crack propagation in bone.

For ethical reasons, in this preliminary phase bovine bone was used. It has been shown that properties of bovine and human bone are comparable (Fung 1980; Norman, Vashishth et al. 1995; Currey 2001; Ritchie, Kinney et al. 2006). In order to control direction of the crack propagation, miniaturized compact tension specimens were cut from the cortical bone of the diaphysis of adult bovine femurs. Specimens (28mm x 28mm x 5mm) were scaled from the geometry recommended in the ASTM E561 standard, similarly to (Behiri and Bonfield 1989; Norman, Vashishth et al. 1992; Malik, Gibeling et al. 2002; Malik, Stover et al. 2003). Two samples were prepared (Fig. 5): longitudinal (tensile stress acted perpendicular to the osteons, i.e. in a circumferential direction respect to the original bone: expected fracture lied parallel to the osteons), and transversal (tensile stress acted parallel to the osteons, i.e. in the axial direction respect to the original bone: expected fracture crossed the osteons). As bone is strongly anisotropic, to drive the crack propagation in the correct direction specimens were crafted with side grooves similar to (Behiri and Bonfield 1989; Norman, Vashishth et al. 1992; Malik, Gibeling et al. 2002; Malik, Stover et al. 2003). Such grooves were wide and rounded (to reduce stress concentration) and aimed at reducing the specimen thickness in the fracture region.



Fig. 5 – Schematic depicting the alignment of the two types of compact tension specimens extracted from the diaphysis of bovine femurs: transversal (T) and longitudinal (L).

On each specimen, nine CG-lines were prepared (1mm wide, spaced by 1mm) perpendicular to the expected crack (Fig. 6). Four such specimens for each type were prepared and tested.

We wanted to ensure that fracture would propagate, driven by initially accumulated energy. To ensure this, the specimens were loaded at a constant speed. The maximum actuator rate for the testing machine (858-MiniBionix, MTS, Minneapolis, MN, USA) used for this experiment was 150mm/s. To allow the actuator to reach its maximum speed before it pulled the specimen, the loading setup allowed a “mechanical play” of 3 mm.

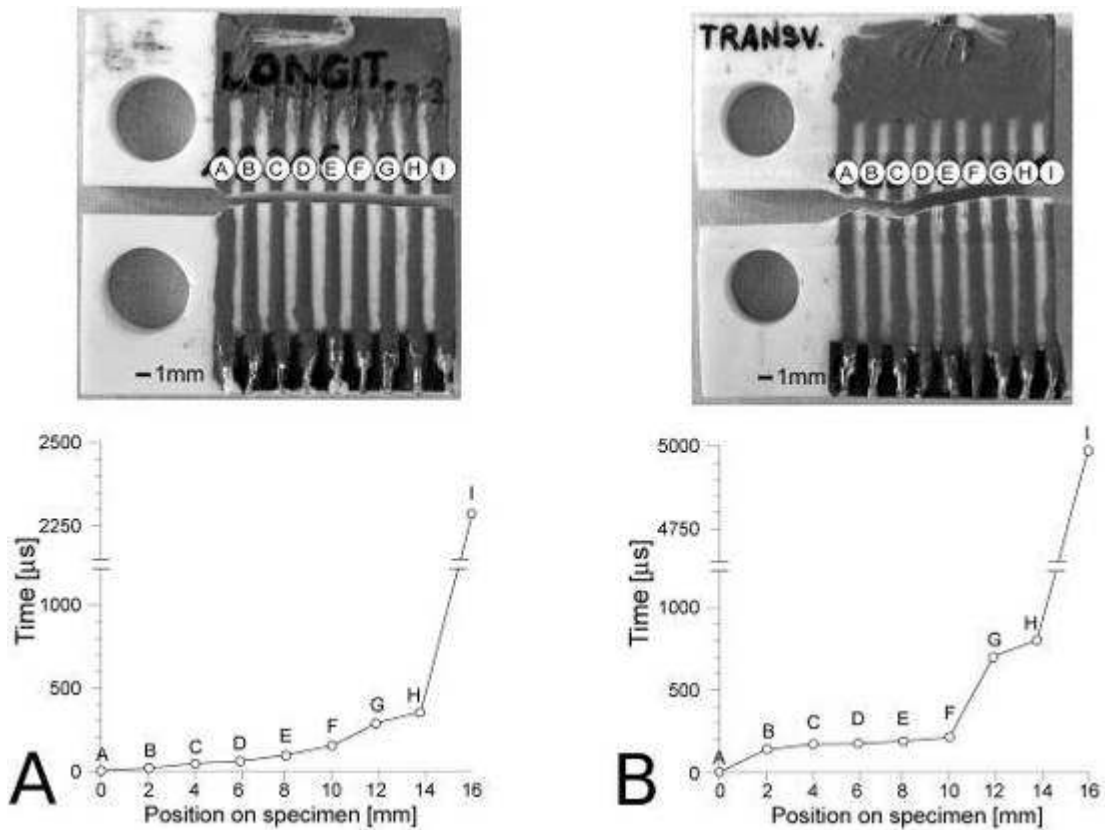


Fig. 6 – Compact tension specimens obtained in the longitudinal (left) and transversal (right) directions. Nine CG-lines were prepared on each specimen (A to I). The graphs indicate the time at which each line failed.

2.4.5.2 Results

The times of disruption of the CG-lines were successfully recorded for all specimens. Recorded times were in the expected sequence, the first line failing being closest to the notch tip, and the last one at the opposite extremity (Fig. 6). Moreover, a pronounced difference existed between the longitudinal and transversal specimens in terms of crack propagation velocity (Table 2): the crack propagated generally faster in the transversal specimens than in the longitudinal ones. The velocity was more uniform across each longitudinal specimen, while it fluctuated in the transversal ones. This is in agreement with the observed anisotropy of cortical bone (Fung 1980; Currey 2001).

Table 2 – Estimate of the crack propagation velocity for the longitudinal and transversal compact tension specimens: average velocity was computed between the 1st and 8th CG-line. Velocity was

estimated based on the distance and the time span between the 1st and the 8th CG-line. The 9th line was not included because the velocity decreased significantly, probably because of a plastic hinge forming at the end of the crack propagation.

| CG-line width | Distance 1 st – 8 th CG-line (mm) | Time spanned 1 st – 8 th CG-line (microseconds) | Average velocity (m/sec) |
|---------------|---|---|--------------------------|
| Longitudinal | 16mm | 687 ± 127 | 23.3 ± 12.6 |
| Transversal | 16mm | 248 ± 237 | 64.5 ± 67.4 |

2.4.6 Testing of the crack-gauge on femoral metaphyses

2.4.6.1 Methods

To assess the suitability of the proposed technique to investigate fracture of real bone, the proximal human femoral metaphysis was chosen as an exemplification. In fact: (i) fractures of the proximal human femur are one of the most common types of fracture (Rockwood, Green et al. 1991; Rüedi and Murphy 2001), and life-threatening for the elderly (WHO 1994); (ii) they are extremely important also for the possible risks associated with contemporary hip resurfacing prostheses (Amstutz, Campbell et al. 2004; Shimmin and Back 2005; Spierings and Derler 2005; Murray, Little et al. 2007). Three human cadaveric femurs with low radiographic density were chosen, to represent elderly subjects possibly undergoing femoral neck fractures (Jeffery 1974; Rockwood, Green et al. 1991; Rüedi and Murphy 2001). Each femur was prepared with a crack-grid (Fig. 1). The CG-lines were directed along the femoral neck axis (i.e. perpendicular to the expected plane of fracture (Rockwood, Green et al. 1991; Rüedi and Murphy 2001)). The circumference of the neck in the narrowest section was on average 80mm. This enabled preparing each specimen with 18-20 CG-lines (actual number depended on the specimen's anatomy), corresponding to a spatial resolution of 2-4 mm (lines were not parallel) in the region where fracture was expected.

The femurs were tested to failure following a validated protocol (Cristofolini, Juszczak et al. 2007), which enabled replicating *in vitro* the spontaneous fractures of the proximal metaphysis. Spontaneous fractures derive from physiological or para-physiological loading (e.g. sudden muscle contraction due to stumbling or misstepping), but not from a traumatic event (spontaneous fractures may result in secondary trauma, but they are not caused by trauma)(Jeffery 1974; Rockwood, Green et al. 1991; Rüedi and Murphy 2001). The femurs were rigidly constrained distally

while a load was applied to the femoral head. The femurs were mounted on the testing machine (Mod.8502, Instron-Corp., Canton, MA, USA) with the diaphysis at an angle of 8° in the frontal plane. Load was applied to the femoral head through a system of rails to avoid transmission of horizontal force components (Fig. 7). A copy of each femoral head was prepared with dental cement (covering 1/5 head diameter) to allow uniform load transfer from the actuator to the head. The actuator moved at 30mm/sec: this caused bone failure in typically 0.2seconds.

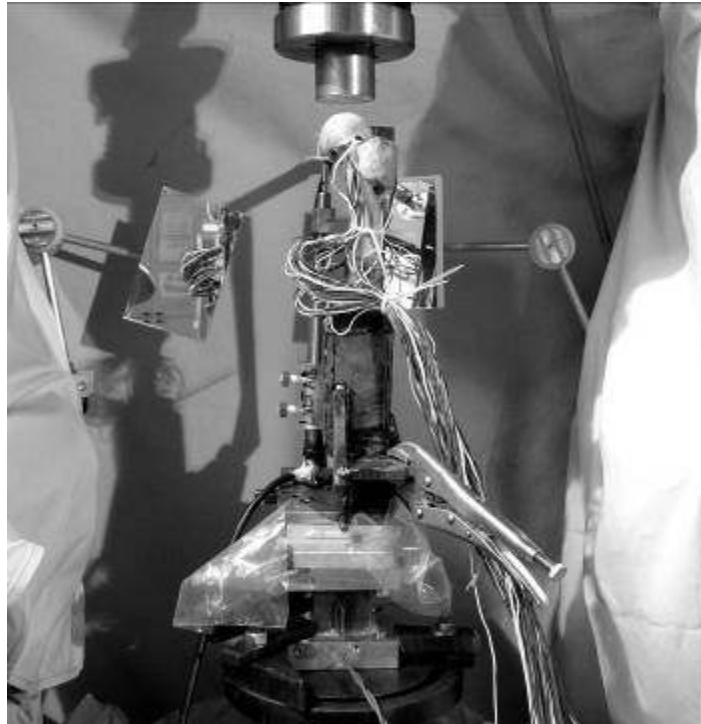


Fig. 7 –Experimental setup used to fracture the proximal femurs *in vitro* (Cristofolini, Juszczuk et al. 2007): the intact femur was mounted on the material testing machine with the diaphysis at 8° from vertical; the cross-rails to eliminate horizontal force components are visible on the top; the two mirrors are visible near the femur (they were oriented so as to reflect the anterior-medial and posterior-medial sides of the femur).

2.4.6.2 Results

All femurs fractured in the expected region (Fig. 8), in a way that was consistent with past *in vitro* experience (Cristofolini, Juszczuk et al. 2007), and with clinically relevant fractures (Jeffery 1974; Rockwood, Green et al. 1991; Rüedi and Murphy 2001). The pattern was quite consistent in all specimens: fracture started in a point on the lateral region. A delay was always observed between failure of the first CG-line, and failure of the subsequent ones, possibly associated with the stress release due to the initial failure. Then the crack propagated at comparable rates on the anterior and posterior sides of the neck. The total time for the entire fracture to occur as recorded by the

crack-grid was compatible with previous observations using high-speed cameras (Cristofolini, Juszcyk et al. 2007).

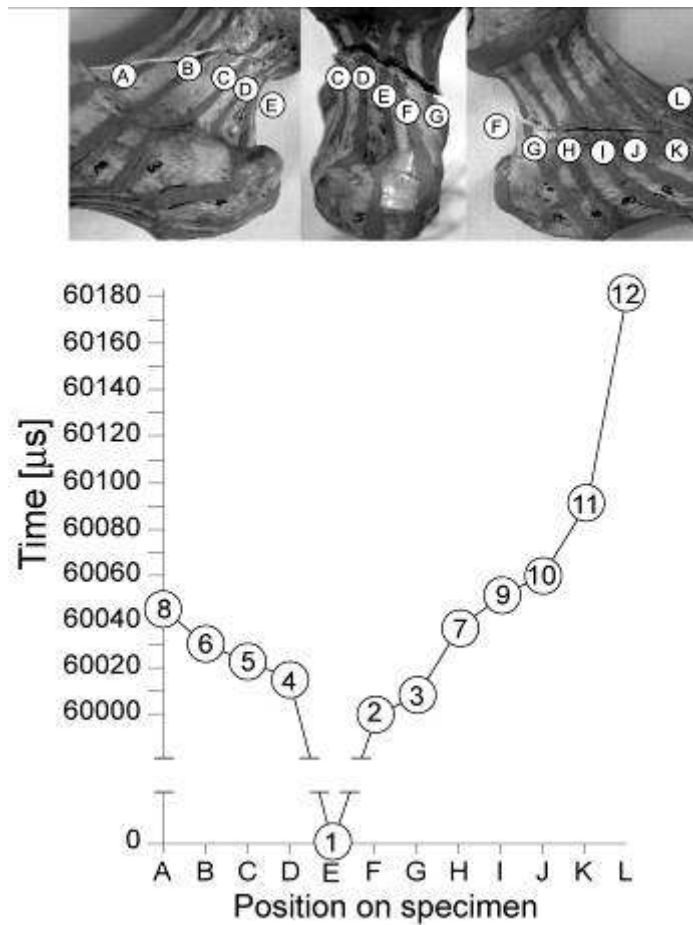


Fig. 8 – Human femur after *in vitro* induced fracture. On top, the anterior, proximal and posterior views of the proximal metaphysis are visible. The CG-lines are labeled with letters. The graph below indicates the time when each CG-line was disrupted. Points are numbered in the same sequence as CG-lines failed: CG-line “E” was the first CG-line to fail. This means, that fracture initiation was comprised within CG-lines D and F.

2.4.7 Discussion

Although the technique proposed seems very promising, there are some limitations that must be addressed. First of all, the spatial resolution of the current technique is of the order of one millimeter. This is comparable to the spatial resolution achieved with other techniques on real bones (e.g.: using contemporary high-speed cameras a pixel size of 0.2-0.5mm was attained – but at a much lower sampling frequency (Cristofolini, Juszcyk et al. 2007)). Commercial devices such as Crack Propagation Pattern (TK-09-CPD01-NRA/DP, Vishay), provide a better resolution (1.27mm).

However, while this CG can only be applied to flat surfaces, the proposed crack-grid can be applied to any geometry, including double-curvature surfaces of bones. It is possible that with some more technical effort the spatial resolution of the proposed crack-grid can be brought down to 0.5mm.

Secondly, the current sampling frequency (700kHz) is relatively high (state-of-the-art high-speed movies do not exceed 15kHz in these applications (Cristofolini, Juszczak et al. 2007)). A frequency of 700kHz is obviously much faster than most mechanical events. The current version was based on inexpensive components. If, for some reason, this scanning frequency is not sufficient, a faster system can be assembled based on more performing electronics.

Third, it is important to remember that the ECD material was not originally designed for this type of application. While extensive validation was carried out for monotonic loading, the properties of this ECD material for a cyclic load have not been characterized.

Fourth, preparation of the CG-lines requires a significant amount of manual work. The entire process for preparing a crack-grid on the bone specimens described above involved approximately 2 hours of a skilled operator. This obviously represents a cost. This is also a source of variation if more specimens are to be prepared. It is worth remarking that when bones are investigated, the irregular anatomy makes it necessary in all cases to acquire the actual position of the constraints, sensors etc using a digitizer. Therefore, this does not necessarily represent a problem. On the other hand, the manual preparation of the crack-grid enables adapting the geometry of the crack-grid to each specimen, considering anatomical details, surface defects and possible regions of high interest.

Acknowledgments

The Authors wish to thank Lorenzo Zani for the technical support; Luigi Lena for the artwork.

Conflict of interest statement

There is no potential conflict of interest: none of the Authors received or will receive direct or indirect benefits from third parties for the performance of this study. Istituto Ortopedico Rizzoli was partially funded by the European Community for the performance of this study (project number: IST-2004-026932; title: Living Human Digital Library; acronym: LHDL).

2.4.8 References

- Amstutz, H. C., P. A. Campbell, et al. (2004). "Fracture of the neck of the femur after surface arthroplasty of the hip." *J. Bone Jt. Surg. Am.* 86: 1874-1877.
- Bayraktar, H. H., E. F. Morgan, et al. (2004). "Comparison of the elastic and yield properties of human femoral trabecular and cortical bone tissue." *J Biomech* 37(1): 27-35.
- Behiri, J. C. and W. Bonfield (1989). "Orientation dependence of the fracture mechanics of cortical bone." *J Biomech* 22(8-9): 863-72.
- Bessho, M., I. Ohnishi, et al. (2007). "Prediction of strength and strain of the proximal femur by a CT-based finite element method." *J Biomech* 40(8): 1745-53.
- Boudet, J. F., S. Ciliberto, et al. (1996). "Dynamics of Crack Propagation in Brittle Materials." *J Phys* 6(10): 1493-1516.
- Cody, D. D., F. J. Hou, et al. (2000). "Short term in vivo precision of proximal femoral finite element modeling." *Ann Biomed Eng* 28(4): 408-14.
- Crawford, R. P., C. E. Cann, et al. (2003). "Finite element models predict in vitro vertebral body compressive strength better than quantitative computed tomography." *Bone* 33(4): 744-50.
- Cristofolini, L., M. Juszczak, et al. (2007). "In vitro replication of spontaneous fractures of the proximal human femur." *Journal of Biomechanics* 40(13): 2837-2845.
- Cristofolini, L., M. Juszczak, et al. (IN PRESS 2009). "Strain distribution in the proximal human femoral metaphysis." *Proc Inst Mech Eng [H]* 223.
- Currey, J. D. (2001). "Bone Strength: What are We Trying to Measure?" *Calcified Tissue International* 68(4): 205-210.
- Fung, Y. C. (1980). *Bone and cartilage. Biomechanics - Mechanical properties of living tissues.* New York, Springer Verlag: 383-415.
- Guyer, E. P. and R. H. Dauskardt (2004). "Electrical technique for monitoring crack growth in thin-film fracture mechanics specimens." *J. Mater. Res.*
- Hansen, U., P. Zioupos, et al. (2008). "The effect of strain rate on the mechanical properties of human cortical bone." *J Biomech Eng* 130(1): 011011.
- Hatakeyama, R., M. Yoshizawa, et al. "A Method for the Measurement of Acoustic Impedance and Speed of Sound in a Small Region of Bone using a Fused Quartz Rod as a Transmission Line." *Japanese Journal of Applied Physics* 39(Part 1, No. 11): 6449.
- Jeffery, C. C. (1974). "Spontaneous fractures of the femoral neck." *Orthop Clin North Am* 5(4): 713-727.
- Kanis, J. A., A. Oden, et al. (2007). "The use of clinical risk factors enhances the performance of BMD in the prediction of hip and osteoporotic fractures in men and women." *Osteoporos Int* 18(8): 1033-46.
- Keaveny, T. M., P. F. Hoffmann, et al. (2008). "Femoral bone strength and its relation to cortical and trabecular changes after treatment with PTH, alendronate, and their combination as assessed by finite element analysis of quantitative CT scans." *J Bone Miner Res* 23(12): 1974-82.

- Lee, T. C., S. Mohsin, et al. (2003). "Detecting microdamage in bone." *J Anat* 203(2): 161-72.
- Malik, C. L., J. C. Gibeling, et al. (2002). "Compliance calibration for fracture testing of equine cortical bone." *J Biomech* 35(5): 701-5.
- Malik, C. L., S. M. Stover, et al. (2003). "Equine cortical bone exhibits rising R-curve fracture mechanics." *J Biomech* 36(2): 191-8.
- Murray, D. W., J. P. Little, et al. (2007). Femoral neck fractures following resurfacing. IMechE Conference: Engineers & Surgeons: joined at the hip, London, Institutions of Mechanical Engineers.
- Nalla, R. K., J. S. Stölken, et al. (2005). "Fracture in human cortical bone: local fracture criteria and toughening mechanisms." *Journal of Biomechanics* 38(7): 1517-1525.
- Norman, T. L., D. Vashishth, et al. (1992). "Effect of groove on bone fracture toughness." *J Biomech* 25(12): 1489-92.
- Norman, T. L., D. Vashishth, et al. (1995). "Fracture toughness of human bone under tension." *J Biomech* 28(3): 309-20.
- Prendergast, P. J. and D. Taylor (1994). "Prediction of bone adaptation using damage accumulation." *J Biomech* 27(8): 1067-76.
- Ritchie, R. O., J. H. Kinney, et al. (2006). Cortical Bone Fracture. Wiley Encyclopedia of Biomedical Engineering. e. Metin Akay.
- Rockwood, C. A. J., D. P. Green, et al. (1991). Rockwood and Green's fractures in adults. Philadelphia, J.B. Lippincott.
- Rüedi, T. P. and W. M. Murphy (2001). AO principles of fracture management. Stuttgart, Georg Thieme Verlag.
- Schileo, E., F. Taddei, et al. (2008). "Subject-specific finite element models implementing a maximum principal strain criterion are able to estimate failure risk and fracture location on human femurs tested in vitro." *J Biomech* 41(2): 356-67.
- Schileo, E., F. Taddei, et al. (2007). "Subject-specific finite element models can accurately predict strain levels in long bones." *J Biomech* 40(13): 2982-9.
- Shimmin, A. J. and D. Back (2005). "Femoral neck fractures following Birmingham hip resurfacing. A national review of 50 cases." *J Bone Joint Surg Br.* 87-B(3): 463-464.
- Smirnov, V. (1968). "A method of measuring the crack propagation velocity in a rock specimen under impact load." *Journal of Mining Science* 4(3): 260-263.
- Spierings, A. B. and S. Derler (2005). "Assessment of hip protectors and corresponding hip fracture risk using stress calculation in the femoral neck." *Med. Eng. Phys.* IN PRESS: IN PRESS.
- Turner, P. J., B. Erickson, et al. (2006). "High-speed photography of the development of microdamage in trabecular bone during compression." *J Mater Res* 21(5): 1093-1100
- Vashishth, D., J. C. Behiri, et al. (1997). "Crack growth resistance in cortical bone: concept of microcrack toughening." *J Biomech* 30(8): 763-9.

- WHO (1994). Assessment of fracture risk and its application to screening for postmenopausal osteoporosis. Report of a WHO study group. WHO Technical Report Series, World Health Organization, Geneva, Switzerland, 843: 1-130.
- Wilkin, T. J. and D. Devendra (2001). "Bone densitometry is not a good predictor of hip fracture." *Bmj* 323(7316): 795-7.
- Yang, Q. D., B. N. Cox, et al. (2006). "Fracture length scales in human cortical bone: the necessity of nonlinear fracture models." *Biomaterials* 27(9): 2095-113.
- Yao, X., P. Wang, et al. (2008). "Experimental study of damage and fracture of cancellous bone using a digital speckle correlation method." *J Biomed Opt* 13(3): 034026.

3 GENERAL BIOMECHANICAL CHARACTERIZATION OF LONG BONES

3.1 LHDL related data acquisition

The Living Human Digital Library research project involved a massive data collection activity, aimed to the creation of the most detailed single-subject collection on biomechanical and anatomo-functional data of the musculoskeletal system. The various methods used in this huge endeavour were documented in detail in a collection of brief technical notes that are now publicly available.

This chapter summaries work done so far at the organ level. Brief description of type of data collected; procedures for handling specimens and data acquisition and list of bone segments tested, is given here.

The detailed description of the methods used for the data collection, is progressively shared by the involved institutions with the rest of the worldwide research community through the Physiome Space service that emerged from the LHDL project.

(www.livinghuman.org , www.biomedtown.org)

Six human long bone segments underwent biomechanical mechanical investigation. Each one was tested in elastic and to failure range with respect to the physiologically most relevant ways (see Table1).

Table 1 Test performed on each bone segment

| BONE SEGMENT | NON DISTRUCTIVE TESTING | TEST TO FAILURE |
|---------------------|--------------------------------|--|
| RADIUS | 4PB / TORSION | 4PB |
| ULNA | 4PB / TORSION | 4PB |
| HUMERUS | 4PB / TORSION | TORSION |
| FEMUR | 4PB / TORSION | SPECIFIC STUDY ON PROSIMAL METAPHYSIS |
| TIBIA | 4PB / TORSION | SPECIFIC STUDY OVER PHISIOLOGICAL FUNCTION AND ANATOMICAL MORPHOLOGY |
| FIBULA | 4PB / TORSION | 4PB |

3.1.1 Whole-bone stiffness

Specimens: The following long bones were fully characterized to assess the whole-bone stiffness: femur, tibia, fibula, first to fifth metatarsal bones. Both right and left limb from the first donor were examined.

Loading configurations: The following loading scenarios were applied:

- Four point bending: the diaphysis was bent by using a four roller configuration in the following directions (Figure 1):
 - Sagittal plane, causing tension on the anterior side
 - Sagittal plane, causing tension on the posterior side
 - Frontal plane, causing tension on the medial side
 - Frontal plane, causing tension on the lateral side

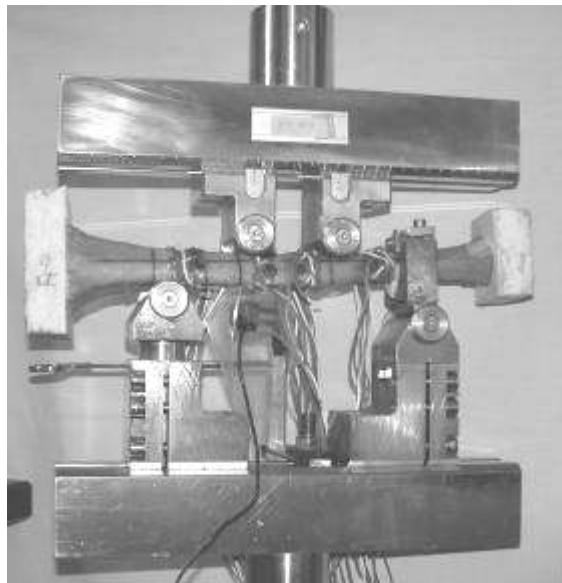


Fig 1. Four point bending of the tibia.

- Torsion about the long axis of the diaphysis was applied by means of pots that clamped the bone extremities:
 - Torque towards intra-rotation of the foot
 - Torque towards extra-rotation of the foot
- In addition, the femur underwent six additional load cases where the femur was tilted by different angles with respect to the vertical while a force was applied

to the femoral head. A constraint was applied so that only the proximal third of the femur was exposed to load.

Measured quantities: Stiffness test consisted in applying loading while deflection was measured by means of high precision displacement transducers.

Applied loads: To prevent tissue damage due to repeated loading, a load equal to 10% of the estimated failure load was applied for each loading configuration.

Loading rate: Load was applied at two loading rates. The highest loading rate was calculated so as to induce a strain rate that would bring the bone to failure in 0.1-0.3 seconds. The lowest loading rate was 10 times lower.

Repetitions: each non destructive loading scenario and loading rate was applied 5 times on each bone

3.1.2 Strain distribution in whole bones

While the whole-bone stiffness was assessed, strain on the bone surface was measured. Strain was measured for all the loading scenarios indicated above.

Strain measurement: triaxial stacked strain rosettes were used. This type of transducer allows measuring all components of surface strain and their direction, even in regions with high strain gradients. Suitable procedures were used to bond the strain gauges to the bone surface without compromising tissue preservation or sensor insulation (Fig 2).

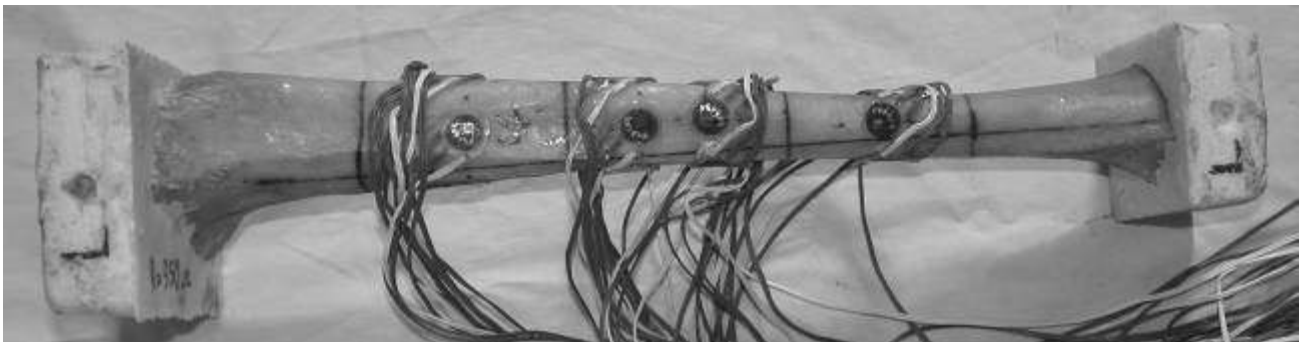


Fig 2. Tibia with triaxial rosettes.

Strain measurement locations: the position of the strain gauges was designed so as to enable sampling the strain distribution in the most relevant regions. The different bones were mapped as follows:

- Femur (four point bending and torsion tests): 12 strain gauges placed around the diaphysis at 3 equally spaced levels
- Femur (six loading directions on the femoral head): 13 strain gauges placed around the head, neck and diaphysis at 3 levels
- Tibia (four point bending and torsion tests): 15 strain gauges placed around the diaphysis at 4 equally spaced levels
- Fibula (four point bending and torsion tests): 8 strain gauges placed around the diaphysis at 4 equally spaced levels

3.1.3 Whole-bone strength

After completion of the stiffness and strain measurement, bone strength was assessed by applying a load ramp until specimen failed.

Loading configurations: The following loading scenarios were applied:

- Femur: load on the femoral head (8° in the frontal plane)
- Tibia: four point bending
- Fibula: four point bending
- Metatarsal bones: torsion

Measured quantities: Load and displacement were acquired during the test, together with strain from the strain gauges (sampling rate 2kHz). High speed videos (10000 frames per second) were recorded for selected specimens to identify the point of fracture initiation. Selected specimens were instrumented with a dedicated proprietary sensor to identify the point of fracture initiation.

Loading rate: Load was applied at the highest loading rate used in the stiffness measurement tests.

This was calculated so as to induce a strain rate that would bring the bone to failure in 0.1-0.3 seconds.

Repetitions: because of the destructive nature of these tests, each specimen could be tested only once.

3.2 STRUCTURAL BEHAVIOUR OF THE LONG BONES OF THE HUMAN LOWER LIMBS

Luca Cristofolini, PhD^{1,2}, Giorgia Conti, MEng^{1,2}, Mateusz Juszczak, MEng^{1,2},
PhD¹, Sara Cremonini MSc¹, Marco Viceconti, PhD¹

¹Laboratorio di Tecnologia Medica, Istituto Ortopedico Rizzoli, Bologna, Italy

²Engineering Faculty, University of Bologna, Italy

Submitted: *J. Biomechanics*

3.2.1 INTRODUCTION

Aim of the present study was:

- Assess the stiffness and strain distributions of the different low limb bones from the same donors;
- Assess if there is any significant effect of viscoelasticity on the strain values within a physiological range of strain rates;
- Assess if the structure and the material properties cause any difference in the behavior in relation to the direction of the applied load, especially considering opposite directions of bending and torsion.

3.2.2 MATERIALS AND METHODS

3.2.2.1 Design of the experiment

The structural stiffness and strain distribution of the long bones of the lower limb were assessed: the proximal metaphysis and the diaphysis of the femur, and the diaphysis of the tibia and fibula were investigated.

3.2.2.2 Specimens

Bone specimens were obtained from two donors who did not suffer from cancer nor musculoskeletal diseases (Table 1). Bone specimens were embalmed following a validated procedure (Ohman, Dall'Ara et al. 2008). Tissue hydration was constantly preserved using moistened cloths. All bone segments (12 in total) were inspected and CT-scanned to exclude fractures or any other defect. Anatomical reference frames were marked on each bone ((Ruff and Hayes 1983; Cristofolini 1997) for the femur; (Conti, Cristofolini et al. 2008) for the tibia and fibula). Anatomical dimensions were measured according to ((Ruff and Hayes 1983), Table 1).

Table 1 – In the first columns the details of the donors are reported. In the following columns the anatomical details of the bone specimens analyzed are reported. The diameter of the head of the femur was measured five times along different directions; the average head diameter, HD, was computed as in (Cristofolini, Juszczak et al. IN PRESS). The ‘biomechanical length’ of the femur (BLF, see also Fig. 2) was defined as in (Ruff and

Hayes 1983); the ‘biomechanical length’ of the tibia and fibula (BLT, see also Fig. 3) was defined as in (Conti, Cristofolini et al. 2008).

| | Age at death (years) | Donors' height (cm) | Donors' Body Weight, BW (kg) | Body Mass Index, BMI (kg/m ²) | Gender | FEMUR | | | | TIBIA AND FIBULA | |
|-----------------|----------------------|---------------------|------------------------------|---|--------|------------------------|------|--------------------------------|------|--------------------------------|------|
| | | | | | | Head Diameter, HD (mm) | | Biomechanical Length, BLF (mm) | | Biomechanical Length, BLT (mm) | |
| | | | | | | Right | Left | Right | Left | Right | Left |
| Donor #1 | 72 | 165 | 63 | 23.1 | female | 47.5 | 47.5 | 427 | 427 | 362 | 364 |
| Donor #2 | 72 | 171 | 64 | 21.9 | female | 46.5 | 47.8 | 415 | 412 | 351 | 346 |

3.2.2.3 Strain measurement

Each bone segment was instrumented with triaxial-stacked strain gauges following a validated procedure (Viceconti, Toni et al. 1992; Cristofolini, Juszczuk et al. IN PRESS):

- Proximal femoral metaphysis: 16 strain gauges (KFG-1-120-D17-23L3M2S, Kyowa, Tokyo, Japan, grid length=1mm) (Fig. 1) (Cristofolini, Juszczuk et al. IN PRESS);
- Femoral diaphysis: 16 strain gauges (KFW-2-350-D17-23L2M2S, Kyowa, grid length=2mm) (Fig. 2);
- Tibial diaphysis: 15 strain gauges (KFW-2-350-D17-23L2M2S, Kyowa, grid length=2mm) (Fig. 3);
- Fibular diaphysis: 8 strain gauges (KFG-1-120-D17-23L3M2S, Kyowa, grid length=1mm) (Fig. 4).

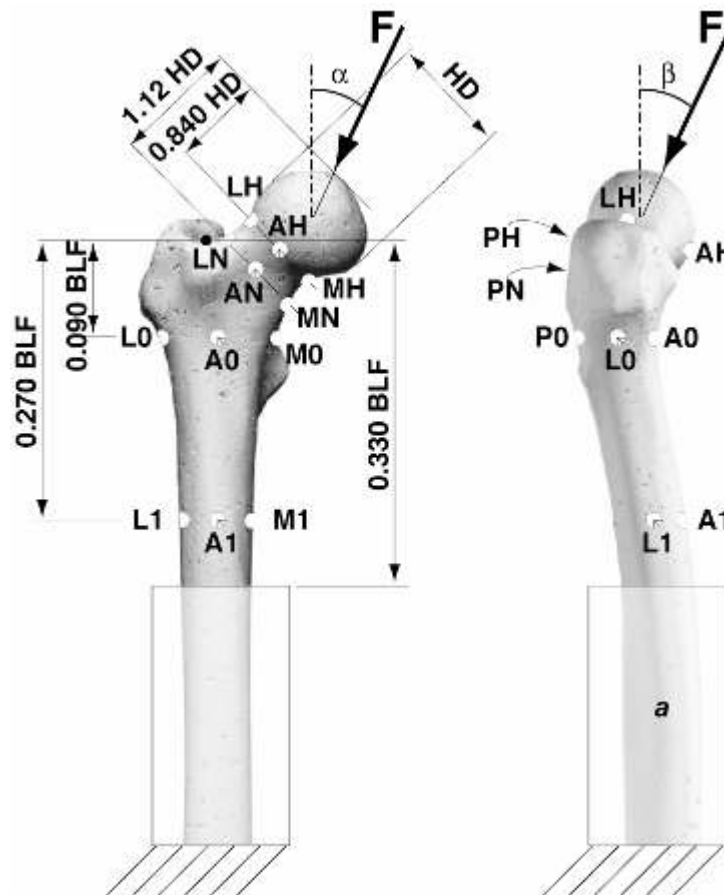


Fig. 1 – Anterior and lateral views of the proximal metaphysis of a right femur. The position of the strain gauges is reported: 4 around the head, close to the articular cartilage (AH, LH, PH, MH); 4 around the neck, distal to the previous ones (AN, LN, PN, MN); 4 around the proximal diaphysis, just below the lesser trochanter (A0, L0, P0, M0); 4 around the proximal part of diaphysis (A1, L1, P1, M1: they were the same as in the femoral diaphysis, Fig. 2). To enable scaling between specimens, all lengths were defined as a fraction of the head diameter (HD) or of the biomechanical length of the femur (BLF). The femur was held distally using a pot made of acrylic bone cement (a). The pot could be tilted so that the hip joint resultant force (F) was applied at the prescribed angles in the frontal plane (α), and in the sagittal plane (β), as in (Cristofolini, Juszczuk et al. IN PRESS).

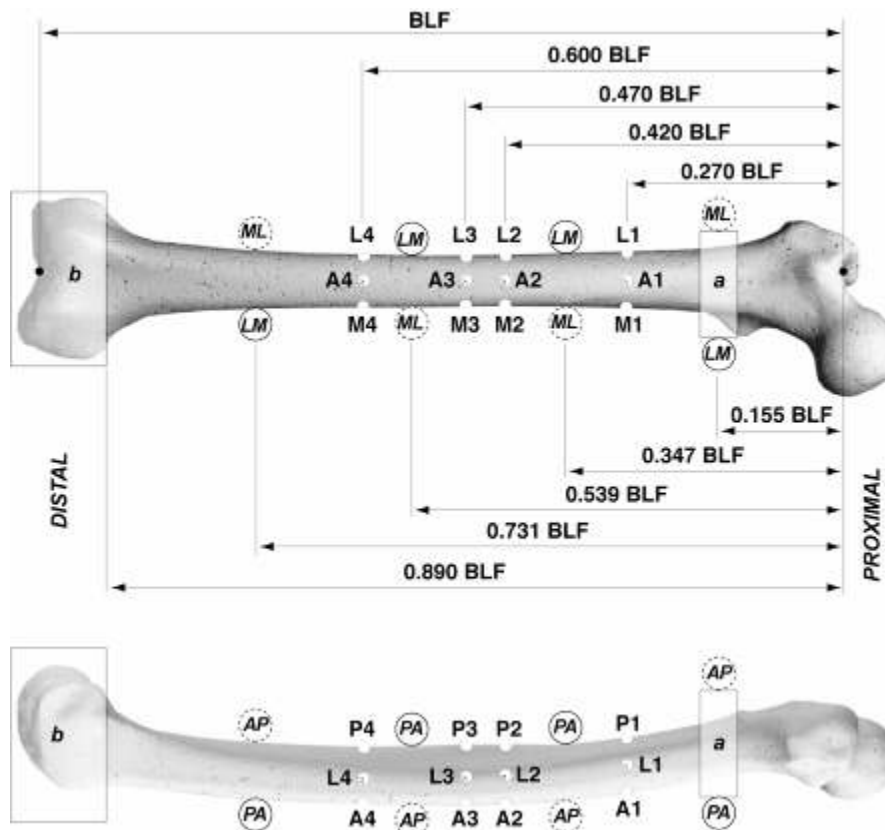


Fig. 2 – Anterior and lateral views of a right femur. The position of the strain gauges is reported: 4 at each of 4 levels, on the Anterior, Lateral, Medial and Posterior sides (gauges A1, L1, P1, M1 were the same as in the proximal femoral metaphysis, Fig. 1). To enable scaling between specimens, all lengths were defined as a fraction of the biomechanical length of the femur (BLF). The torsional load was applied by means of proximal (a) and distal (b) pots made of acrylic bone cement. Also indicated is the position of the rollers to apply four-point-bending in the different directions (Table 2): rollers (LM) acted in a frontal plane generating tension on the medial side; rollers (ML) generated tension on the lateral side; rollers (PA) acted in a sagittal plane generating tension on the anterior side; rollers (AP) generated tension on the posterior side. The most proximal rollers always rested on the flat faces of pot (a) to prevent the specimen from rotating axially.

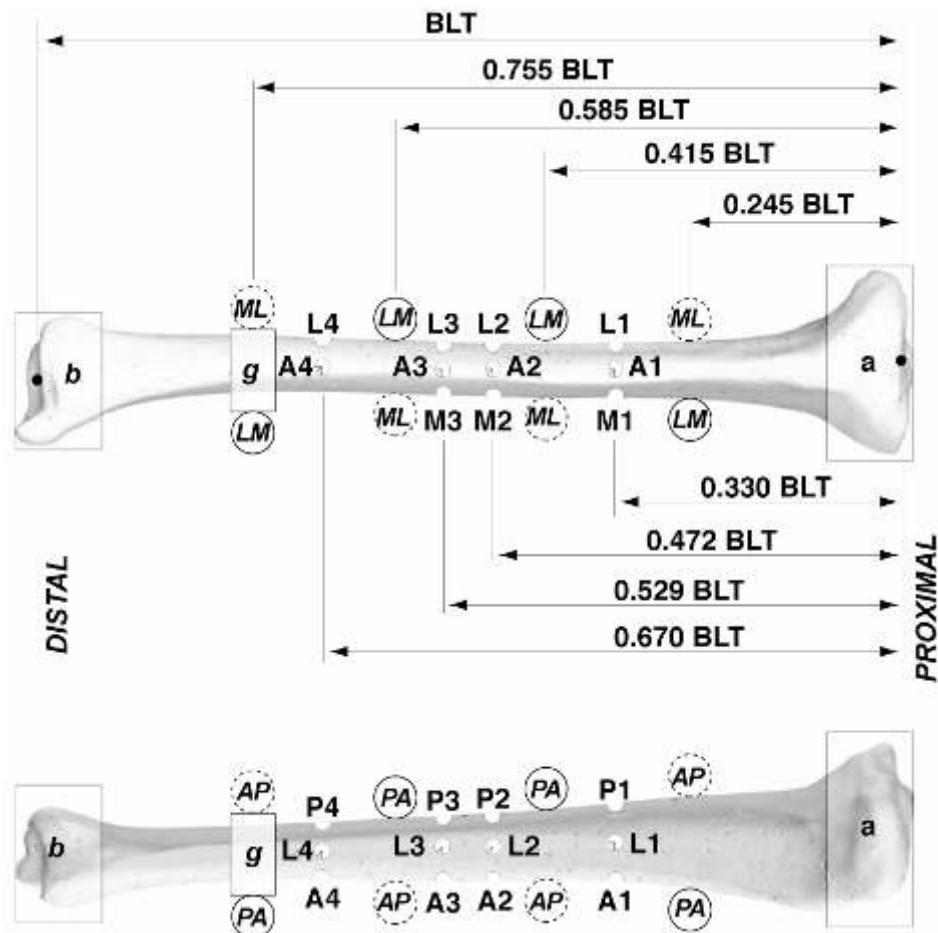


Fig. 3 – Anterior and lateral views of a right tibia. The position of the strain gauges is reported: 4 at each of 4 levels, on the Anterior, Lateral, Medial and Posterior sides (only the most distal level had 3 gauges: M4 was not installed). To enable scaling between specimens, all lengths were defined as a fraction of the biomechanical length of the tibia (BLT). The torsional load was applied by means of a proximal (a) and a distal (b) pot made of acrylic bone cement. Also indicated is the position of the rollers to apply four-point-bending in the different directions (Table 2): rollers (LM) acted in a frontal plane generating tension on the medial side; rollers (ML) generated tension on the lateral side; rollers (PA) acted in a sagittal plane generating tension on the anterior side; rollers (AP) generated tension on the posterior side. The most proximal rollers always rested on the flat faces of pot (g) to prevent the specimen from rotating axially.

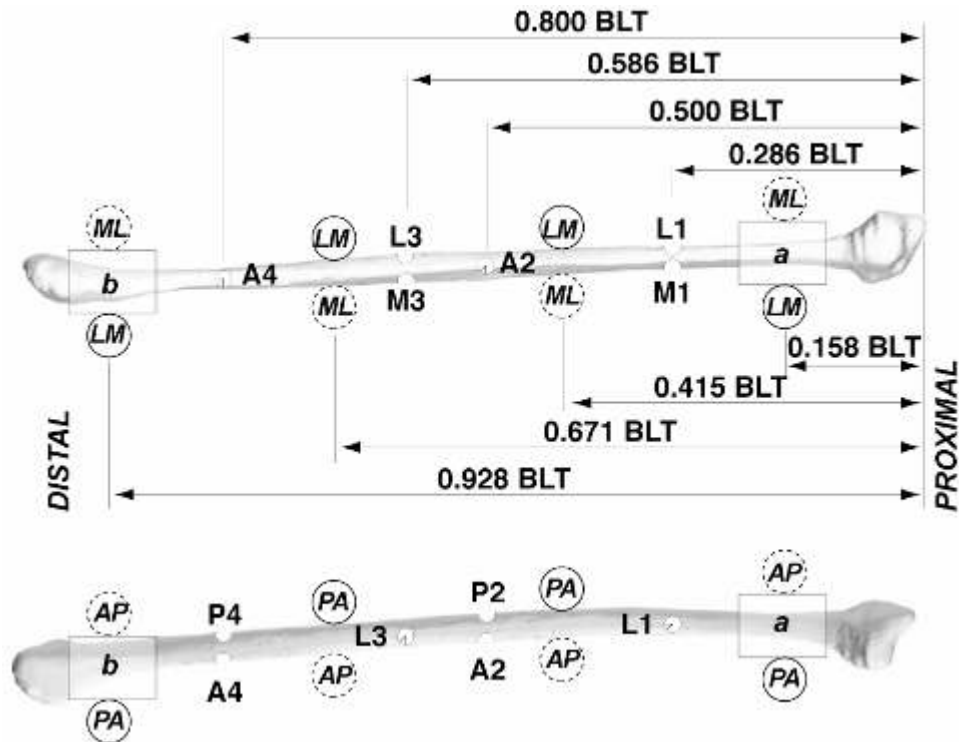


Fig. 4 – Anterior and lateral views of a right fibula. The position of the strain gauges is reported: 2 at each of 4 levels (either Anterior and Posterior, or Lateral and Medial). To enable scaling between specimens, all lengths were defined as a fraction of the biomechanical length (BLT). The torsional load was applied by means of a proximal (a) and a distal (b) pot made of acrylic bone cement. Also indicated is the position of the rollers to apply four-point-bending in the different directions (Table 2): rollers (LM) acted in a frontal plane generating tension on the medial side; rollers (ML) generated tension on the lateral side; rollers (PA) acted in a sagittal plane generating tension on the anterior side; rollers (AP) generated tension on the posterior side. The most proximal rollers always rested on the flat faces of pot (a) to prevent the specimen from rotating axially.

A grid excitation of 0.5V was selected to avoid heating. Strains and load-displacement data from the testing machine were sampled at 2000Hz, using a 50-channel data logger (System-6000, Vishay Micro-Measurement, USA). Principal strains (ϵ_1 and ϵ_2) were computed based on the three grids of each strain gauge.

3.2.2.4 *In vitro* loading

All specimens were tested using an axial-torsional servo-hydraulic machine (858-MiniBionix, MTS, Minneapolis, USA). For each type of loading, suitable loading setups were designed (using hinges and universal joints) that avoided any additional load components.

To investigate the strain distribution in the proximal metaphysis, a single force was applied to the femoral head at different directions, simulating the hip joint resultant force during daily loading (Fig. 1 (Cristofolini, Juszczuk et al. IN PRESS)). Muscle forces were not simulated, as they do not significantly alter the stress distribution in the proximal metaphysis (Cristofolini, Viceconti et al. 1995; Cody, Gross et al. 1999; Keyak, Kaneko et al. 2005; Taddei, Cristofolini et al. 2006; Cristofolini, Juszczuk et al. 2007). Four configurations were designed to cover the physiological range of loading directions during a variety of activities (Bergmann, Deuretzbacher et al. 2001). The cone spanned by the hip joint resultant force was calculated: LC1-LC4 (Table 2) corresponded to the extreme angles of the resultant force in the frontal and sagittal planes (Taddei, Cristofolini et al. 2006). To replicate a loading configuration used in the literature to replicate simplified single-leg stance, the hip joint resultant force was applied parallel to the femoral diaphysis (LC5 in Table 2). The last configuration (LC6 in Table 2) has been proposed to *in vitro* replicate spontaneous fractures of the proximal femur (i.e. not associated with any primary trauma, but due to sudden application of para-physiological load peaks, e.g. while mis-stepping or stumbling) (Cristofolini, Juszczuk et al. 2007).

The procedure for four-point-bending of the diaphysis of the femur, tibia and fibula was consistent with (Cristofolini, Viceconti et al. 1996; Cristofolini and Viceconti 2000; Heiner and Brown 2001; Gray, Taddei et al. 2008): equally spaced rollers generated bending either in the frontal plane and sagittal plane (Figs.2-4). Deflection at the mid-point was measured by a single-arm Extensometer (632.06H-20, MTS, Minneapolis, USA). Bending in each plane was exerted in both opposite direction to assess if a difference existed (Table 2). Bending stiffness was defined as the average slope of the load-deflection curve between 10% and 90% of the full load.

The procedure for torsional testing of the diaphysis of the femur, tibia and fibula was consistent with (Cristofolini, Viceconti et al. 1996; Cristofolini and Viceconti 2000; Heiner and Brown 2001; Gray, Taddei et al. 2008): rotation was recorded while the testing machine applied a controlled torque to the extremities of the diaphysis. Torsion was exerted in both opposite direction to assess if a difference existed (Table 2). Torsional stiffness was defined as the average slope of the torque-rotation curve between 10% and 90% of the full load.

To avoid risk of damage during testing, the failure load for each configuration was estimated with preliminary Finite Element models, using a validated procedure (Schileo,

Taddei et al. 2007; Schileo, Taddei et al. 2008). The applied load was 10% of the estimated failure load.

To cover the range of physiological strain rates, load was applied at two different speeds:

- High-strain-rate: the load ramp was tuned so that the strain rate in the most stressed regions was 0.05s^{-1} . As bone tissue fails when strain exceeds 0.007-0.01 (Bayraktar, Morgan et al. 2004), such strain rate would generate failure in the order of 0.2 seconds. This is the typical timescale of physiological and para-physiological loading (Bergmann, Deuretzbacher et al. 2001; Bergmann, Graichen et al. 2004).
- Low-strain-rate: a strain rate ten times lower than high-strain-rate was implemented to replicate quasi-static loading events;
- For both strain rates, the maximum load was held for 2 seconds before unloading.

Each loading configuration was tested six times on each specimen, dismounting and realigning the entire loading setup between repetitions. Bone specimens were allowed to recover at least 3 minutes between repetitions.

3.2.5 Statistical analysis

Linearity between force and strain was checked by linear regression separately for each strain gauge and each specimen.

To assess the effect of the loading direction and loading rate on the stiffness of the bones, a Factorial ANOVA (with Scheffe post-hoc test) was performed separately for the two donors and for each bone segment (femur, tibia, fibula). A power analysis was performed for statistically non-significant effects. The following independent factors were examined:

- Donor's side (right, left)
- Loading configuration (6 configurations for the proximal metaphysis, 4 for four-point-bending, 2 for torsion);
- Test speed (high-strain-rate, low-strain-rate).

A similar analysis was performed also on the strain distribution, where the strain measurement location was included as an additional factor.

To assess the effect of opposite directions of loading (e.g. intra-rotations vs. extra-rotation) on the strain distribution, the correlation between the strain measured with opposite directions of applied load was investigated by means of linear regression.

To assess the effect of the loading rate on the strain distribution, the correlation between the strain measured at high-strain-rate and low-strain-rate was investigated by means of linear regression.

All statistical analyses were performed using dedicated software (StatView-5.0.1, SAS-Institute, Cary, NC, USA, and SPSS-16.0, SPSS Inc., Chicago, IL, USA).

3.2.3 RESULTS

3.2.3.1 Linearity and creep

Linearity between load and displacement was excellent ($R^2 \geq 0.98$). Also load-strain and displacement-strain linearity was excellent ($R^2 \geq 0.97$ where strain exceeded 100 microstrain).

Strain magnitude tended to increase over time by typically 0.1-3.0% of the initial value while load was held (for 2 seconds). After unloading, strain returned rapidly to zero, with residual strain (3 minutes after unloading) of 0.5%-4% percent of the peak value.

Strain measurement repeatability (intra-specimen variability) was good: the Coefficient of Variation (CoV) between replicates under the same conditions was on average 0.4% for the proximal femoral metaphysis, 2.5% for four-point-bending, and 0.5% for torsion.

3.3.3.2 Stiffness and strain distribution

The right specimen was generally stiffer than the controlateral one both in bending and in torsion for both donors (Figs. 5-7; Factorial ANOVA, $p < 0.001$). The only exception was the bending stiffness of the femoral diaphysis: the difference between controlateral specimens was not significant, for both donors (Factorial ANOVA, $p > 0.1$, power=0.4).

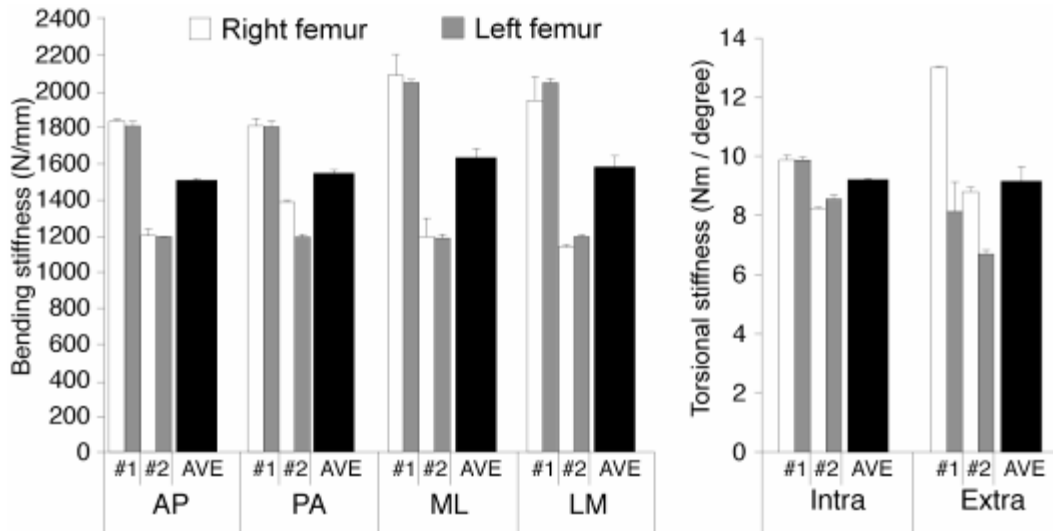


Fig. 5 – Stiffness of the diaphysis of the femur for the right and left specimens of donors #1 and #2 (average \pm standard deviation between 6 test repetitions), and on average (average \pm standard deviation between 4 specimens). Bending stiffness was measured as in a sagittal plane, with tension on the posterior (AP) and anterior side (PA), and in a frontal plane, with tension on the lateral (ML) and medial side (LM). Torsional stiffness was measured applying intra-rotation (Intra) and extra-rotation (Extra) of the distal extremity. Data represented here correspond to the low-strain-rate; similar trends were observed for the high-strain-rate.

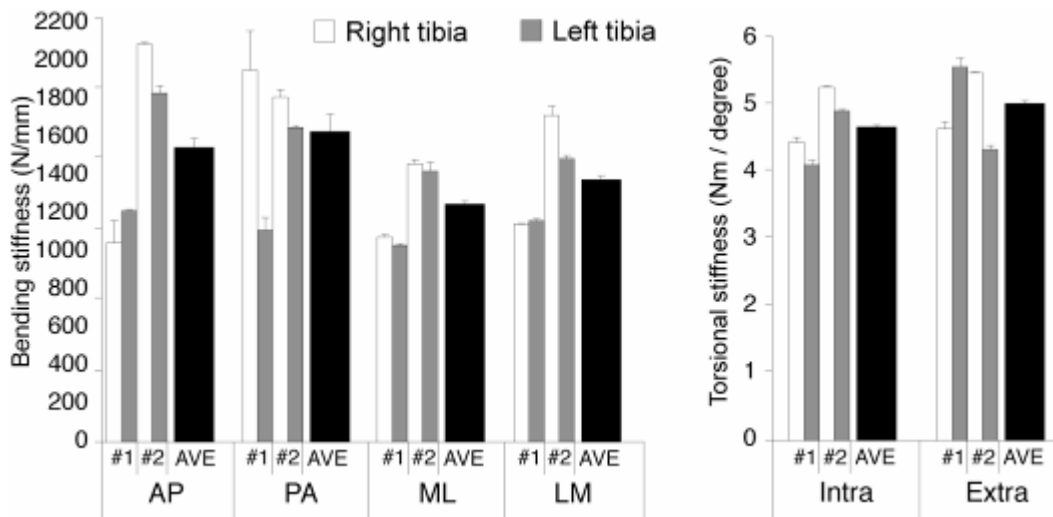


Fig. 6 – Stiffness of the diaphysis of the tibia for the right and left specimens of donors #1 and #2 (average \pm standard deviation between 6 test repetitions), and on average (average \pm standard deviation between 4 specimens). Bending stiffness was measured as in a sagittal plane, with tension on the posterior (AP) and anterior side (PA), and in a frontal plane, with tension on the lateral (ML) and medial side (LM). Torsional stiffness was measured applying intra-rotation (Intra) and extra-rotation (Extra) of the distal extremity. Data represented here correspond to the low-strain-rate; similar trends were observed for the high-strain-rate.

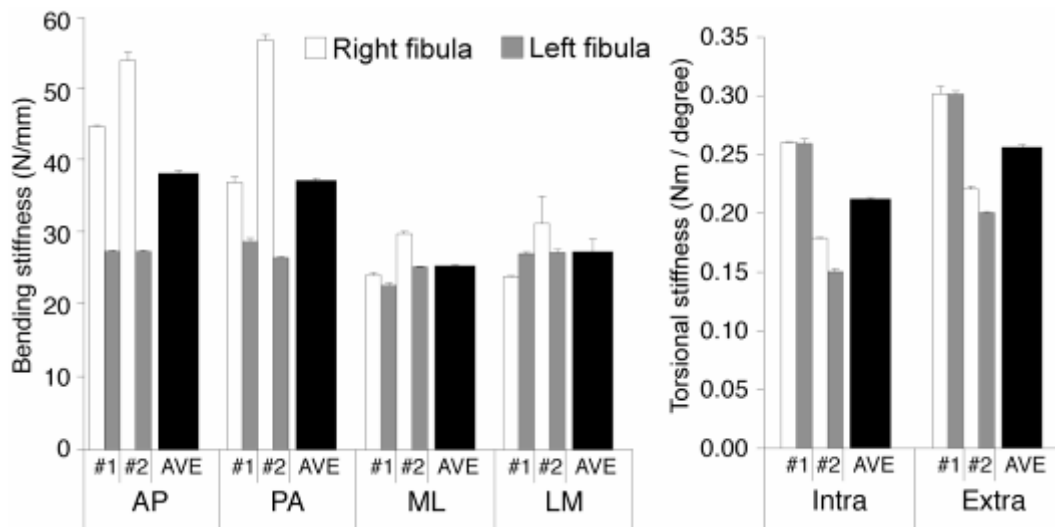


Fig. 7 – Stiffness of the diaphysis of the fibula for the right and left specimens of donors #1 and #2 (average \pm standard deviation between 6 test repetitions), and on average (average \pm standard deviation between 4 specimens). Bending stiffness was measured as in a sagittal plane, with tension on the posterior (AP) and anterior side (PA), and in a frontal plane, with tension on the lateral (ML) and medial side (LM). Torsional stiffness was measured applying intra-rotation (Intra) and extra-rotation (Extra) of the distal extremity. Data represented here correspond to the low-strain-rate; similar trends were observed for the high-strain-rate.

Similarly, the strain distribution differed significantly between contralateral specimens (Factorial ANOVA, $p < 0.0005$, for the femur, tibia and fibula). Also significant was the difference between strains measured at different locations (Factorial ANOVA, $p < 0.0005$, in all bone segments). For space reasons, more details about the strain distribution are not reported on web site dedicated LHDH project.

3.2.3.3 Effect of loading rate

Most bones were slightly stiffer at high-strain-rate than at low-strain-rate, although this difference was not always significant (Table 3). Slightly lower strain values were found at high-strain-rate for the proximal metaphysis and diaphysis of the femur for all loading configurations, while this difference was not significant in the tibia and fibula (Table 3, Fig. 8).

Table 2 – Details of the loading configurations applied to the femur, tibia and fibula: direction and magnitude of applied loads.

| | DIRECTION OF APPLIED LOAD | FEMUR | TIBIA | FIBULA |
|----------------------------|---|------------------------------------|---------|--------|
| PROXIMAL METAPHYSIS | <i>Direction of applied force (α and β defined in Fig. 1):</i> | <i>Magnitude of applied force:</i> | of N.A. | N.A. |
| S | LC1: Max flexion: $\alpha=0^\circ$, $\beta=+18^\circ$ | 0.75BW | | |
| | LC2: Max abduction: $\alpha=+3^\circ$, $\beta=0^\circ$ | | | |
| | LC3: Max extension: $\alpha=0^\circ$, $\beta=-3^\circ$ | | | |
| | LC4: Max adduction: $\alpha=+24^\circ$, $\beta=0^\circ$ | | | |
| | LC5: Neutral: $\alpha=0^\circ$, $\beta=0^\circ$ | | | |

| | | | | |
|---------------------------|--|---|---|---|
| FOUR-POINT-BENDING | <i>Direction of applied flexion:</i> | <i>Magnitude of applied force at each roller:</i> | <i>Magnitude of applied force at each roller:</i> | <i>Magnitude of applied force at each roller:</i> |
| | AP: bending in sagittal plane (tensor on posterior side) | 0.563 BW | 0.243 BW | 0.0324 BW |
| | PA bending in sagittal plane (tensor on anterior side) | | | |
| | ML: bending in frontal plane (tensor on lateral side) | | | |
| | LM: bending in frontal plane (tensor on medial side) | | | |
| TORSION | <i>Direction of applied torque:</i> | <i>Magnitude of applied torque:</i> | <i>Magnitude of applied torque:</i> | <i>Magnitude of applied torque:</i> |
| | INTRA: torque causing intra-rotation of the distal extremity | 42.1 BW*mm | 11.9 BW*mm | 0.985BW*mm |
| | EXTRA: torque causing extra-rotation of the distal extremity | | | |

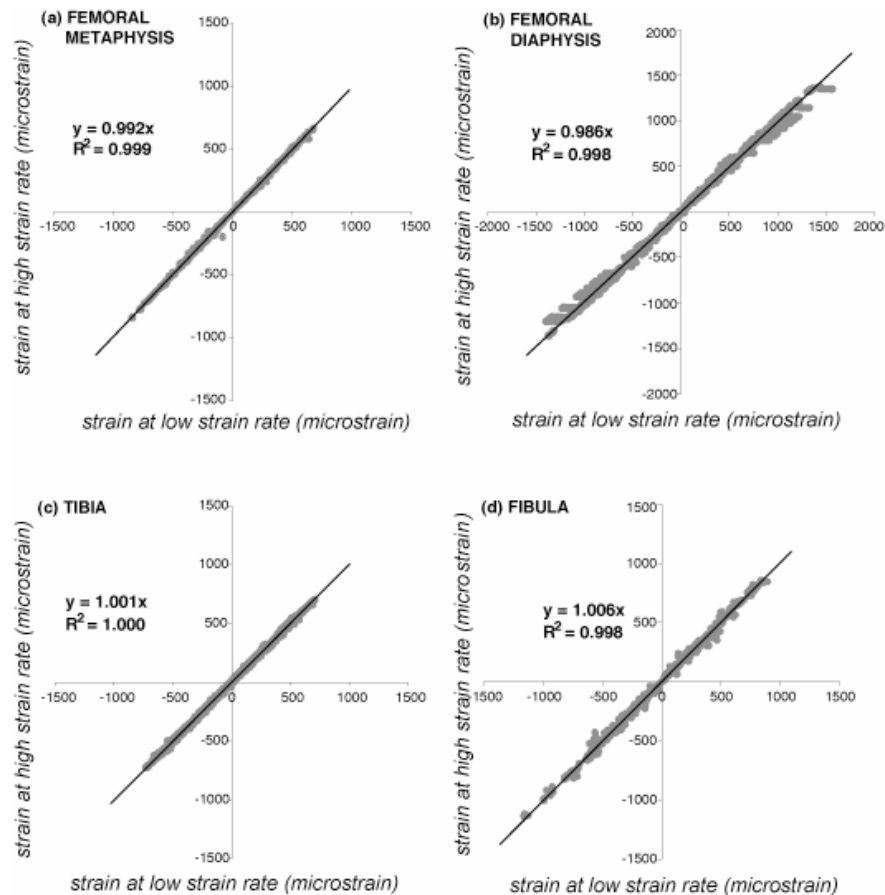


Fig. 8 – Correlation between strain at low-strain-rate and high-strain-rate for the proximal metaphysis of the femur (a), the diaphysis of the femur (b), tibia (c) and fibula (d). All specimens (right and left from both donors), all loading configurations and all strain measurement locations are pooled. A slope equal to 1.000 would indicate that identical strain values are obtained at both strain rates; a slope lower than 1.000 indicates that strains are lower when a higher strain rate is applied.

3.2.3.4 Effect of loading direction

The direction of the applied load had a significant effect on the bending stiffness (factorial ANOVA, $p < 0.0005$, Figs. 5-7). The femur was stiffer in the frontal than in the sagittal plane (Scheffe test, $p < 0.0005$). The tibia and fibula were stiffer in the sagittal than in the frontal plane (Scheffe test, $p < 0.0005$). Remarkably, differences existed also between bending in opposite directions in the same plane (Table 3). Similarly, the direction of the applied torque (intra-rotation vs extra-rotation) had a significant effect on the stiffness (Factorial ANOVA, $p < 0.0005$ for all bone segments, Figs. 5-7).

Table 3 – In the first part (three rows), the significance of the loading rate is reported for the structural stiffness and for the strain distribution. In the last part, the significance of the differences between specific load configurations is reported: opposite directions of loading are compared for the stiffness and for the strain distribution. Significance is expressed in terms of Scheffe post-hoc p-value.

| | | FEMUR | TIBIA | FIBULA |
|---|---|--|---|--|
| Effect of loading rate | Proximal metaphysis | Slightly lower strain at high-strain-rate ($p < 0.1$) | N.A. | N.A. |
| | Diaphysis: four-point-bending | Similar stiffness at high- and low-strain-rate ($p > 0.2$) Lower strain at high-strain-rate ($p < 0.05$) | Similar stiffness at high- and low-strain-rate ($p > 0.2$) Similar strain at both strain rates ($p > 0.1$) | 16% Stiffer at high-strain-rate ($p < 0.005$) Similar strain at both strain rates ($p > 0.1$) |
| | Diaphysis: torsion | 4% Stiffer at high-strain-rate ($p < 0.005$) Lower strain at high-strain-rate ($p < 0.005$) | 6% Stiffer at high-strain-rate ($p < 0.05$) Similar strain at both strain rates ($p > 0.1$) | Similar stiffness at high- and low-strain-rate ($p > 0.2$) Similar strain at both strain rates ($p > 0.1$) |
| Effect of opposite directions of applied load | Diaphysis: four-point-bending in sagittal plane | Stiffer when anterior side was in tension ($p < 0.0005$) Different strain distribution for opposite directions of bending ($p < 0.0005$) | Stiffer when posterior side was in tension ($p < 0.0005$) Different strain distribution for opposite directions of bending ($p < 0.0005$) | Stiffer when posterior side was in tension ($p < 0.05$) Different strain distribution for opposite directions of bending ($p < 0.0005$) |
| | Diaphysis: four-point-bending in frontal plane | Stiffer when lateral side was in tension ($p < 0.0005$) Different strain distribution for opposite directions of bending ($p < 0.0005$) | Stiffer when medial side was in tension ($p < 0.02$) Different strain distribution for opposite directions of bending ($p < 0.0005$) | Stiffer when medial side was in tension ($p < 0.002$) Different strain distribution for opposite directions of bending ($p < 0.0005$) |
| | Diaphysis: torsion | Stiffer in intra-rotation than extra-rotation ($p < 0.0005$) Similar strain distribution for opposite directions of torsion ($p > 0.5$, power > 0.8) | Stiffer in extra-rotation than intra-rotation ($p < 0.0005$) Different strain distribution for opposite directions of torsion ($p < 0.0005$) | Stiffer in extra-rotation than intra-rotation ($p < 0.0005$) Similar strain distribution for opposite directions of torsion ($p > 0.2$) |

Also the strain distribution was significantly affected by the direction of the applied load (Factorial ANOVA, $p < 0.0005$ for all bone segments). Such difference existed not only between the most obvious configurations (e.g. bending in the frontal vs sagittal planes), but also for opposite directions of loading (Table 3). As an example, the effects of opposite directions of torsion are compared in Fig. 9.

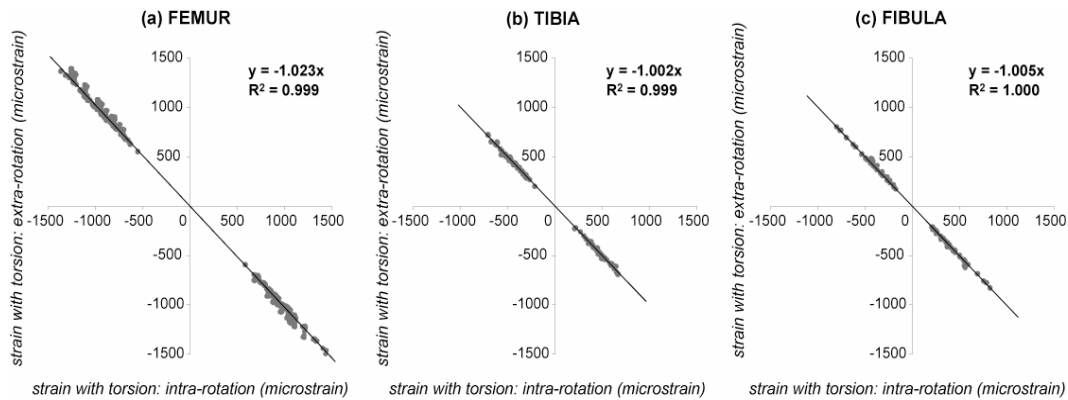


Fig. 9 – Correlation between strain when a torque was applied in two opposite directions (intra-rotation vs extra-rotation of the distal extremity). Strains are plotted separately for the diaphysis of the femur (a), tibia (b) and fibula (c). All specimens (right and left from both donors), all loading configurations and all strain measurement locations are pooled. A slope equal to one would indicate that identical strain values are obtained for opposite loading directions; a slope lower than unity indicates that strains are lower when extra-rotation is applied to the distal extremity. Data represented here correspond to the low-strain-rate (similar results were obtained at high-strain-rate).

Acknowledgments

The Authors wish to thank Caroline Öhman and Andrea Malandrino for their support in digitizing the landmarks, Keith Smith for revising the script, and Luigi Lena for the artwork. This work was partially supported by the European Community (project number: IST-2004-026932; title: Living Human Digital Library; acronym: LHDL)

3.2.4 References

- Bayraktar, H. H., E. F. Morgan, et al. (2004). "Comparison of the elastic and yield properties of human femoral trabecular and cortical bone tissue." J Biomech **37**(1): 27-35.
- Bergmann, G., G. Deuretzbacher, et al. (2001). "Hip contact forces and gait patterns from routine activities." J Biomech **34**(7): 859-71.
- Bergmann, G., F. Graichen, et al. (2004). "Hip contact forces during stumbling." Langenbecks Arch. Surg. **389**: 51-59.
- Cody, D. D., G. J. Gross, et al. (1999). "Femoral strength is better predicted by finite element models than QCT and DXA." J Biomech **32**(10): 1013-20.
- Conti, G., L. Cristofolini, et al. (2008). "Comparison of three standard anatomical reference frames for the tibia-fibula complex." J Biomech **41**(16): 3384-3389.
- Cristofolini, L. (1997). "A critical analysis of stress shielding evaluation of hip prostheses." Critical Reviews in Biomedical Engineering **25:4&5**: 409-483.
- Cristofolini, L., M. Juszczak, et al. (2007). "In vitro replication of spontaneous fractures of the proximal human femur." J. Biomechanics **40**(13): 2837-2845.
- Cristofolini, L., M. Juszczak, et al. (IN PRESS). "Strain distribution in the proximal human femoral metaphysis." Proc Inst Mech Eng [H].
- Cristofolini, L. and M. Viceconti (2000). "Mechanical validation of whole bone composite tibia models." J Biomech **33**(3): 279-88.
- Cristofolini, L., M. Viceconti, et al. (1996). "Mechanical validation of whole bone composite femur models." J Biomech **29**(4): 525-35.
- Cristofolini, L., M. Viceconti, et al. (1995). "Influence of thigh muscles on the axial strains in a proximal femur during early stance in gait." J Biomech **28**(5): 617-624.
- Gray, H. A., F. Taddei, et al. (2008). "Experimental validation of a finite element model of a human cadaveric tibia." J. Biomech. Engineering **130**(3): 031016-1 (9 pages).
- Heiner, A. D. and T. D. Brown (2001). "Structural properties of a new design of composite replicate femurs and tibias." J Biomech **34**(6): 773-81.
- Keyak, J. H., T. S. Kaneko, et al. (2005). "Predicting proximal femoral strength using structural engineering models." Clin Orthop Relat Res(437): 219-28.
- Ohman, C., E. Dall'Ara, et al. (2008). "The effects of embalming using a 4% formalin solution on the compressive mechanical properties of human cortical bone." Clin Biomech (Bristol, Avon) **23**(10): 1294-8.
- Ruff, C. B. and W. C. Hayes (1983). "Cross-sectional Geometry of Pecos Pueblo Femora and Tibiae - A Biomechanical Investigation: I. Method and General Patterns of Variation." Am. J. Phys. Anthropol. **60**: 359-381.
- Schileo, E., F. Taddei, et al. (2008). "Subject-specific finite element models implementing a maximum principal strain criterion are able to estimate failure risk and fracture location on human femurs tested in vitro." J Biomech **41**(2): 356-67.
- Schileo, E., F. Taddei, et al. (2007). "Subject-specific finite element models can accurately predict strain levels in long bones." J Biomech **40**(13): 2982-9.
- Taddei, F., L. Cristofolini, et al. (2006). "Subject-specific finite element models of long bones: An in vitro evaluation of the overall accuracy." J Biomech **39**(13): 2457-67.
- Viceconti, M., A. Toni, et al. (1992). Strain gauge analysis of hard tissues: factors influencing measurements. Experimental Mechanics. Technology transfer between

high tech engineering and biomechanics. E. G. Little. Amsterdam, Elsevier Science
Publisher B.V.: 177-184.

4.1 STRAIN DISTRIBUTION IN THE PROXIMAL HUMAN FEMORAL METAPHYSIS

Luca Cristofolini, Ph.D. ^{1,2}, Mateusz Juszczak, M.Eng. ^{1,2}, Fulvia Taddei, Ph.D. ¹, Marco Viceconti, Ph.D. ¹

¹ Laboratorio di Tecnologia Medica, Istituto Ortopedico Rizzoli, Bologna, Italy

² Engineering Faculty, University of Bologna, Italy

This paper is in press on Proceedings of the Institution of Mechanical Engineers, PartH, Journal of Engineering in Medicine.

4.1.1 ABSTRACT

There is a significant interest in the state of stress/strain in the proximal femoral metaphysis, because of its relevance for hip fractures and prosthetic replacements. The scope of this work was to provide a better understanding of the strain distribution, and of its correlation with the different directions of loading, and with bone quality. Twelve pairs of human femurs were instrumented with strain gauges. Six loading configurations were designed to cover the range of directions spanned by the hip joint force. Inter-specimen variability was reduced if paired specimens were considered. Principal strain magnitude varied greatly between loading configurations. This suggests that different loading configurations need to be simulated *in vitro*. The strain magnitude varied between locations, but on average was compatible with the strain values measured *in vivo*. The strain magnitudes and the direction of principal tensile strain in the head and neck were compatible with the spontaneous fractures of the proximal femur reported in some subjects. Principal tensile strain was significantly larger where cortical bone was thinner; compressive strain was larger where cortical bone was thicker. The direction of principal strain varied significantly between measurement locations, but varied little between loading configurations. This suggests that the anatomy and the distribution of anisotropic material properties enable the proximal femur to adequately respond to the changing direction of daily loading.

Keywords: proximal human femoral metaphysis; strain distribution; loading condition; paired and unpaired variability; direction of principal strain

List of abbreviations:

| | |
|-----------------|--|
| ε_1 | maximum principal strain |
| ε_2 | minimum principal strain |
| θ_p | angle of the principal planes (counter-clockwise) |
| BW | Body Weight |
| FE | Finite Element |
| LC | load configuration (six different configurations were tested: LC1-LC6) |
| AH | strain gauge on the anterior side of the head |
| LH | strain gauge on the lateral side of the head |
| PH | strain gauge on the posterior side of the head |
| MH | strain gauge on the medial side of the head |
| AN | strain gauge on the anterior side of the neck |
| PN | strain gauge on the posterior side of the neck |
| MN | strain gauge on the medial side of the neck |
| A1 | strain gauge on the anterior side, below the lesser trochanter |
| L1 | strain gauge on the lateral side, below the lesser trochanter |
| P1 | strain gauge on the posterior side, below the lesser trochanter |
| M1 | strain gauge on the medial side, below the lesser trochanter |

4.1.2 INTRODUCTION

Strain distribution in the proximal femur always had a great interest in biomechanics. The recent resurgence of epiphyseal hip prostheses requires a deep understanding of the stress distribution in the proximal femoral metaphysis, because of the potential risk of neck fracture and adverse bone remodeling (Amstutz, Campbell et al. 2004; Grigoris, Roberts et al. 2006; McMinn and Daniel 2006). Also, the increased rate of traumatic and spontaneous fractures (i.e.: caused by sudden loading and muscle contraction, not by trauma) of the proximal femur associated with the aging population (Grisso, Kelsey et al. 1991; Rockwood, Green et al. 1991) suggests that more research should focus on the biomechanics of such fractures, to improve the understanding of their etiology (Yang, Shen et al. 1996; Cristofolini, Juszczuk et al. 2007). Recently, a multi-scale approach was taken by many researchers to investigate musculoskeletal biomechanics in general (Fenner, Brook et al. 2008), and especially focusing on the proximal femoral metaphysis (Cristofolini, Taddei et al. 2008; Viceconti, Taddei et al. 2008): this approach requires quantitative information about the strain distribution under load.

The stress/strain distribution in the femur has been extensively studied in the past (Fung 1980; Roesler 1987; Fabeck, Tolley et al. 2002). However, most of the published experimental studies were designed to investigate the effect of hip stems (Cristofolini 1997). Therefore, the loading configuration (including inclusion of selected muscle groups) and the strain measurement procedures proposed in the literature mostly focus on the diaphysis and might not be suitable to investigate the proximal metaphysis. Failure of the proximal femoral metaphysis has often been investigated *in vitro*, but the strain distribution was not assessed (e.g.: (Yang, Shen et al. 1996; Lochmüller, Groll et al. 2002; Cristofolini, Juszczuk et al. 2007)). The strain distribution in the intact and resurfaced femur has often been investigated using a single loading configuration (Crick, Wagner et al. 1985; Field and Rushton 1989). In no case triaxial strain gauges were used: thus, strains could be measured only along selected direction, but principal strains (ε_1 and ε_2) and the angle (θ_p) of the principal planes could not be resolved. None of the experimental studies above could indicate if different configurations (associated with different motor tasks) would stress the proximal metaphysis in significantly different fashions. Also, no study so far indicated if using paired specimens would reduce inter-specimen strain variability.

In addition, it is well known (Carter and Spengler 1978; Fung 1980) that in the diaphyseal region the cortical bone is thicker if compared to the metaphyses, where cortical bone is thinner. Different load transfer, and possibly different failure mechanism, is associated with different thickness of the cortical bone (Carter and Spengler 1978; Fung 1980; Roesler 1987). It would be interesting to assess whether physiological loading induces different stress/strain patterns where the cortical bone is thicker (hence uptaking most of the load) if compared to those regions where cortical bone is thinner (hence, most of the load is uptaken by the trabecular bone).

Finally, several authors suggest that bone geometry and density are adjusted by bone remodeling so as to attain a constant level of stress/strain (e.g.: (Lanyon 1980; Huiskes, Weinans et al. 1987)). However there is no consensus whether such physiological level of strain is constant or varies between subjects.

The aims of this work were:

- To implement a validated procedure to measure strain in the proximal femoral metaphysis with a realistic, simplified and relevant set of loading configurations;
- To provide an indication of the typical strain distribution (including principal strains and angle of principal planes) in the proximal metaphysis;
- To estimate strain variability between paired and unpaired femurs;
- To assess if there is a correlation between strain distribution and local thickness of the cortical bone;
- To assess if physiological bone strain vary between femurs in relation to bone quality or bone dimensions.

4.1.3 MATERIALS AND METHODS

4.1.3.1 Test specimens

Twelve pairs of fresh-frozen femur specimens were obtained through IIAM (Jessup, PA, USA) from donors who did not suffer of musculoskeletal pathologies (Table 1). They were DEXA-scanned (Excel-Plus, Norland, USA) and CT-scanned (HiSpeed, General Electric, USA) to document bone quality and lack of abnormality or defects. Anatomical dimensions were measured (Ruff and Hayes 1983; Cristofolini 1997; Cristofolini and Viceconti 1999).

- The biomechanical length, BL, was measured between the trochanteric fossa and the intercondylar fossa.
- The diameter of the head was measured five times along different directions; the average head diameter, HD, was computed.

The density values found (Table 1) cover the entire range from physiological to osteopenic to osteoporotic bone according to (WHO 1994; NIH 2000). The distal extremities of the femurs were potted with acrylic cement once the anatomical axes were identified (Ruff and Hayes 1983; Cristofolini 1997; Cristofolini and Viceconti 1999). During experimental tests, the femurs were wrapped in cloths soaked with physiological solution (room temperature: 27-30°C); they were stored sealed in bags at -25°C when not in use.

Table 1 – Details of the specimens investigated. In the first four columns, details of the donors are listed. Bone quality is reported in the 6th and 7th column for each femur (T-score of the bone density referred to the young reference population, and Z-score referred to the age-matched population, based on the Norland DEXA scanner reference population). Biomechanical dimensions (Ruff and Hayes 1983; Cristofolini 1997; Cristofolini and Viceconti 1999) are reported in the last two columns. Average and standard deviation are summarized in the last two lines for the entire sample.

| DONORS' DETAILS | | | | FEMURS' DETAILS | | | | |
|-----------------|--------------|-------------------|-------------------|-----------------|---------|---------|-------------------------------|------------------------|
| Sex | Age at death | Donor Height (cm) | Donor Weight (kg) | SIDE | T-score | Z-score | Biomechanical length, BL (mm) | Head diameter, HD (mm) |
| male | 67 | 173 | 82 | Left | -1.89 | -0.66 | 415 | 49.7 |
| | | | | Right | -1.74 | -0.51 | 415 | 50.6 |

| | | | | | | | | |
|--------|----|-----|-----|-------|-------|-------|-----|------|
| male | 60 | 178 | 82 | Left | -0.75 | 0.39 | 419 | 50.3 |
| | | | | Right | -2.16 | -1.18 | 421 | 51.1 |
| male | 72 | 173 | 100 | Left | -0.90 | 0.48 | 408 | 46.7 |
| | | | | Right | -1.37 | 0.01 | 414 | 46.6 |
| male | 70 | 175 | 90 | Left | -2.65 | -1.33 | 443 | 47.7 |
| | | | | Right | -2.26 | -0.93 | 443 | 48.4 |
| male | 51 | 175 | 164 | Left | -0.70 | -0.04 | 463 | 53.5 |
| | | | | Right | -0.11 | 0.55 | 466 | 54.4 |
| male | 68 | 178 | 98 | Left | -2.58 | -1.32 | 424 | 51.5 |
| | | | | Right | -2.89 | -1.62 | 427 | 52.1 |
| female | 83 | 157 | 48 | Right | -3.03 | -1.36 | 425 | 46.6 |
| | | | | Left | -3.00 | -1.33 | 421 | 46.8 |
| male | 80 | 178 | 88 | Right | -2.97 | -1.51 | 437 | 52.0 |
| | | | | Left | -3.42 | -1.96 | 439 | 51.9 |
| male | 67 | 175 | 88 | RIGHT | -3.21 | -1.99 | 423 | 52.0 |
| | | | | LEFT | -3.36 | -2.13 | 423 | 52.0 |
| male | 71 | 178 | 91 | RIGHT | -1.87 | -0.52 | 443 | 53.3 |
| | | | | LEFT | -1.49 | -0.15 | 445 | 53.7 |
| male | 82 | 175 | 78 | RIGHT | -3.95 | -2.49 | 427 | 50.3 |
| | | | | LEFT | -4.09 | -2.62 | 432 | 49.4 |
| male | 73 | 175 | 73 | RIGHT | -4.32 | -2.91 | 433 | 48.7 |
| | | | | LEFT | -4.10 | -2.69 | 433 | 46.9 |
| MEAN | 70 | 174 | 90 | - | -2.45 | -1.16 | 431 | 50.3 |
| SD | 9 | 6 | 27 | - | 1.18 | 1.04 | 15 | 2.5 |

4.1.3.2 Strain measurement

Triaxial stacked strain gauges (KFG-3-120-D17-11L3M2S, Kyowa, Tokyo, Japan, three grids at 0°-45°-90°, grid length of 3 mm) were bonded at eleven locations (Fig.1):

- Four around the head, close to the articular cartilage (Anterior, Lateral, Posterior, Medial sides);
- Three around the neck, distal to the previous ones (Anterior, Posterior, Medial: space on the lateral side was insufficient to host one additional strain gauge);
- Four around the proximal diaphysis, just below the lesser trochanter (Anterior, Lateral, Posterior, Medial).

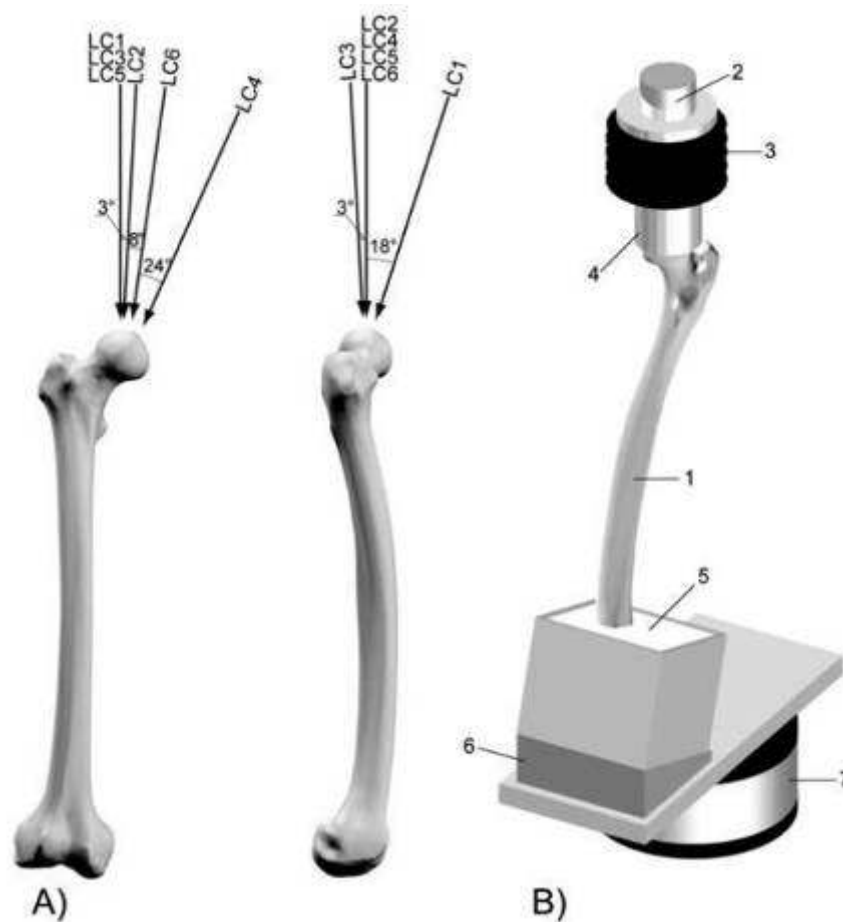


Fig. 1 – Sketch of a right femur with an indication of the position of the strain gauges: lateral, anterior, medial, and posterior views. To allow comparable positioning between specimens, the three levels were defined as a fraction of the femur dimensions (biomechanical length and head diameter). The position around the neck of strain gauges MH, MN, and LH corresponded to the frontal plane defined by (Ruff and Hayes 1983). The position around the neck of the strain gauges AH, AN, PH, PN corresponded to the mid thickness of the neck at the corresponding level. The position around the femur of the strain gauges A1, L1, P1, M1 corresponded to the mid thickness of the diaphysis at that level.

The actual position where the strain gauge was bonded sometimes was adjusted by up to 4 mm, when small defects (pores, ridges or grooves) made the bone surface unsuitable for bonding a strain gauge.

The measurement locations around the head (AH, LH, PH, MH) and neck (AN, PN, MN) were consistent with preliminary experience (Cristofolini, Juszczak et al. 2006). The measurement locations around the diaphysis (A1,L1,P1,M1) were consistent with previously published protocols for testing hip stems (Cristofolini 1997; Cristofolini and Viceconti 1999). The area for strain measurement was prepared with an established procedure for wet cadaveric specimens (Viceconti, Toni et al. 1992), which included:

1. Cleaning the surface from soft tissues with a scalp, and sandpaper;
2. Accurate cleaning and degreasing first with ethanol, then with a cocktail of acetone and 2-propanol (RMS1, HBM, Darmstadt, Germany);
3. Filling the pores and waterproofing the bone surface with two layers of polyurethane protective (PU120, HBM);
4. Smoothing and removing the excess of polyurethane with fine sandpaper (#400);
5. Bonding the strain gauges with cyanoacrylate glue (CC-33A, Kyowa);
6. Protecting and waterproofing the strain gauges with three layers of polyurethane protective (PU120, HBM).

A grid excitation of 0.5V was selected to avoid heating. Strains were sampled at 10Hz, with a low-pass cutoff of 1Hz, using a multi-channel data logger (System-6000, Vishay Micro-Measurement, USA). Principal strains (ε_1 and ε_2) and the angle (θ_p) of the principal planes, were computed based on the readout from the three grids of each strain gauge (Dally and Riley 2005).

4.1.3.3 Measurement of cortical bone thickness

After test completion the femurs were sectioned in correspondence of the strain gauges. The thickness of the cortical bone was measured under an optical microscope with a scaled ocular (SMZ-2T, Nikon, Tokyo, Japan).

4.1.3.4 Analysis of reinforcement caused by strain gauges

Strain gauges are known to cause reinforcement, especially on low-modulus materials and on thin structures (Beatty and Chewning 1979; Perry 1985; Little, Tocher et al. 1990; Ajovalasit and Zuccarello 2005). This leads to an underestimation of the actual strain. As the cortical bone is extremely thin in the metaphyseal region, we suspected that reinforcing would significantly bias strain measurements. The reinforcement caused by the strain gauge

was estimated based on the nominal technical specifications of the strain gauges, assuming parallel loading of the bone thin shell and the strain gauge (Perry 1985; Little, Tocher et al. 1990; Ajovalasit and Zuccarello 2005). A typical Young modulus of 15.0 to 18.0 GPa was assigned to the cortical bone based on the literature (Carter and Spengler 1978; Fung 1980; Currey 1998). Only the cortical shell was included in this estimate. As the contribution of the trabecular bone to structural stiffness was neglected, this analysis provides an overestimate of the reinforcing effect.

4.1.3.5 *In vitro* loading configurations

In order to investigate the strain distribution in the proximal metaphysis, a set of simplified loading configurations was chosen. A single force was applied to the femoral head at different directions, simulating the hip joint resultant force during daily loading (Fig. 2). Muscle forces were not simulated, as experimental and Finite Element (FE) studies indicated they do not significantly alter the stress distribution in the proximal metaphysis (Cristofolini, Viceconti et al. 1995; Cody, Gross et al. 1999; Keyak, Kaneko et al. 2005; Cristofolini, Juszczuk et al. 2006; Cristofolini, Juszczuk et al. 2007). The following load configurations were investigated (Fig. 2):

- LC1-LC4: These configurations were designed to cover the physiological range of loading directions during a variety of activities (including level walking at different speeds, single-leg-stance, stair-climbing and -descending, standing up from seated (Bergmann, Deuretzbacher et al. 2001)). The cone spanned by the hip joint resultant force was calculated: LC1-LC4 corresponded to the extreme angles of the resultant force in the frontal and sagittal planes (Taddei, Cristofolini et al. 2006). These configurations did not correspond to any specific motor task.
- LC5: To replicate a loading configuration frequently used in the literature to replicate simplified single-leg stance, (e.g.: (Rohlmann, Mossner et al. 1983; Lotz, Cheal et al. 1991; Augat, Reeb et al. 1996; Lochmüller, Groll et al. 2002)), the femur was tested when the hip joint resultant force was parallel to the femoral diaphysis.
- LC6: The last configuration has been proposed to *in vitro* replicate spontaneous fractures (i.e. not associated with any primary trauma) of the proximal femur (Cristofolini, Juszczuk et al. 2007): spontaneous fractures occur when a subject applies a sudden para-physiological load peak (while mis-stepping or stumbling). In this configuration (which corresponds to single-leg-stance (Bergmann, Deuretzbacher et al. 2001)), the femur was tilted by 8° in the frontal plane. (Cristofolini, Juszczuk et al.

2007) used a previously validated FE model (Taddei, Cristofolini et al. 2006) to show that stresses are highest in the proximal femoral metaphysis for this loading configuration.

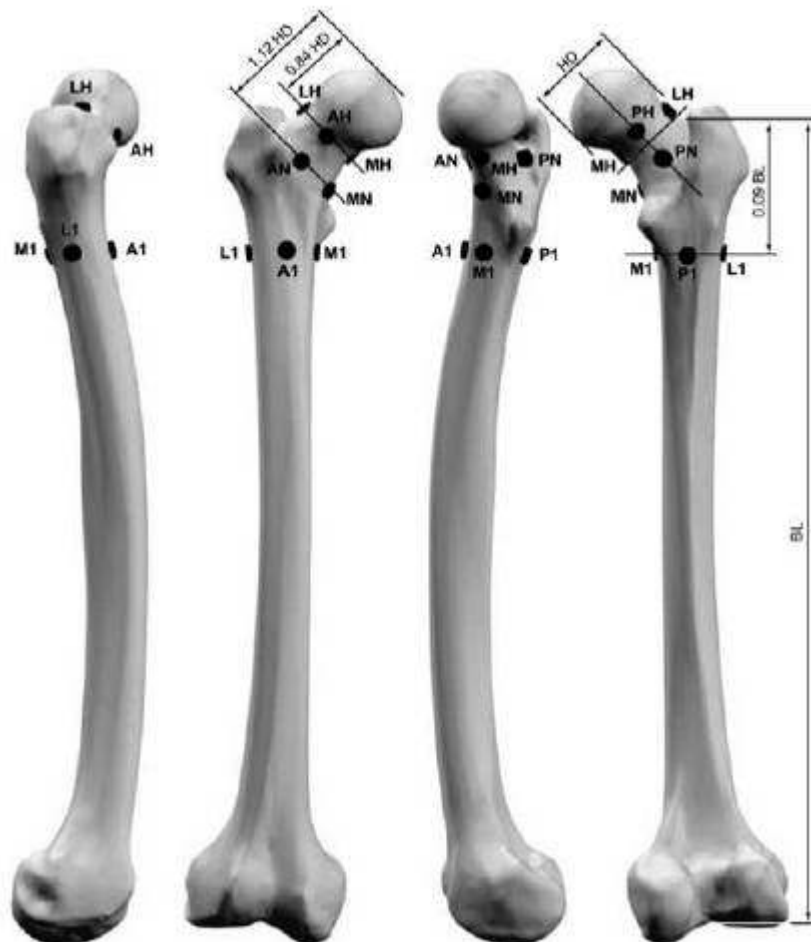


Fig. 2 – A) Schematic of a right femur (anterior and lateral views) showing the direction of the hip joint force for the different loading configurations: configuration LC1-LC4 covered the extreme directions of the hip joint resultant force in the sagittal and frontal planes; LC5 corresponded to the force parallel to the femoral diaphysis; LC6 replicated the same angles used in destructive tests of the proximal femur (Cristofolini, Juszczak et al. 2007). B) Experimental setup including: (1) the femur specimen; (2) the actuator of the testing machine with (3) the system of rails to avoid transmission of horizontal force components; (4) the copy of the femoral head to allow uniform load transfer from the actuator to the femoral head; (5) the distal pot of acrylic cement holding the femur distally; (6) the interchangeable wedges to hold the femur at the assigned angle (LC4: 24° in the frontal plane and 0° in the sagittal plane, in this instance) on top of the (7) load cell of the testing machine.

The femur specimens were mounted on top of the load cell of the testing machine using interchangeable wedges to tilt the bone by the assigned angles (Fig. 2). The force was applied vertical by the actuator of the testing machine to the femoral head through a system

of rails to avoid transmission of horizontal force components, similarly to (Cristofolini 1997; Cristofolini and Viceconti 1999). A copy of each femoral head was prepared with acrylic cement (covering a height equivalent to 1/5 of the head diameter) to allow uniform load application. Load was applied at a constant displacement rate of 2 mm/sec. In order to avoid bone damage due to repeated loading, load was limited to 0.75 of the Body Weight (BW) of the relative donor. For all loading configurations the maximum force was held for thirty seconds to allow a constant time for a repeatable amount of creep to take place. Each loading configuration was repeated 6 times on each specimen. The specimen was allowed to recover for 5 minutes between repetitions. In addition, each loading configuration was replicated by applying the force in 6 equal increments. This sequence of loads allowed measuring strains at different strain levels, checking material linearity, quantifying viscoelastic phenomena and irreversible strains.

4.1.3.6 Statistics

Linearity between force and strain was checked by linear regression separately for each strain gauge and each specimen.

To obtain a single output for each strain gauge and each specimen, the average was calculated over all repetitions for the principal strains (ε_1 and ε_2) for the angle (θ_p) of the principal planes. To estimate the measurement repeatability (intra-specimen variability) the standard deviation of the principal strains (ε_1 and ε_2) and angle (θ_p) was computed between repetitions, for each strain gauge and each specimen. The Coefficient of Variation (CoV: standard deviation expressed as % of the average) was computed for each measurement location. To avoid fictitiously increasing the CoV with close-to-zero data, measurement locations where strain was lower than 100 microstrain were excluded.

To estimate the inter-specimen repeatability (unpaired inter-specimen variability), the standard deviation and CoV of the principal strains (ε_1 and ε_2) and angle (θ_p) was computed between specimens (one specimen was randomly chosen of each pair of femurs), for each strain gauge. To estimate the within-pair repeatability (paired inter-specimen variability), the root-mean-squared average and CoV of the difference between paired femurs was computed for each strain gauge. In order to test the hypothesis that paired inter-specimen variability was lower than unpaired inter-specimen variability, a Levene's test was performed on the respective variances (Montgomery 2005).

The significance of the effect of the loading configuration was assessed by means of a factorial ANOVA, where the strain measurement location and the loading configuration

were independent factors. A Fisher PLSD post-hoc test was performed to assess which loading configurations differed most significantly.

The correlation between the local thickness of cortical bone and the strain in the same region was investigated. Bone thickness was assigned to two categories: thin (≤ 1.0 mm: typically all the head and neck region, except the medial part of the neck – gauge MN) and thick (> 1.0 mm: typically the gauge on the medial part of the neck –MN- and the more distal ones –A1, L1, P1, M1). Correlation between cortical thickness and strain was assessed by means of a factorial ANOVA both pooling together all loading configurations, and splitting by loading configuration.

To investigate the correlation between bone quality (assessed from DEXA) and anatomical dimensions (biomechanical length, BL, and head diameter, HD) and strain values, the Pearson's correlation coefficient was computed both pooling together all strain measurement locations, and splitting by measurement location.

All statistical analyses were performed using dedicated software (StatView-5.0.1, SAS-Institute, Cary, NC, USA, and SPSS 16.0, SPSS Inc., Chicago, IL, USA). A level of confidence $p=0.05$ was assumed for statistical significance.

4.1.3 RESULTS

The cortex in the region where the most proximal strain gauges are installed (e.g.: AH, LH, PH, AN, PN) in some cases was as thin as 0.2 mm. The thickness of the strain gauges used in this study was 0.085 mm, with an average Young modulus (estimated on the sandwich structure of the triaxial stacked strain gauges) of 6.4 GPa (Cristofolini and Viceconti 2000). The reinforcing associated with the strain gauges in the proximal metaphysis leads to underestimate the actual strain by less than 1%, up to 15%, and varied from region to region and between specimens because of the uneven thickness of the cortical shell. The reinforcement was lower than 4% where cortical bone was thicker than 1 mm.

Strain increased linearly with load for each individual grid, and each loading configuration: $R^2 \geq 0.99$ for 98% of the cases where strains reached a value of 100 microstrain or larger. This confirms that the bone can be assumed to behave linearly with good approximation for the strain range and strain rates used in this study.

Strain readout at the beginning and at the end of the thirty-second force holding was compared. Strain magnitude tended to increase over time by typically 0.1-3.0% of the initial

value. This confirms the presence of viscoelastic phenomena, and the need to define a time when strains are measured after force application. However, these creep effects are detectable but not such as to significantly alter the strain pattern. After unloading, strains returned rapidly to zero, with residual strains of 0.5%-4% percent of the peak value being found five minutes after unloading.

Measurement repeatability (intra-specimen variability) was good (Table 2): the CoV between replicates under the same conditions was on average 0.4% for the principal strain. Also, the angle (θ_p) of the principal planes varied on average by 0.3° (standard deviation) between replicates under the same conditions.

Table 2 – Measurement repeatability of the principal strains: the coefficient of variations reported. Ranges are reported, in relation to the different loading configurations.

| | Measurement repeatability (intra-specimen variability) | Unpaired inter-specimen variability | Paired inter-specimen variability |
|--|---|---|---|
| Head region (gauges AH,LH,PH,MH) | 1 - 4% | 30 - 62% | 20 - 50% |
| Neck region (gauges AN,PN,MN) | | 20 - 62% | 11 - 45% |
| Proximal diaphysis (gauges A1,L1,P1,M1) | | 16 - 53% | 20 - 34% |

The principal strains averaged over all specimens, measurement locations, and loading configurations were 217 microstrain (ϵ_1) and -309 microstrain (ϵ_2) respectively. Tension was generally predominant on the lateral side while compression was predominant medially (Fig. 3). Tensile and compressive strain were comparable on the anterior and posterior sides (Fig. 4). Strain had the same order of magnitude in the head region, neck region and in the proximal diaphysis (Fig. 3-4).

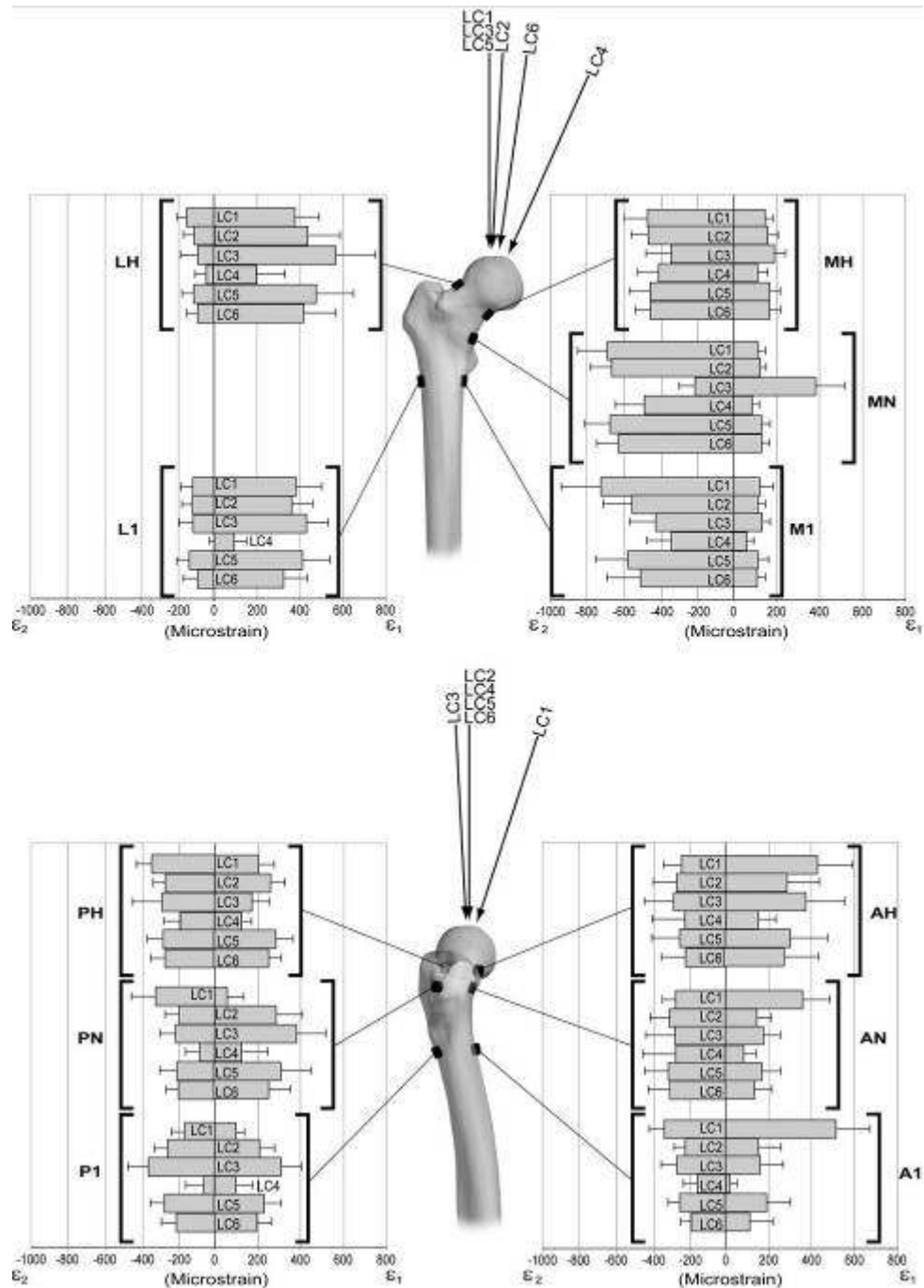


Fig. 3 – Maximum and minimum principal strains (ϵ_1 and ϵ_2 , in microstrain) on the lateral and medial sides of the femur. Average and standard deviation between 24 femurs is reported for the six loading configurations.

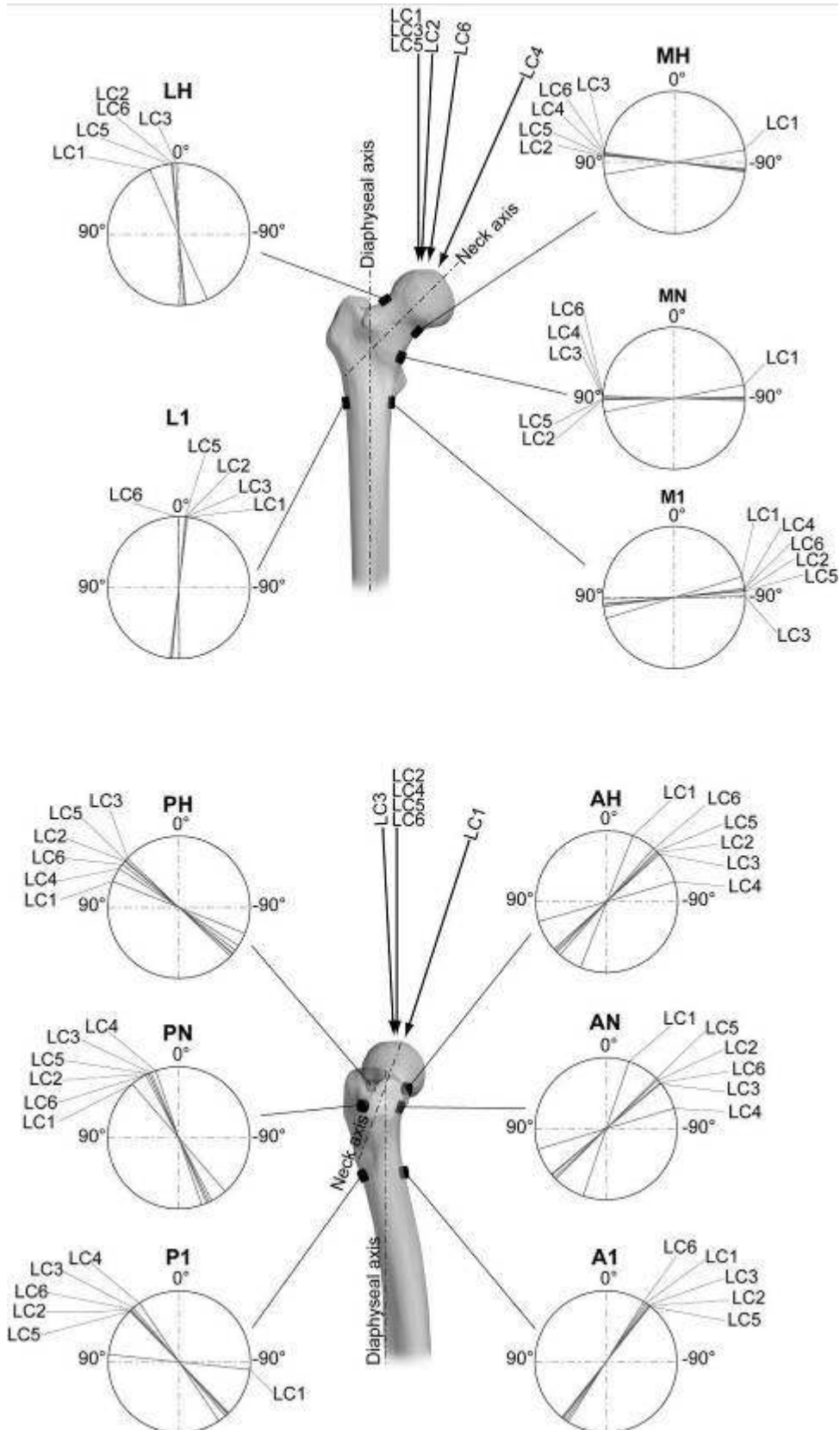


Fig. 4 – Direction of the principal planes. The angle (α_p , positive counter-clockwise) of the maximum tensile principal strain (ϵ_1) was measured with respect to the neck axis in the head and neck region (AH, LH, PH, MH, AN, PN, MN), with respect to the axis of the diaphysis for the strain gauges below the lesser trochanter (A1, L1, P1, M1). The average between 24 femurs is reported for the six loading configurations, for each

measurement location.

The unpaired inter-specimen variability (for the same loading configuration and same strain gauge) affecting the principal strain was larger in the head and neck region, and slightly lower in the diaphysis (Table 2). Variability was one third lower when paired specimens were compared (Table 2). This difference was statistically significant at all strain measurement locations and for all loading configurations (Levene's test, $p < 0.05$).

In the lateral gauges the direction of the maximum principal strain (ϵ_1) lied within $\pm 6^\circ$ from the neck axis (LH) or from the axis of the diaphysis (L1) for all load cases, with the exception of LC1 that was at 24° in LH (Fig. 5). In the medial gauges ϵ_1 was nearly perpendicular ($\pm 8^\circ$) the neck axis (MH, MN) or to the axis of the diaphysis (M1) for all load cases, with the exception of LC1 that was between -80° and -73° (Fig. 5). In the anterior gauges (Fig. 6), the direction of ϵ_1 was close to 45° ($\pm 6^\circ$) from the neck axis (AH, AN) or from the axis of the diaphysis (A1) for all load cases, with the exception of LC1 that was between -22° and -19° (AH, AN) and LC4 (between -74° and -73° in AH, AN). In the posterior gauges (Fig. 6), ϵ_1 lied between 23° and 53° from the neck axis (PH, PN) or from the axis of the diaphysis (P1) for all load cases, with the exception of LC1 and LC4 that differed greatly from each other, and varied between 19° and 84° .

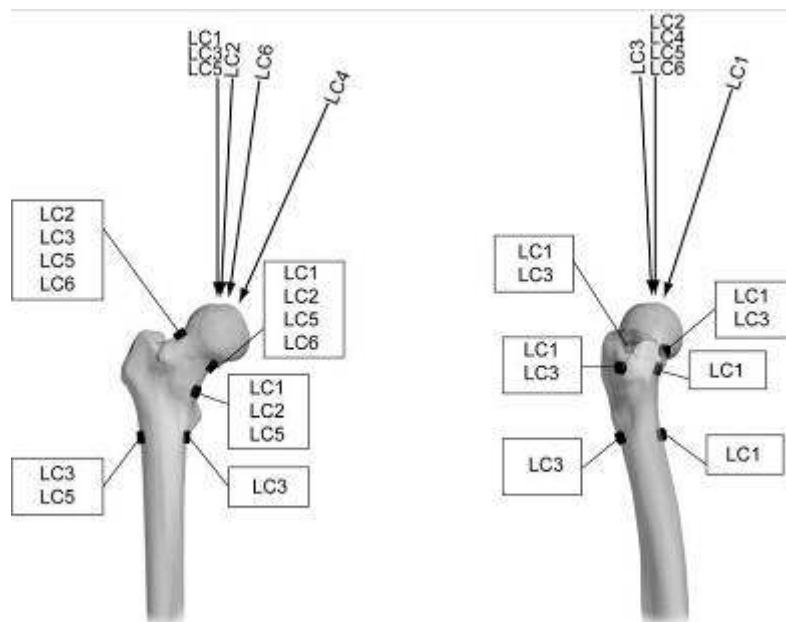


Fig. 5 – Schematic of a right femur (anterior and lateral views), with the indication for each strain measurement location of which loading configuration(s) caused the largest absolute principal strain (Fisher PLSD post-hoc $p < 0.05$). When more loading configurations caused large strain, but did not differ significantly from each other (Fisher PLSD post-hoc $p > 0.05$), they are all indicated. Also indicated is the direction of the hip joint resultant force for each loading configuration, similar to Fig. 2.

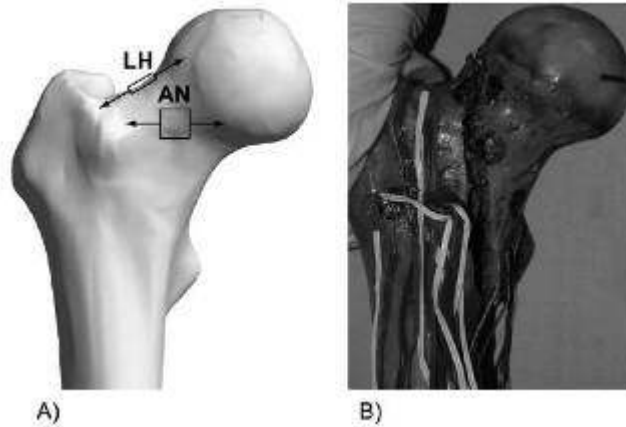


Fig. 6 – A) Schematic of the direction of principal tensile strain ϵ_1 found in the head and neck in this study for most loading configurations. B) Typical image of a femur fractured *in vitro* when a loading configuration identical to LC6 was applied

The angle (θ_p) of the principal planes varied on average by 9° (standard deviation) between unpaired specimens. This inter-specimen variability was larger on the anterior and posterior sides of the head and neck (AH, AN, PH, PN: standard deviation was on average 15°), and smaller on the medial and lateral parts of the neck, and below the lesser trochanter. Similarly to what happened for the values of the principal strains, such variability decreased by nearly one third when paired specimens were compared.

The direction of the applied force had a highly significant effect (ANOVA, $p < 0.0001$) on both principal strains (ϵ_1 and ϵ_2 , Fig. 3 and 4). Also, the strain values varied significantly from location to location (ANOVA, $p < 0.0001$). The location of the largest strains changed in relation to the direction of the applied force. In fact, the lateral part of the head (gauge LH) was the most stressed region for most loading configurations (Fisher PLSD post-hoc, $p < 0.05$). The anterior side (AH, A1) became more stressed when the force was tilted in the frontal plane (LC1). When the force direction was closest to the neck axis (LC4) a more uniform distribution of strain was visible in the head and neck regions.

A correlation was found between the local thickness of cortical bone and the strain values in the same region. The principal tensile strain (ϵ_1) was significantly larger in the regions where the cortical bone was thinner than 1 mm (Table 3). The opposite happened for the principal compressive strain (ϵ_2): it was significantly larger in the regions where the cortical bone was thicker than 1 mm (Table 3).

Table 3 – Significance of correlation between indicators of bone geometry/quality, and magnitude of principal strain

| | | |
|--|---|---|
| | Principal tensile strain (ϵ_1) | Principal compressive strain (ϵ_2) |
|--|---|---|

| | | |
|--|---|---|
| Local thickness of cortical bone | ANOVA, $p < 0.0001$ | ANOVA, $p < 0.0001$ |
| DEXA-assessed bone density (overall) | Pearson's coefficient = -0.111 $p = 0.0004$ | Pearson's coefficient = -0.063 $p = 0.04$ |
| DEXA-assessed bone density (head and neck region, split by strain gauge) | $\text{abs}(\text{Pearson's coefficient}) > 0.05$ $p < 0.05$ | $\text{abs}(\text{Pearson's coefficient}) > 0.05$ $p < 0.05$ |
| DEXA-assessed bone density (proximal diaphysis, split by strain gauge) | $\text{abs}(\text{Pearson's coefficient}) < 0.05$ $p > 0.1$ | $\text{abs}(\text{Pearson's coefficient}) < 0.05$ $p > 0.1$ |
| Biomechanical length, BL | Pearson's coefficient = $+0.092$ $p = 0.0032$ | Pearson's coefficient = -0.094 $p = 0.0025$ |
| Head diameter, HD | Pearson's coefficient = $+0.047$ $p = 0.1$ | Pearson's coefficient = -0.076 $p = 0.015$ |

A low but significant correlation was found between DEXA values and principal tensile and compressive strains (Table 3), when all gauges were pooled together. At a detailed inspection, it was found that such difference was significant for the strain measured in the head and neck region, but not significant below the lesser trochanter (Table 3).

Also, a low but significant correlation was found between biomechanical length (BL) and principal tensile and compressive strain (Table 3). The correlation between head diameter and principal tensile strain (ϵ_1) was not significant, while the correlation between head diameter and principal compressive strain (ϵ_2) was significant (Table 3).

4.1.4 DISCUSSION

The recent resurgence of epiphyseal hip prostheses (Amstutz, Campbell et al. 2004; Grigoris, Roberts et al. 2006; McMinn and Daniel 2006), and the increased rate of traumatic and spontaneous fractures of the proximal femur (Grisso, Kelsey et al. 1991; Rockwood, Green et al. 1991) calls for a better understanding of the stress distribution in the proximal femoral metaphysis. The focus of this work was to better understand the strain distribution in the proximal femur, and its biomechanical determinants.

A procedure was implemented that allowed measuring principal strain and the angle of principal planes at eleven measurement locations, when different loading configurations were applied. Similarly to previous work (Cristofolini, Juszczak et al. 2006; Taddei, Cristofolini et al. 2006), simplified loading configurations were chosen that covered the whole range of angles spanned by the hip joint resultant force (Bergmann, Deuretzbacher et al. 2001). The present results confirm that significantly different strain distributions are obtained with different loading configurations. A similar conclusion was drawn based on theoretical considerations (Fabeck, Tolley et al. 2002) and when testing mouse femurs (Voide, van Lenthe et al. 2008). Therefore, it is recommended that the entire cone of the hip joint resultant force be explored, for instance by testing the extreme angles, like in this study.

The unpaired inter-specimen strain variability was 30%-62% of the measured strain in the head region, 20%-62% in the neck, and 16%-53% in the diaphysis. To the Authors' knowledge, inter-specimen strain variability has never been reported for the proximal metaphysis. A review of the literature (Cristofolini 1997) shows that the reported inter-specimen variability ranges between 13% and 800% when inspecting the femoral diaphysis, which is compatible with the variability found here. An inter-specimen variability of 27–42% was reported for the failure load of the proximal femoral metaphysis (Lochmüller, Groll et al. 2002; Eckstein, Wunderer et al. 2004; Duchemin, Skalli et al. 2006).

The variability was reduced by a factor 0.4-0.8 (depending on measurement location and load configuration) when paired specimens were compared. Similarly, (Eckstein, Wunderer et al. 2004) reported that paired inter-specimen variability affecting failure load of the proximal femoral metaphysis (12%) was 3.5 times lower than unpaired inter-specimen variability (42%). This indicates that paired specimens should be used whenever possible to allow more powerful comparisons. However, even paired inter-specimen variability was one order of magnitude larger than intra-specimen variability. Part of the paired inter-specimen variability is due to the fact that we had to adjust the actual strain measurement location between specimens (difference in position between paired specimens of up to 4 mm), due to small defects on the bone surface. Therefore, using paired specimens can only partially reduce test variability. If better repeatability is sought, composite femur models should be considered (Cristofolini, Viceconti et al. 1996; Heiner and Brown 2001).

The strains varied significantly in relation to the measurement location and load configuration. The average principal tensile strain (ϵ_1) was 217 microstrain; the average principal compressive strain (ϵ_2) was -309 microstrain. Such values were recorded when a

force of 0.75BW was applied. The typical load values recorded for physiological activities such as level walking at different speeds, single-leg-stance, stair-climbing and -descending, standing up from seated (Bergmann, Deuretzbacher et al. 2001) are 1.9-2.6BW. If a proportion is applied (linear behaviour of bone in the strain range used this study was confirmed) considering a force of 2.5BW, the strain values recorded here scale respectively to 725 (ϵ_1) and -1029 microstrain (ϵ_2). These values are comparable with those measured *in vitro* by (Field and Rushton 1989) (up to 1800microstrain with 1500N hip joint resultant force). The present values also compare favorably with *in vivo* recorded strains: peak strain in the human femur during walking was -393 microstrain (ϵ_2), and 1198 microstrain (ϵ_1); during strain climbing, strain ranged -194 to -948 (ϵ_2), and 1013 to 1454 microstrain (ϵ_1); during one-legged stance, strain ranged -60 to -435 (ϵ_2), and 1225 to 1463 microstrain (ϵ_1) (Aamodt, Lund-Larsen et al. 1997). *In vivo* peak strain in the human tibia during walking was -434 microstrain (ϵ_2), and 395 microstrain (ϵ_1); during running, peak strain was -578 microstrain (ϵ_2), and 847 microstrain (ϵ_1) (Lanyon, Hampson et al. 1975).

In fact, physiological strain (to prevent bone remodeling and resorption) is assumed to be in the range of 1000 microstrain (Lanyon 1980). It must be remarked that, while average strain was close to such value, inter-specimen strain variability in this study was quite high (up to 62%). This suggests that physiological strain may indeed vary between subjects. This hypothesis is further supported by the fact that, although the applied force was scaled by donor's body weight, strain distribution was correlated with subject-specific indicators such as bone quality (DEXA-assessed density), and gross dimensions (biomechanical length, head diameter). Such correlation was low (indicating that bone quality and gross dimensions are not the only factors determining the strain distribution), but statistically significant.

In para-physiological tasks (e.g.: stumbling or mis-stepping), hip resultant forces up to 7.2-8.7BW were occasionally recorded (Bergmann, Graichen et al. 1993; Bergmann, Graichen et al. 2004). The largest principal tensile strain found here was 497 microstrain (average of 24 femurs for location LH, loading configuration LC3). If such peak strain is scaled to 8.7BW, a strain peak of 5762 microstrain is obtained. Such strain value would be sub-critical. In fact, it can be assumed that healthy bone fails when principal tensile strain (ϵ_1) exceeds 7300 microstrain (Bayraktar, Morgan et al. 2004). However, a peak of more than 730 microstrain was measured in four specimens (these femurs were characterized by low DEXA density, and should be classified as osteoporotic (WHO 1994; NIH 2000)): this

would scale to 8468 microstrain for the loads encountered in stumbling and mis-stepping (8.7BW). Thus, the strain peak in such four femurs is compatible with the spontaneous fractures (i.e.: caused by sudden loading and muscle contraction, not by trauma (Rockwood, Green et al. 1991; Cotton, Whitehead et al. 1994; WHO 1994)) observed in osteoporotic subjects as a consequence of occasional overloading events such as stumbling or mis-stepping. Also, the location of the measured strain peak (LH) is in agreement with the failure mode observed *in vitro* for this type of loading (Cristofolini, Juszczuk et al. 2007).

Principal tensile strain was generally aligned with the axis of the neck/diaphysis on the lateral side, and was perpendicular on the medial side. This confirms the predominance of bending in the frontal plane, in agreement with the literature (Cristofolini and Viceconti 1999). Principal strains were generally close to 45° from the axis of the neck/diaphysis on the anterior and posterior sides for most strain measurement locations and load cases. This suggests the presence of shear stress on the anterior and posterior sides (the main exception being LC1, that tended to generate torsion). This is in agreement with previous theoretical considerations (Fabeck, Tolley et al. 2002). The direction of principal strains varied by a relatively small angle between loading configurations (less than 6.7° at all strain measurement locations), if LC1 and LC4 were excluded. As strain measurements were performed when the applied force was tilted to cover the cone spanned by the hip joint resultant (Bergmann, Deuretzbacher et al. 2001), this suggests that the principal strain directions vary little for most physiological motor tasks. Hence, the state of stress in the proximal metaphysis allows structural optimization (in terms of local tissue arrangement, and anisotropy) to face most physiological tasks. This should be put in relation to the optimized shape of the femoral neck (Fabeck, Tolley et al. 2002).

It is remarkable that the direction of principal tensile strain (ϵ_1) in the head and neck region (Fig. 8) for most loading configurations was in agreement with the direction of the spontaneous fractures observed clinically (Grisso, Kelsey et al. 1991; Rockwood, Green et al. 1991), and reported experimentally (Cotton, Whitehead et al. 1994; Yang, Shen et al. 1996; Cody, Gross et al. 1999; Keyak, Skinner et al. 2001; Cristofolini, Juszczuk et al. 2007).

Fig. 8 – A) Schematic of the direction of principal tensile strain ϵ_1 found in the head and neck in this study for most loading configurations. B) Typical image of a femur fractured *in vitro* when a loading configuration identical to LC6 was applied (Cristofolini, Juszczuk et al. 2007).

The principal tensile strain (ϵ_1) was significantly larger where the cortical bone was thinner than 1 mm, while the principal compressive strain (ϵ_2) was significantly larger where the

cortical bone was thicker than 1 mm. This observation is possibly related to the fact that bone tissue is weaker in tension than in compression (Carter and Spengler 1978; Fung 1980; Lanyon 1980; Roesler 1987): where the structure is loaded in compression, the bone adapts itself by simply increasing the amount of material resisting to the load (increased cortical thickness); where high tensile stress is present, a simple increase of the bone mass would be inefficient and the structure adapts itself by assuming a more complex morphology (thin cortical shell and 3-dimensional arrangement of the trabecular bone).

There are some limitations that should be discussed. First of all, in order to make the test setup as simple as possible (Currey 2008), muscle forces were not simulated. It has been reported that the internal stresses in the femoral diaphysis decrease if the muscles forces are taken into account (Taylor, Tanner et al. 1996; Duda, Schneider et al. 1997). However, experimental and FE studies indicated that muscle forces do not significantly alter the stress distribution in the proximal femoral metaphysis (Cristofolini, Viceconti et al. 1995; Cody, Gross et al. 1999; Keyak, Kaneko et al. 2005; Cristofolini, Juszczuk et al. 2006; Cristofolini, Juszczuk et al. 2007).

Using strain gauges in the metaphyseal region (where bone is particularly thin) can cause a significant reinforcing effect (up to 15% of the measured strain). The fact that the estimated reinforcement varied by one order of magnitude from region to region and between specimens makes it impossible to satisfactorily compensate for such error. The effect of reinforcement becomes negligible when bone strains are compared under different conditions (e.g.: intact versus implanted) by computing a strain ratio on the same specimen (Cristofolini, Cappello et al. 1994; Cristofolini 1997). Also, this artifact becomes small (<4%) where the cortical bone is thicker than 1 mm. It must be noticed that the reinforcing effect was estimated including only the contribution of the cortical shell to structural stiffness. As the trabecular bone was neglected, these estimates provide an indication of the upper boundary of such error.

In conclusion, this study provided a deeper understanding of the strain distribution in the proximal femoral metaphysis. The typical patterns of principal strain and angle of the principal planes were analyzed when different loading configurations were simulated. The reasons for inter-specimen variability were investigated both within the same pair and between pairs. Dependence of strain on local bone characteristics, and also on subject-specific biomechanical factors was demonstrated.

Acknowledgments: The Authors wish to thank Enrico Schileo, Martino Pani and Fulvia Taddei for the valuable discussions; Elena Varini, Francesco Pallini and Mauro Della Motta for the support during the tests; Barbara Bordini and Manuela De Clerico for the statistical analysis; Luigi Lena for the artwork. This work was partially supported by the European Community (project number: IST-2004-026932; title: Living Human Digital Library; acronym: LHDL).

4.1.5 References

- Aamodt, A., J. Lund-Larsen, et al. (1997). "In vivo measurements show tensile axial strain in the proximal lateral aspect of the human femur." J Orthop Res. 15(6): 927-931.
- Ajovalasit, A. and B. Zuccarello (2005). "Local reinforcement effect of a strain gauge installation on low modulus materials." J. Strain Analysis in Engineering Design 40(7): 643-654.
- Amstutz, H. C., P. A. Campbell, et al. (2004). "Fracture of the neck of the femur after surface arthroplasty of the hip." J. Bone Jt. Surg. Am. 86: 1874-1877.
- Augat, P., H. Reeb, et al. (1996). "Prediction of fracture load at different skeletal sites by geometrical properties of the cortical shell." J. Bone and Mineral Research 11(9): 1356-1363.
- Bayraktar, H. H., E. F. Morgan, et al. (2004). "Comparison of the elastic and yield properties of human femoral trabecular and cortical bone tissue." J Biomech 37(1): 27-35.
- Beatty, M. F. and S. W. Chewning (1979). "Numerical analysis of the reinforcement effect of a strain gage applied to a soft material." Int. J. Engineering Sci. 17: 907-915.
- Bergmann, G., G. Deuretzbacher, et al. (2001). "Hip contact forces and gait patterns from routine activities." J Biomech 34(7): 859-71.
- Bergmann, G., F. Graichen, et al. (1993). "Hip joint loading during walking and running, measured in two patients." J Biomech. 26: 969-990.
- Bergmann, G., F. Graichen, et al. (2004). "Hip contact forces during stumbling." Langenbecks Arch. Surg. 389: 51-59.
- Carter, D. R. and D. M. Spengler (1978). "Mechanical properties and composition of cortical bone." Clin Orthop Relat Res. 135: 192-217.
- Cody, D. D., G. J. Gross, et al. (1999). "Femoral strength is better predicted by finite element models than QCT and DXA." J Biomech 32(10): 1013-20.
- Cotton, D. W. K., C. L. Whitehead, et al. (1994). "Are hip fractures caused by falling and breaking or breaking and falling? Photoelastic stress analysis." Forensic Science International 65(2): 105-112.
- Crick, D., J. Wagner, et al. (1985). "Comportement mécanique de l'épiphyse supérieure de fémur resurfacé et incidence des variations anatomiques et des différentes types de cupules." Acta Orthop. Belg. 51: 168-178.
- Cristofolini, L. (1997). "A critical analysis of stress shielding evaluation of hip prostheses." Critical Reviews in Biomedical Engineering 25:4&5: 409-483.

- Cristofolini, L., A. Cappello, et al. (1994). "Experimental errors in the application of photoelastic coatings on human femurs with uncemented hip stems." Strain 30(3): 95-103.
- Cristofolini, L., M. Juszczak, et al. (2007). "In vitro replication of spontaneous fractures of the proximal human femur." J. Biomechanics 40(13): 2837-2845.
- Cristofolini, L., M. Juszczak, et al. (2006). Biomechanical testing of the proximal femoral epiphysis: intact and implanted condition. 8th Biennial Conference on Engineering Systems Design and Analysis ASME-ESDA 2006, Turin, ASME.
- Cristofolini, L., F. Taddei, et al. (2008). "Multiscale investigation of the functional properties of the human femur." Philos Transact A Math Phys Eng Sci 366(1879): 3319-41.
- Cristofolini, L. and M. Viceconti (1999). "Towards the standardization of in vitro load transfer investigations of hip prostheses." Journal of Strain Analysis for Engineering Design 34(1): 1-15.
- Cristofolini, L. and M. Viceconti (2000). "Development and validation of a technique for strain measurement inside polymethylmethacrylate." J. Strain Analysis in Engineering Design 35(1): 21-33.
- Cristofolini, L., M. Viceconti, et al. (1996). "Mechanical validation of whole bone composite femur models." J Biomech 29(4): 525-35.
- Cristofolini, L., M. Viceconti, et al. (1995). "Influence of thigh muscles on the axial strains in a proximal femur during early stance in gait." J Biomech 28(5): 617-624.
- Currey, J. (1998). Cortical bone. Handbook of biomaterial properties. J. Black and G. Hastings. London, Chapman & Hall: 3-14.
- Currey, J. (2008). "Whole-bone mechanics: 'the best is the enemy of the good'." Vet J 177(1): 1-2.
- Dally, J. W. and W. F. Riley (2005). Experimental stress analysis. Knoxville, College House Enterprises.
- Duchemin, L., W. Skalli, et al. (2006). Femoral fracture load and failure energy in two load configurations: an in vitro study. 16th EORS Annual meeting, Bologna, CLUEB.
- Duda, G. N., E. Schneider, et al. (1997). "Internal forces and moments in the femur during walking." J Biomech 30: 933-941.
- Eckstein, F., C. Wunderer, et al. (2004). "Reproducibility and side differences of mechanical tests for determining the structural strength of the proximal femur." J. Bone and Mineral Research 19(3): 379-385.
- Fabeck, L., M. Tolley, et al. (2002). "Theoretical study of the decrease in the femoral neck anteversion during growth." Cells Tissues Organs 171(4): 269-75.
- Fenner, J. W., B. Brook, et al. (2008). "The EuroPhysiome, STEP and a roadmap for the virtual physiological human." Philos Transact A Math Phys Eng Sci 366(1878): 2979-99.
- Field, R. E. and N. Rushton (1989). "Proximal femoral surface strain gauge analysis of a new epiphyseal prosthesis." J. Biomed. Eng. 11: 123-129.
- Fung, Y. C. (1980). Bone and cartilage. Biomechanics - Mechanical properties of living tissues. New York, Springer Verlag: 383-415.
- Grigoris, P., P. Roberts, et al. (2006). "Hip resurfacing arthroplasty: the evolution of contemporary designs." Proc. Instn. Mech. Engrs. Part H: J. Engineering in Medicine 220(2): 95-105.
- Grisso, J. A., J. L. Kelsey, et al. (1991). "Risk factors for falls as a cause of hip fracture in women. The Northeast Hip Fracture Study Group." N. Engl. J. Med. 324(19): 1326-31.

- Heiner, A. D. and T. D. Brown (2001). "Structural properties of a new design of composite replicate femurs and tibias." J Biomech 34(6): 773-81.
- Huiskes, R., H. Weinans, et al. (1987). "Adaptive bone-remodeling theory applied to prosthetic-design analysis." J Biomech 20(11-12): 1135-50.
- Keyak, J. H., T. S. Kaneko, et al. (2005). "Predicting proximal femoral strength using structural engineering models." Clin Orthop Relat Res(437): 219-28.
- Keyak, J. H., H. B. Skinner, et al. (2001). "Effect of force direction on femoral fracture load for two types of loading conditions." J Orthop Res 19(4): 539-44.
- Lanyon, I. E. (1980). Bone remodelling, mechanical stress, and osteoporosis. Osteoporosis. H. F. De Luca. Baltimore, University Park Press: 129-138.
- Lanyon, L. E., W. G. J. Hampson, et al. (1975). "Bone deformation recorded in vivo from strain gauges attached to the human tibial shaft." Acta Orthop. Scand. 46: 256-268.
- Little, E. G., D. Tocher, et al. (1990). "Strain gauge reinforcement of plastics." Strain 26: 91-98.
- Lochmüller, E.-M., O. Groll, et al. (2002). "Mechanical strength of the proximal femur as predicted from geometric and densitometric bone properties at the lower limb versus the distal radius." Bone 30(1): 207-216.
- Lotz, J. C., E. J. Cheal, et al. (1991). "Fracture prediction for the proximal femur using finite element models: Part I--Linear analysis." J Biomech Eng 113(4): 353-60.
- McMinn, D. and J. Daniel (2006). "History and modern concepts in surface replacement." Proc. Instn. Mech. Engrs. Part H: J. Engineering in Medicine 220(2): 239-251.
- Montgomery, D. C. (2005). Design and analysis of experiments. New York, J. Wiley.
- NIH (2000). Consensus Statement on Osteoporosis Prevention, Diagnosis, and Therapy, NIH Consens Statement Online, US Department of Health and Human Services, National Institute of Health, 2000 March 27-29; 17(1): 1-36.
- Perry, C. C. (1985). "Strain-gage reinforcement effects on low-modulus materials." Experimental techniques 9: 25-27.
- Rockwood, C. A. J., D. P. Green, et al. (1991). Rockwood and Green's fractures in adults. Philadelphia, J.B. Lippincott.
- Roesler, H. (1987). "The history of some fundamental concepts in bone biomechanics." J Biomech. 20: 1025-1034.
- Rohlmann, A., U. Mossner, et al. (1983). "Finite-element- analysis and experimental investigation in a femur with hip endoprosthesis." J Biomech. 16: 727-742.
- Ruff, C. B. and W. C. Hayes (1983). "Cross-sectional Geometry of Pecos Pueblo Femora and Tibiae - A Biomechanical Investigation: I. Method and General Patterns of Variation." Am. J. Phys. Anthropol. 60: 359-381.
- Taddei, F., L. Cristofolini, et al. (2006). "Subject-specific finite element models of long bones: An in vitro evaluation of the overall accuracy." J Biomech 39(13): 2457-67.
- Taylor, M. E., K. E. Tanner, et al. (1996). "Stress and strain distribution within the intact femur: compression or bending?" Med. Eng. Phys. 18: 122-131.
- Viceconti, M., F. Taddei, et al. (2008). "Multiscale modelling of the skeleton for the prediction of the risk of fracture." Clin Biomech (Bristol, Avon).
- Viceconti, M., A. Toni, et al. (1992). Strain gauge analysis of hard tissues: factors influencing measurements. Experimental Mechanics. Technology transfer between high tech engineering and biomechanics. E. G. Little. Amsterdam, Elsevier Science Publisher B.V.: 177-184.

- Voide, R., G. H. van Lenthe, et al. (2008). "Femoral stiffness and strength critically depend on loading angle: a parametric study in a mouse-inbred strain." Biomed Tech (Berl) 53(3): 122-9.
- WHO (1994). Assessment of fracture risk and its application to screening for postmenopausal osteoporosis. Report of a WHO study group. WHO Technical Report Series, World Health Organization, Geneva, Switzerland, 843: 1-130.
- Yang, K.-H.-, K. L. Shen, et al. (1996). "The relationship between loading conditions and fracture patterns of the proximal femur." J. Biomech. Eng. 118(4): 575-578.

4.2 IN VITRO REPLICATION OF SPONTANEOUS FRACTURES OF THE PROXIMAL HUMAN FEMUR

Luca Cristofolini, PhD ^{1,2}, Mateusz Juszczak, MEng ^{1,2}, Saulo Martelli, MEng ^{1,2}, Fulvia Taddei, PhD ¹, Marco Viceconti, PhD ¹

¹Laboratorio di Tecnologia Medica, Istituti Ortopedici Rizzoli, Bologna, Italy

²Engineering Faculty, University of Bologna, Italy

The author has significantly contributed into creation of the experimental setup and executing measurements. **This work was published on Journal of Biomechanics.**

4.2.1 ABSTRACT

Spontaneous fractures (ie: caused by sudden loading and muscle contraction, not by trauma) represent a significant percentage of proximal femur fractures. They are particularly relevant as may occur in elderly (osteoporotic) subjects, but also in relation to epiphyseal prostheses. Despite its clinical and legal relevance, this type of fracture has seldom been investigated. Studies concerning spontaneous fractures are based on a variety of loading scenarios. There is no evidence, nor consensus on the most relevant loading scenario. The aim of this work was to develop and validate an experimental method to replicate spontaneous fractures *in vitro* based on clinically relevant loading. Primary goals were: (i) repeatability and reproducibility, (ii) clinical relevance. A validated numerical model was used to identify the most critical loading scenario that can lead to head-neck fractures, and to determine if it is necessary to include muscle forces when the head-neck region is under investigation. The numerical model indicated that the most relevant loading scenario is when the resultant joint force is applied to the head at 8° from the diaphysis. Furthermore, it was found that it is not essential to include the muscles when investigating head-neck fractures. The experimental setup was consequently designed. The procedure included high-speed filming of the fracture event. Clinically relevant fracture modes were obtained on 10 cadaveric femurs. Failure load should be reported as a fraction of donor's body-weight to reduce variability. The proposed method can be used to investigate the reason and mechanism of failure of natural and operated proximal femurs.

Keywords:

Fracture testing, simulation of spontaneous fracture, proximal femoral metaphysis, *in vitro* test to failure, Finite Element models

4.2.2 INTRODUCTION

Spontaneous fractures of the hip can be defined as those fractures deriving from physiological or sudden loading, but not from a traumatic event (they may eventually result in secondary trauma, but they are not caused by trauma)(Cotton et al., 1994; Jeffery, 1974; Rockwood et al., 1991; Rüedi and Murphy, 2001). They most frequently occur in elderly (osteoporotic) subjects. (Yang et al., 1996) developed two *in vitro* simulations (later replicated numerically by (Gomez-Benito et al., 2005)) to determine the biomechanical background for spontaneous hip fractures. They suggested that abnormal muscle contraction of the rotator muscles could induce hip fracture. In addition, bone fractures may occur as a consequence of excessive cyclic loading (Cotton, et al., 1994; Jeffery, 1974; Rockwood, et al., 1991; Rüedi and Murphy, 2001). However, cyclic fractures typically occur because of excessive load/activity, and usually do not involve the proximal femur. As the focus of this paper is on fractures of the proximal femur occurring in elderly subjects, cyclic fractures will not be considered hereafter. There are mainly two reasons to investigate the biomechanics of spontaneous fractures of the proximal femoral metaphysis:

- 1) A significant fraction (though not the majority) of fractures of the untreated hip in the elderly are not associated with a primary traumatic event(Cotton, et al., 1994; Rockwood, et al., 1991; Rüedi and Murphy, 2001). While the actual estimate of such fraction is difficult (elderly patients are often unable to report whether they fell before or after the fracture), it must account for 10% to 60% of the hip fractures (Grisso et al., 1991; Michelson et al., 1995; Muckle, 1976). (Mayhew et al., 2005) suggested that buckling of the thin cortical shell could be one failure-initiating event if the underlying trabeculae are weakened by osteoporosis.
- 2) With the recent return to resurfacing prostheses, concerns exist about risk of neck fractures due to physiological loading (Amstutz et al., 2004; Shimmin and Back, 2005; Shimmin et al., 2005; Siebel et al., 2006). This event is clinically undesirable. It also has serious legal implications (especially in the case of spontaneous fractures).

In most cases, patients cannot recall what motor task was performed at the time of fracture, or report having been stumbling or tripping on an obstacle (Grisso, et al., 1991; Michelson, et al., 1995). In the first case the motor task is unknown, but even in the second case the direction of the applied loads is hard to determine. Therefore, there is no clear indication as

to which is the relevant loading mode when spontaneous fractures occur. Additionally, the type of fracture that will develop and the required load cannot be easily predicted *a priori* (Jarvinen et al., 2005).

Traumatic femoral fractures due to impact on the greater trochanter as a consequence of sideways fall have been extensively investigated *in vitro* (Deler et al., 2005; Eckstein et al., 2004; Keyak et al., 1998; Lang et al., 1997; Lochmüller et al., 1998; Mayhew, et al., 2005). Traumatic and spontaneous fractures exhibit different cracking modes and regions (Backman, 1957; Cotton, et al., 1994; Eckstein, et al., 2004; Keyak, 2000; Keyak et al., 2001; Rockwood, et al., 1991).

Several numerical and *in vitro* studies have been carried out attempting to simulate spontaneous fractures. However, there is no consensus concerning the relevant loading scenario to be simulated. The direction of the force applied on the femoral head ranges between 0° (Lochmüller et al., 2002; Lochmüller et al., 2000; Lochmüller, et al., 1998; Lotz et al., 1991), 11° (Link et al., 2003), 20° (Keyak, et al., 1998; Keyak, 2000; Lang, et al., 1997), 24° (Smith et al., 1992), and 25° (Cody et al., 1999; Delaere et al., 1989) in the frontal plane, or even perpendicular to the shaft (Dalen et al., 1976). In other cases (e.g.: (Alho et al., 1988; Ota et al., 1999; Patel and Murphy, 2006)) the loading direction is not specified (with limitations discussed elsewhere (Cristofolini, 2007)). This lack of agreement concerning the loading scenario undermines comparison between tests, as the direction of the load severely affects the stress distribution (Cristofolini, 1997; Cristofolini and Viceconti, 1999; Voide et al., 2006), hence failure. Keyak *et al* addressed the issue of the loading direction (Keyak et al., 2001) and tried to assess the relevance of the muscle force on simulated failure (Keyak et al., 2005). Their conclusions were that it should not be necessary to simulate the muscles, and single-leg-stance (resultant force at 10° in the frontal plane) and stair-climbing (30° in the sagittal plane) are the most relevant loading conditions. However, their indications cannot be considered conclusive, as they never tested experimentally the single-leg stance loading condition they identified (in all experiments they applied a resultant force at 20° in the frontal plane (Keyak, et al., 1998; Keyak, et al., 2005; Keyak, et al., 2001)). In addition in the cited work (Keyak, et al., 2001), they did not provide any indications on the femoral region subjected to the highest stress-strain levels in the one-leg-stance configuration, thus providing no numerical evidence that this configuration may result in clinically relevant neck fractures. Therefore, there is a need for more extensive work based on state-of-the-art FE models, to confirm which is, the most relevant loading scenario for replicating *in vitro* spontaneous neck fractures.

The goals of this work were to:

- Develop a rationale and identify the most relevant loading scenario to recreate *in vitro* spontaneous hip fractures;
- Develop the simplest possible testing protocol so as to increase repeatability and reproducibility (including assessment of the need to apply the muscle forces in the *in vitro* setup);
- Validate such protocol by testing a sample of human femurs, and assessing the fractures recreated *in vitro*, in comparison with those observed in the clinical practice.

4.2.3 MATERIALS AND METHODS

4.2.3.1 Identification of the most critical loading scenario: FE simulations

A highly detailed Finite Element (FE) model of a human femur, which was previously validated against experimental measurements (Taddei et al., 2006) was used to complement this study. A relevant donor for the FE study was selected (male, died 51 of intracerebral hemorrhage, free of musculoskeletal disease, smoker, osteoporotic, 175 cm tall, weighing 75 kg). The FE model included a dedicated material mapping strategy to assign suitable material properties to each element (Taddei et al., 2004; Taddei et al., 2006). It was used to perform a preliminary sensitivity analysis to address the following two questions:

- 1) Does the application of the muscle forces (below the intertrochanteric region) affect the strain distribution in the head-neck region, or is it sufficient to apply the joint load with the right direction and intensity? This question was addressed by simulating inclusion and exclusion of the muscle forces, when the same resultant joint force was simulated under simulated single-leg stance during gait (Bergmann, 2001; Bergmann et al., 2001).
- 2) Which is the direction of the hip joint resultant force that can cause the highest risk of failure in the head-neck region with respect to the diaphyseal one, to obtain clinically relevant failure scenario for the proximal femur? In fact, a preliminary study indicated that when unsuitable scenarios are applied, diaphyseal fractures might occur before the head-neck region fails. Once the first question was answered, the second one was addressed by exploring the five most frequent loading scenarios (level walking, stair

climbing and descending, one-leg stance, standing up), as reported in (Bergmann, 2001; Bergmann, et al., 2001).

The model consisted of 76,026 10-node tetrahedral elements. The inhomogeneous material properties were derived from the calibrated Computed Tomography (CT) dataset of the same femur (Taddei, et al., 2004) and resulted in 381 different materials. More details are reported in (Taddei, et al., 2006).

4.2.3.2 Experimental setup, measurements and recording

The *in vitro* set-up was designed based on previous experience with non-destructive testing of the proximal femur (Cristofolini, 1997; Cristofolini et al., 2003; Cristofolini and Viceconti, 1999; Cristofolini et al., 1995).

The femur specimens were prepared with a set of reference axes to allow for reproducible alignment throughout the test, following a validated protocol (Cristofolini and Viceconti, 1999; Ruff and Hayes, 1983). The femurs were stored at -25°C when not in use. During the test they were wrapped in clothes soaked with physiological solution and tested at a room temperature of $27\text{-}30^{\circ}\text{C}$.

The femoral condyles were potted in a steel box with dental cement meeting the ISO 5833 requirements. The femur was mounted on top of the load cell of the testing machine with the diaphysis at an angle of 8° in the frontal plane (as defined by the sensitivity analysis performed with the FE, Section 3.1). Load was applied to the femora head through a system of rails to avoid transmission of horizontal force components (Fig. 1). A copy of each femoral head was prepared with dental cement (covering $1/5$ head diameter) to allow uniform load transfer from the actuator to the head. Muscle forces were not simulated, as the FE models indicated this is not necessary in this application (Section 3.1).



Fig. 1 – Experimental setup used to fracture the proximal femurs *in vitro*. Left: overview of the testing setup where the high-speed camera is visible on the left (directly facing the superior-lateral part of the femur),

together with the light source; the bone specimen is under the testing machine on the right. Centre: Intact femur mounted on the material testing machine with the diaphysis at 8° from vertical; the cross-rails to eliminate horizontal force components are visible on the top; the two mirrors are visible near the femur (they were oriented so as to reflect the anterior-medial and posterior-medial sides of the femur). Right: detail of the proximal femur, with the mirrors and the copy of the femoral head for applying the load to the femur. The strain gauges bonded on the bone surface were part of a separate study.

Load was applied at a constant displacement rate of 2mm/sec, which resulted in the femurs failing within 0.5-2 seconds. Load and displacement were recorded by the testing machine (8502, Instron, Canton, MA, USA) at 1000Hz.

During the destructive test the event was filmed by means of a high-speed camera (FastCam-X1024PCI, Photron, U.K.) at 3000-9000 frames/second (actual frame rate depended on the size of the field of vision cropped for each specimen). The camera pointed at the superior-lateral part of the neck. Two mirrors were used to film at the same time the anterior-medial and posterior-medial portions of the neck.

4.2.3.3 Assessment of the test protocol

The test protocol above was applied to 10 cadaveric human femurs (Table 1) to confirm if clinically relevant failure modes and fracture load could be obtained. Specimens were chosen from relatively aged donors so as to represent the target population. Suitable fresh-frozen bone specimens were obtained through IIAM (Jessup, PA, USA). They were DEXA-scanned (Excel-Plus, Norland, USA) and CT-scanned (HiSpeed, General Electric, USA) to document bone quality and lack of abnormality or defects. Anatomical dimensions (head diameter and biomechanical length) were measured (Table 1 (Ruff and Hayes, 1983))

Table 1 – Details of the twelve femur specimens investigated. In the first four columns, details of the donor are listed. Bone quality is reported in the 6th and 7th column (bone density as % of the young reference population, and of the age-matched population computed based on the Norland DEXA scanner reference population). Biomechanical dimensions (Ruff and Hayes, 1983) are reported in the 8th and 9th columns. Failure load in Newton and as a fraction of the donor's Body Weight is reported. The failure mode is reported in the last three columns: based on anatomical location (Rockwood, et al., 1991); AO Müller Classification (31-A= extracapsular trochanteric; 31-B= intracapsular neck; 31-C= intracapsular head)(Rüedi and Murphy, 2001);

Pauwels' classification based on fracture direction (I= fracture nearly perpendicular to femoral diaphysis; II = nearly perpendicular to neck axis; III = nearly parallel to femoral diaphysis)(Pauwels, 1935).

| DONOR'S DETAILS | | | | FEMUR'S DATA | | | | | FAILURE LOAD | | FAILURE MODE | | |
|-----------------|--------------|-------------------|-------------------|--------------|-----------------------|-------------------|----------------------------|---------------------|--------------|-------|---|-------------|------------|
| Sex | Age at death | Donor Height (cm) | Donor Weight (kg) | SIDE | DEXA% young reference | DEXA% age matched | Average head diameter (mm) | Biomech length (mm) | N | x BW | Anatomical location | AO Müller | Pauwels |
| M | 67 | 173 | 82 | Left | 75.9% | 90.0% | 49.7 | 415 | 11370 | 14.13 | intracapsular: base neck | 31B | III |
| M | 72 | 173 | 100 | Right | 82.5% | 100.1% | 46.6 | 414 | 11170 | 11.39 | intracapsular: transcervical (+ subcapital) | 31B (+ 31C) | III (+ II) |
| M | 70 | 175 | 90 | Left | 66.2% | 79.6% | 47.7 | 443 | 11770 | 13.33 | transcervical extracapsular | 31B (+ 31A) | III |
| M | 51 | 175 | 164 | Left | 91.0% | 99.4% | 53.5 | 463 | 16040 | 9.97 | extracapsular: base neck | 31B | II |
| F | 83 | 157 | 48 | Left | 60.9% | 77.8% | 46.8 | 421 | 7931 | 16.84 | intracapsular: transcervical | 31B | III |
| M | 80 | 178 | 88 | Right | 62.2% | 76.4% | 52.0 | 437 | 7093 | 8.22 | intracapsular: transcervical | 31B | III |
| M | 67 | 175 | 88 | Right | 59.1% | 70.0% | 52.0 | 423 | 7427 | 8.60 | intracapsular: transcervical | 31B | III |
| M | 71 | 178 | 91 | Right | 76.2% | 92.0% | 53.3 | 443 | 7921 | 8.87 | intracapsular: transcervical (near base neck) | 31B | II |
| M | 82 | 175 | 78 | Left | 47.9% | 58.9% | 49.4 | 432 | 6401 | 8.37 | intracapsular: transcervical | 31B | III |
| M | 73 | 175 | 73 | Left | 47.7% | 58.2% | 46.9 | 433 | 6319 | 8.82 | intracapsular: transcervical (near base neck) | 31B | III |

Note ⁽¹⁾: failed due to transcervical fracture, but subcapital fracture initiated in parallel;

Note ⁽²⁾: started from lateral cartilage edge, propagated below lesser trochanter;

Note ⁽³⁾: started from lateral cartilage edge, bifurcated and propagated along cartilage edge;

Note ⁽⁴⁾: started from lateral cartilage edge, propagated along the neck (above lesser trochanter).

4.2.4 RESULTS

4.2.4.1 Most critical loading scenario: FE simulations

In the FE model, the inclusion/exclusion of the abductor muscles affected the strain distribution in the superior aspect of the head-neck region (Fig. 2). However, this effect was quite moderate. Moreover, higher peak tensile strains were found when the muscles were not simulated. Therefore, exclusion of the muscles tends to slightly overestimate the risk of fracture (when the same joint resultant force is applied).

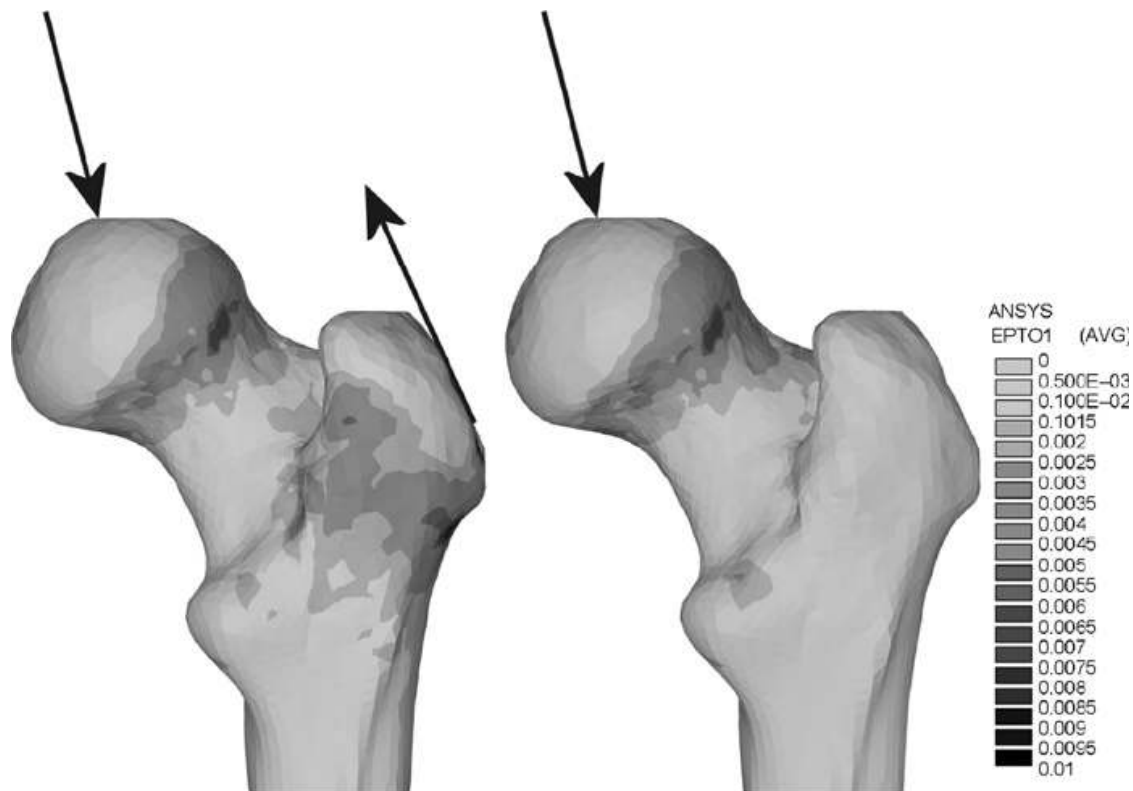


Fig. 2 – Principal tensile strain in the proximal femur when the abductor muscles are simulated (left) and when these muscles are not simulated, while the same resultant force is applied to the femoral head (right). The plots show that minimal strain alterations are induced in the head-neck region by the inclusion/exclusion of the abducting muscles.

The finite element models indicated that, among the directions recorded by (Bergmann, 2001; Bergmann, et al., 2001), the loading scenario that generates the highest risk of failure of the neck region is the one-leg stance configuration, when the force lies in the frontal plane at 8° from the diaphysis (Fig. 3). In fact, while other scenarios have a larger stress below the trochanteric region or in the diaphysis, this is the condition with the highest risk in the neck (ie: the loading scenario that, if incrementally scaled, may lead to a fracture in the head-neck region first).

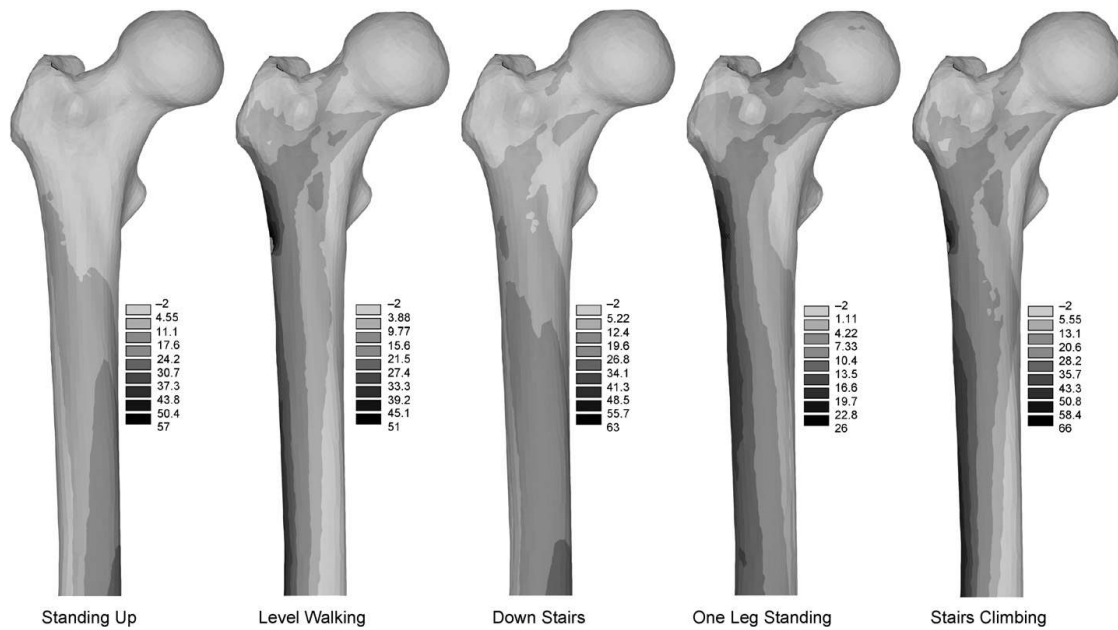


Fig. 3 –Principal tensile stress distribution as predicted by Finite Element analysis for five different loading scenarios. Different scales are used for the five loading scenarios, to allow comparison between the head-neck and diaphyseal region within the same case. These plots were explored to determine for which loading scenario the stress in the head-neck region is higher, in comparison with the diaphysis (i.e. proximal fractures are more likely than diaphyseal ones)

4.2.4.2 Results from 10 bone specimens

The test protocol was successfully applied to all specimens, with fractures occurring in the head-neck region (ie: the region where spontaneous fractures are most likely to occur). *In vitro* fractures varied from specimen to specimen, and ranged from cervical to inter-trochanteric (Fig. 4). Most of the fractures (80%, Table 1) initiated from the most proximal portion of the neck.

Load-displacement curves were highly linear ($R^2 > 0.99$) for most of the loading ramp. Linearity decreased only in the last few hundred Newton, prior to sudden failure. The failure load was 9344 ± 3140 N, corresponding to 10.9 ± 3.0 Body Weight (BW), Table 1.

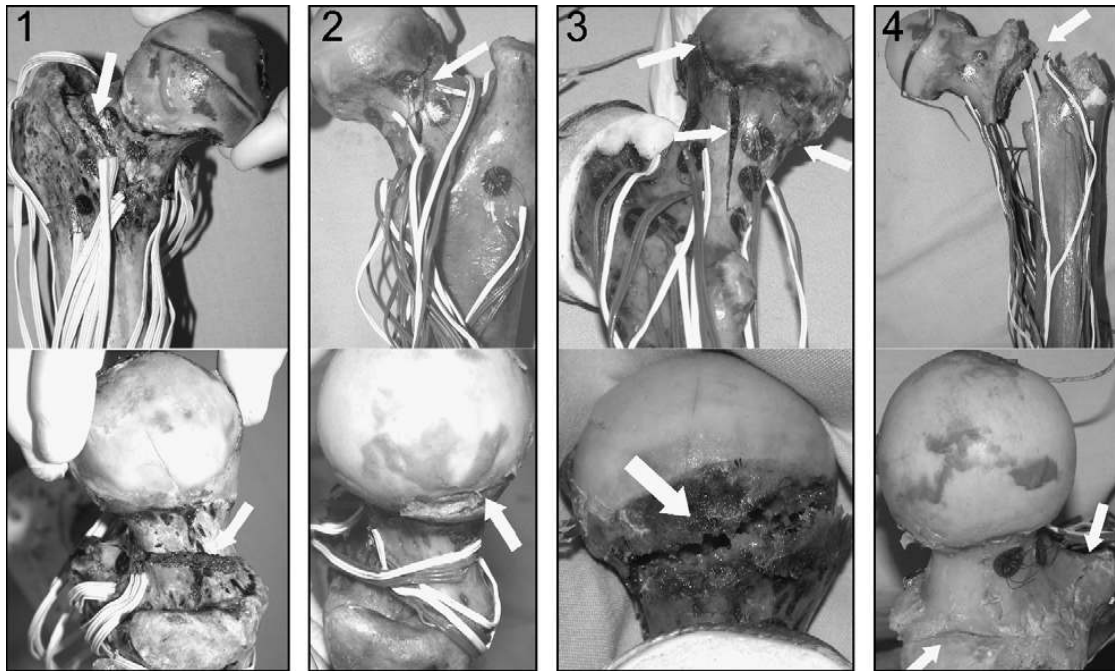


Fig. 4 – Typical fractures found in the *in vitro* fractured specimens (highlighted by the white pointers). 1) Base-of-the-neck fracture, close to the greater trochanter (top: frontal view; bottom: detail from the lateral-superior side of the neck). 2) Cervical fracture, showing two crack initiation sites laterally, which indicate uniform fracture risk area (top: posterior view on top; bottom: detail from the lateral-superior side of the neck). 3) Cervical fracture, propagating parallel to the neck, and including a secondary subcapital crack on the medial side (top: posterior view; bottom: lateral view of the head). Strain gauges can be seen, that were not part of this study. 4) Extracapsular (base-of-the-neck) fracture (top: anterior view; bottom: detail from supero-posterior side of the neck).

High-speed movie were successfully obtained for all specimens. They allowed observing the exact time when fracture initiated, and how it propagated across the bone (Fig. 5). A sample movie is available from the Journal website A sample movie is available from the Journal website.

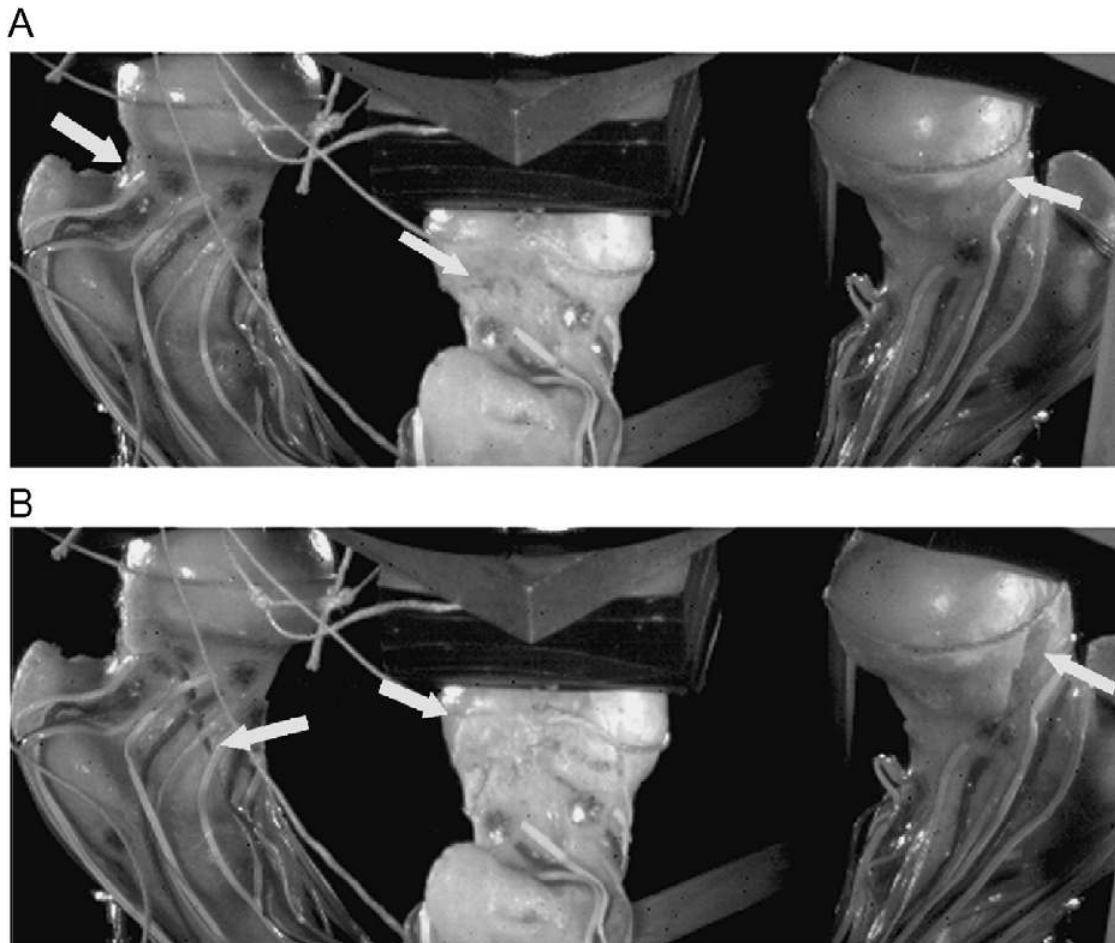


Fig. 5 – Frames obtained from a high-speed movie during a fracture test on a right femur. The image in the center of each picture is a direct view of the femoral neck from superior-lateral; the ones on the left and right (postero-medial and antero-medial views of the neck respectively) are reflected images obtained from the two mirrors placed next to the femur and suitably oriented (Fig. 1). Picture A shows the instant when the crack starts opening on the lateral part of the neck (indicated by the white pointer). Picture B (2.8 milliseconds after Picture A) shows a later stage of propagation. Strain gauges can be seen, that were not part of this study. Also, strings are visible that were glued to several points of the head and neck (they were slack, and bonded to unloaded regions): they were used to prevent excessive spreading of bone fragment upon fracture. The pictures have low resolution (1 pixel = approximately 0.2mm on the physical specimen) because they were acquired by the high-speed camera; view is clearer when the movie provided in the Supplementary Material is watched.

4.2.5. DISCUSSION AND CONCLUSIONS

Spontaneous fractures of the hip are caused by occasional overloads during daily activities, and are associated with hip resurfacing implants (Cotton, et al., 1994; Jeffery, 1974; Rockwood, et al., 1991; Rüedi and Murphy, 2001). They are associated with poor bone

quality due to age and osteoporosis. In fact, a decrease of bone tissue toughness is associated with age(Wang and Puram, 2004).

Despite some preliminary study(Keyak, et al., 2005; Keyak, et al., 2001), there is no strong indication concerning the most relevant loading scenario for replicating spontaneous neck fractures *in vitro*. The final scope of this paper was to design a knowledge-based test setup to simulate *in vitro* spontaneous fractures of the proximal femur. The three original goals were successfully met:

- Based on a validated FE model, the most critical loading scenario (among the possible motor tasks that a subject typically performs when spontaneous fractures occur) was identified, which should be simulated *in vitro*
- Based on past experience and on the current FE simulations, the simplest possible testing protocol was designed and implemented. It was demonstrated that it is not necessary to simulate the action of the muscles to investigate fractures in the head-neck region. This enables simplification and better reproducibility both of experimental simulations and of *in vitro* test setups.
- Application of the protocol to 10 femur specimens confirmed its feasibility and reproducibility. Clinically relevant fractures were obtained *in vitro* in all specimens, with failure loads which were compatible with occasional overloads (Bergmann, 2001; Bergmann, et al., 2001).

The loading scenario identified as most critical here is compatible with numerical studies (Daniel et al., 2006; Keyak, et al., 2001), and is quite similar to the one used by (Link, et al., 2003) (11° in the frontal plane). Also, this study indicated that it is not necessary to simulate the muscle forces to create a suitable stress state in the head-neck, region in accordance with previously published works (Cody, et al., 1999; Keyak, et al., 2005).

It must be stressed that the scope of this study was to recreate *in vitro* the conditions for spontaneous fractures of the proximal caused by a single sudden loading event (typically in elderly subjects), as opposed to fatigue fractures, which are caused by cyclic loading (usually associated with active subjects, and involving other regions than the proximal femur (Cotton, et al., 1994; Jeffery, 1974; Rockwood, et al., 1991; Rüedi and Murphy, 2001)). Consistently with most of similar works, the authors recommend simulation of a single loading ramp, as this seems to best represent the occasional overloading leading to non-traumatic fractures)(Grisso, et al., 1991; Jeffery, 1974; Michelson, et al., 1995; Muckle,

1976; Rockwood, et al., 1991). Others (Lochmüller, et al., 2002; Lochmüller, et al., 2000; Lochmüller, et al., 1998) have chosen to apply loading cycles of increasing magnitude.

The most common fracture initiation site was the subcapital region (80% of the specimens). This is the most common type of spontaneous fractures (Cotton, et al., 1994; Pauwels, 1935; Rockwood, et al., 1991). Indeed, a similar fraction of subcapital fractures was obtained *in vitro* by others (69% (Cody, et al., 1999) and 94% (Keyak, et al., 2001)).

The failure loads found here ($9344\pm 3140\text{N}$) are comparable with the values reported in the literature: (Ota, et al., 1999) reported a failure load of 8400N (loading direction not specified); (Link, et al., 2003) reported a failure load of $8890\pm 3770\text{N}$ (simulated stance); (Duchemin et al., 2006) reported a failure load of $9032\pm 3412\text{N}$ (11° in the frontal plane); (Smith, et al., 1992) reported a range of 4937-16148N; (Cody, et al., 1999) reported a value of $9920\pm 3219\text{N}$ (25° in the frontal plane). Such values are found in occasional overloading events such as stumbling or miss-stepping (Bergmann, 2001; Bergmann, et al., 2001), which are a suspected cause of spontaneous fractures (Cotton, et al., 1994; Rockwood, et al., 1991; Rüedi and Murphy, 2001).

The variability of the failure load expressed in N in this study (Coefficient of Variation $\text{CoV}=34\%$) is comparable to the values reported in the literature: (Lochmüller, et al., 2002; Lochmüller, et al., 1998) reported $\text{CoV}=27\text{-}39\%$; (Duchemin, et al., 2006) $\text{CoV}=38\%$, (Eckstein, et al., 2004; Link, et al., 2003) $\text{CoV}=42\%$ (both values are referred to a sample with a wider age range)(Cody, et al., 1999) $\text{CoV}=32\%$. In fact, a comparison on paired femurs (Eckstein, et al., 2004) indicated that the lower bound for repeatability is 15%.

It must be noticed that variability was reduced when the failure load was expressed in terms of fraction of the donor's BW, rather than in N: the Coefficient of Variation decreased from 33.6% to 27.5%. This supports the idea of reporting bone strength as a fraction of BW rather than in absolute terms, and is in agreement with the findings of (Lochmüller, et al., 1998).

It is worth remarking that the strength of the femur measured under this loading scenario is a potential predictor of neck strength when the femur is subjected to a lateral impact (Duchemin, et al., 2006; Keyak, 2000; Lochmüller, et al., 2002).

There are some limitations of this work that should be discussed. First, the sample size investigated was relatively small. However, the scope of the experimental tests was not to measure the average strength of the femur on a given population, but to provide a validation to the methodology.

Moreover, as no *in vivo* recording is available for such traumatic events, the FE simulation relied on scaled muscle forces based on stance conditions (Bergmann, 2001; Bergmann, et al., 2001), similarly to (Keyak, et al., 2005).

The test protocol developed and validated herein can thus be applied to investigate spontaneous fractures of the natural femur. It could also be extended to address neck fractures in the presence of epiphyseal prostheses.

Acknowledgments

The Authors wish to thank Enrico Schileo, PhD, Elena Varini, PhD, Francesco Pallini, MEng and Mauro Della Motta, MEng for the support during the tests; Francesco Traina, MD, for the advice on fracture classification; Andrea Bertuolo, MEng of EyePro System, Trento, Italy for the valuable consultancy with high-speed cameras; Mr. Luigi Lena for the artwork.

4.2.6 References

- Alho, A., Husby, T., Hoiseth, A., 1988. Bone mineral content and mechanical strength. An *ex vivo* study on human femora at autopsy. *Clin Orthop Relat Res.* 227, 292-297.
- Amstutz, H.C., Campbell, P.A., Le Duff, M.J., 2004. Fracture of the neck of the femur after surface arthroplasty of the hip. *J. Bone Jt. Surg. Am.* 86, 1874-1877.
- Backman, S., 1957. The proximal end of the femur: investigations with special reference to the etiology of femoral neck fractures; anatomical studies; roentgen projections; theoretical stress calculations; experimental production of fractures. *Acta radiol* 1-166.
- Bergmann, G., 2001. Hip 98 - Loading of the hip joint. Free University of Berlin, (Compact Disk ISBN 3980784800)
- Bergmann, G., Deuretzbacher, G., Heller, M., Graichen, F., Rohlmann, A., Strauss, J., Duda, G.N., 2001. Hip contact forces and gait patterns from routine activities. *J Biomech* 34, 859-871.
- Cody, D.D., Gross, G.J., Hou, F.J., Spencer, H.J., Goldstein, S.A., Fyhrie, D.P., 1999. Femoral strength is better predicted by finite element models than QCT and DXA. *J Biomech* 32, 1013-1020.

- Cotton, D.W.K., Whitehead, C.L., Vyas, S., Cooper, C., Patterson, E.A., 1994. Are hip fractures caused by falling and breaking or breaking and falling? Photoelastic stress analysis. *Forensic Science International* 65, 105-112.
- Cristofolini, L., 1997. A critical analysis of stress shielding evaluation of hip prostheses. *Critical Reviews in Biomedical Engineering* 25:4&5, 409-483.
- Cristofolini, L., 2007. Comments on: "Fractures of the proximal femur: correlates of radiological evidence of osteoporosis" (published on *Skeletal Radiology* 35: 202-211). *Skeletal Radiology* In press,
- Cristofolini, L., Saponara Teutonico, A., Monti, L., Cappello, A., Toni, A., 2003. Comparative in vitro study on the long term performance of cemented hip stems: Validation of a protocol to discriminate between "good" and "bad" designs. *J. Biomechanics* 36, 1603-1615.
- Cristofolini, L., Viceconti, M., 1999. Towards the standardization of in vitro load transfer investigations of hip prostheses. *Journal of Strain Analysis for Engineering Design* 34, 1-15.
- Cristofolini, L., Viceconti, M., Toni, A., Giunti, A., 1995. Influence of thigh muscles on the axial strains in a proximal femur during early stance in gait. *J Biomech* 28, 617-624.
- Dalen, N., Hellstrom, L.G., Jacobson, B., 1976. Bone mineral content and mechanical strength of the femoral neck. *Acta Orthop. Scand.* 47, 503-508.
- Daniel, M., Igljic, A., Kralj-Igljic, V., One-legged stance - A representative body position for the long term effect of the hip contact stress. 2006, 5th World Congress of Biomechanics Book of Abstracts. Published as *J. Biomechanics* 39 (supplement1), Munich, 29 July - 4 August 2006.
- Delaere, O., Dhem, A., Bourgois, R., 1989. Cancellous bone and mechanical strength of the femoral neck. *Arch. Orthop. Trauma Surg.* 108, 72-75.
- Deler, S., Spierings, A.B., Schmitt, K.-U., 2005. Anatomical model for the mechanical testing of hip protectors. *Med. Eng. Phys.* 27, 475-485.
- Duchemin, L., Skalli, W., Topouchian, V., Benissa, M., Mitton, D., Femoral fracture load and failure energy in two load configurations: an in vitro study. 2006, 16th EORS Annual meeting, Bologna,
- Eckstein, F., Wunderer, C., Boehm, H., Kuhn, V., Priemel, M., Link, T.M., Lochmüller, E.-M., 2004. Reproducibility and side differences of mechanical tests for determining the structural strength of the proximal femur. *J. Bone and Mineral Research* 19, 379-385.

- Gomez-Benito, M.J., Garcia-Aznar, J.M., Doblare, M., 2005. Finite element prediction of proximal femoral fracture patterns under different loads. *J. Biomech. Eng.* 127, 9-14.
- Grisso, J.A., Kelsey, J.L., Strom, B.L., Chiu, G.Y., Maislin, G., O'Brien, L.A., Hoffman, S., Kaplan, F., 1991. Risk factors for falls as a cause of hip fracture in women. The Northeast Hip Fracture Study Group. *N. Engl. J. Med.* 324, 1326-1331.
- Jarvinen, T.L., Sievanen, H., Jokihaara, J., Einhorn, T.A., 2005. Revival of bone strength: the bottom line. *J. Bone and Mineral Research* 20, 717-720.
- Jeffery, C.C., 1974. Spontaneous fractures of the femoral neck. *Orthop Clin North Am* 5, 713-727.
- Keyak, J.C., Rossi, S.A., Jones, K.A., Skinner, H.B., 1998. Prediction of femoral fracture load using automated finite element modeling. *J Biomech.* 31, 125-133.
- Keyak, J.H., 2000. Relationships between femoral fracture loads for two load configurations. *J Biomech.* 33, 499-502.
- Keyak, J.H., Kaneko, T.S., Tehranzadeh, J., Skinner, H.B., 2005. Predicting proximal femoral strength using structural engineering models. *Clin Orthop Relat Res* 219-228.
- Keyak, J.H., Rossi, S.A., Jones, K.A., Les, C.M., Skinner, H.B., 2001. Prediction of fracture location in the proximal femur using finite element models. *Med Eng Phys* 23, 657-664.
- Keyak, J.H., Skinner, H.B., Fleming, J.A., 2001. Effect of force direction on femoral fracture load for two types of loading conditions. *J Orthop Res* 19, 539-544.
- Lang, T.F., Keyak, J.H., Heitz, M.W., Augat, P., Lu, Y., Mathur, A., Genant, H.K., 1997. Volumetric quantitative computed tomography of the proximal femur: precision and relation to bone strength. *Bone* 21, 101-108.
- Link, T.M., Vieth, V., Langenberg, R., Meier, N., Lotter, A., Newitt, D., Majumdar, S., 2003. Structure analysis of high resolution magnetic resonance imaging of the proximal femur: in vitro correlation with biomechanical strength and BMD. *Calcif Tissue Int* 72, 156-165.
- Lochmüller, E.-M., Groll, O., Kuhn, V., Eckstein, F., 2002. Mechanical strength of the proximal femur as predicted from geometric and densitometric bone properties at the lower limb versus the distal radius. *Bone* 30, 207-216.
- Lochmüller, E.-M., Miller, P., Bürklein, D., Wehr, U., Rambeck, W., Eckstein, F., 2000. In situ femoral dual-energy X-ray absorptiometry related to ash weight, bone size and

- density, and its relationship with mechanical failure loads of the proximal femur. *Osteoporos Int.* 11, 361-367.
- Lochmüller, E.-M., Zeller, J.-B., Kaiser, D., Eckstein, F., Landgraf, J., Putz, R., Steldinger, R., 1998. Correlation of femoral and lumbar DXA and calcaneal ultrasound, measured in situ with intact soft tissues, with the in vitro failure loads of the proximal femur. *Osteoporos Int.* 8, 591-598.
- Lotz, J.C., Cheal, E.J., Hayes, W.C., 1991. Fracture prediction for the proximal femur using finite element models: Part I--Linear analysis. *J Biomech Eng* 113, 353-360.
- Mayhew, P.M., Thomas, C.D., Clement, J.G., Loveridge, N., Beck, T.J., Bonfield, W., Burgoyne, C.J., Reeve, J., 2005. Relation between age, femoral neck cortical stability, and hip fracture risk. *Lancet* 366, 129-135.
- Michelson, J.D., Myers, A., Jinnah, R., Cox, Q., Van Natta, M., 1995. Epidemiology of hip fractures among the elderly. Risk factors for fracture type. *Clin Orthop Relat Res.* 129-135.
- Muckle, D.S., 1976. Iatrogenic factors in femoral neck fractures. *Injury* 8, 98-101.
- Ota, T., Yamamoto, I., Morita, R., 1999. Fracture simulation of the femoral bone using the finite-element method: how a fracture initiates and proceeds. *J. Bone Miner. Metab.* 17, 108-112.
- Patel, S.H., Murphy, K.P., 2006. Fractures of the proximal femur: correlates of radiological evidence of osteoporosis. *Skeletal Radiology* 35, 202-211.
- Pauwels, F., 1935. Der Schenkenholsbruck, em mechanisches Problem. *Grundlagen des Heilungsvorganges. Prognose un kausale Therapie.* *Z Orthop Chir* 6,
- Rockwood, C.A.J., Green, D.P., Bucholz, R.W., 1991. *Rockwood and Green's fractures in adults.* J.B. Lippincott, Philadelphia
- Rüedi, T.P., Murphy, W.M., 2001. *AO principles of fracture management.* Georg Thieme Verlag, Stuttgart (3-13-117441-2 (LTV))
- Ruff, C.B., Hayes, W.C., 1983. Cross-sectional Geometry of Pecos Pueblo Femora and Tibiae - A Biomechanical Investigation: I. Method and General Patterns of Variation. *Am. J. Phys. Anthropol.* 60, 359-381.
- Shimmin, A.J., Back, D., 2005. Femoral neck fractures following Birmingham hip resurfacing. A national review of 50 cases. *J Bone Joint Surg Br.* 87-B, 463-464.
- Shimmin, A.J., Bare, J., Back, D.L., 2005. Complications associated with hip resurfacing arthroplasty. *Orthopaedic Clin. North America* 36, 187-193.

- Siebel, T., Maubach, S., Morlock, M.M., 2006. Lessons learned from early clinical experience of 300 ASR hip resurfacing implantations. Proc. Instn. Mech. Engrs. Part H: J. Engineering in Medicine 220, 345-353.
- Smith, M.D., Cody, D.D., Goldstein, S.A., Cooperman, A.M., Matthews, L.S., Flynn, M.J., 1992. Proximal femoral bone density and its correlation to fracture load and hip-screw penetration load. Clin Orthop Relat Res 244-251.
- Taddei, F., Cristofolini, L., Martelli, S., Gill, H.S., Viceconti, M., 2006. Subject-specific finite element models of long bones: An in vitro evaluation of the overall accuracy. J Biomech 39, 2457-2467.
- Taddei, F., Pancanti, A., Viceconti, M., 2004. An improved method for the automatic mapping of computed tomography numbers onto finite element models. Med Eng Phys 26, 61-69.
- Taddei, F., Schileo, E., Helgason, B., Cristofolini, L., Viceconti, M., 2006. The material mapping strategy influences the accuracy of CT-based finite element models of bones: An evaluation against experimental measurements. Med Eng Phys
- Voide, R., Van Lenthe, G.H., Müller, R., Femoral neck stiffness critically depends on loading direction. 2006, 5th World Congress of Biomechanics Book of Abstracts. Published as J. Biomechanics 39 (supplement1), Munich, 29 July - 4 August 2006.
- Wang, X., Puram, S., 2004. The toughness of cortical bone and its relationship with age. Ann Biomed Eng 32, 123-135.
- Yang, K.-H.-, Shen, K.L., Demetropoulos, C.K., King, A.I., Kolodziej, P., Levine, R.S., Fitzgerald, R.H.J., 1996. The relationship between loading conditions and fracture patterns of the proximal femur. J. Biomech. Eng. 118, 575-578.

5 CONCLUSIONS

CONCLUSIONS

All aims of researches developed within presented thesis were satisfied

1. A marker for different medical imaging techniques were developed and assisted to multi-level measurements merging, satisfying all previously defined requirements (not-magnetic, no artefacts, no bone damage).
2. Three anatomical coordinate systems were compared to support defining of the most reproducible coordinate system for tracing of anatomical plans. The system proposed by Ruff *et al* (1983) is preferable when the bone surface can be accessed *in vitro*.
3. A load cell able to reproduce the position of applied force during *in vitro* tests of long bones was developed and validated. This device has been used providing an extra data for the FEM validation, with accuracy of less than 2mm.
4. Then a novel technique called the Crack Grid has been developed. Able to distinguish crack initiation point with 3mm spatial resolution at 700kHz sampling rate.
5. All specified by LHDL-project data has been successfully acquired. The whole bone stiffness, strength and strain distribution related data were obtained for human radius, ulna, humerus, femur, tibia and fibula.
6. Loading direction and loading velocity relations were measured providing deeper insight into bone-structure viscoelastic behaviour.
7. Specific studies addressed to the proximal femur were conducted. An insight to understanding of proximal femur structure and its load bearing capabilities has been provided by strain gauges measurements.
8. An experimental method to replicate spontaneous fractures *in vitro*, has been completed and clinically relevant fractures were obtained. Within this method a mechanism of failure of natural and operated proximal femurs can be investigated.
9. The know-how developed about testing the proximal femur was also applied to testing and optimizing proximal epiphyseal replacement of the femur.

Reassuming, the main goal, to asses enormous dataset of human long bones biomechanics at organ level has been achieved, both for the LHDL project and specific research questions. Furthermore, this project has shown a power of interdisciplinary framework, once all datasets from all levels set together at one digital library.

APPENDIX

***APPENDIX: Stress-shielding and stress-concentration
of contemporary epiphyseal hip prostheses***

Luca Cristofolini, PhD ^{1,2}, Mateusz Juszczak, MEng ^{1,2}, Fulvia Taddei, PhD ¹, Richard E.
Field, PhD, FRCS³, Neil Rushton, MD, FRCS, FIMMM ⁴,
Marco Viceconti, Ph.D. ¹

¹ Laboratorio di Tecnologia Medica, Istituto Ortopedico Rizzoli, Bologna, Italy

² Engineering Faculty, University of Bologna, Italy

³ The Orthopaedic Research Unit, St Helier Hospital, London, UK

⁴ The Orthopaedic Research Unit, University of Cambridge, UK

This paper has been published on Proceedings of the Institution of Mechanical Engineers, PartH,
Journal of Engineering in Medicine. 2009/01/01/.

The author of the thesis has contributed to this work with statistical elaboration of the data.

ABSTRACT

After the first early failures, proximal femoral epiphyseal replacement is becoming popular again. Prosthesis-to-bone load transfer is critical for two reasons: stress-shielding is suspected of being responsible of a number of failures of early epiphyseal prostheses; stress-concentration is probably responsible of the relevant number of early femoral neck fractures in resurfaced patients. The scope of this work was to experimentally investigate the load transfer of a commercial epiphyseal prosthesis (BHR) and an innovative prototype proximal epiphyseal replacement (Prototype). To investigate bone surface strain, 10 cadaveric femurs were instrumented with 15 triaxial strain gauges. In addition the cement layer of the Prototype was instrumented with embedded gauges to estimate the strain in the adjacent trabecular bone. Six different loading configurations were investigated, with and without muscles. BHR: Significant stress-shielding was observed on the posterior side of the head-neck region (strain was halved); a pronounced stress-concentration was observed on the anterior surface (up to 5x in some specimens); BHR was quite sensitive to the different loading configurations. Prototype: the largest stress-shielding was observed in the neck region (lower than the BHR: alteration <20%); some stress-concentration was observed at the head region, close to the rim of the prosthesis (alteration <20%); the different loading configurations had similar effects. Such large alterations with respect to the pre-operative conditions were found only in regions where strain level was low. Conversely, alterations were moderate where strain was higher. Thus, prosthesis-to-bone load transfer of both devices has been elucidated; the Prototype preserved a stress distribution closer to the physiological condition.

Keywords: Epiphyseal hip prostheses; femoral head resurfacing; stress shielding; stress concentration; load transfer; in vitro bone testing; embedded strain gauges; physiological loading; proximal femur

List of abbreviations:

| | |
|------------------|---|
| ε_1 | maximum principal strain |
| ε_2 | minimum principal strain |
| θ_p | angle (θ_p) of the principal planes (counter-clockwise) |
| BW | Body Weight |
| FE | Finite Element |
| LCx | loading configuration (six different configurations were tested: LC1-LC5 and LCA) |
| AH, LH, PH, MH | strain gauges on the anterior, lateral, posterior and medial sides of the head |
| AN, PN, MN | strain gauges on the anterior, posterior and medial sides of the neck |
| A1, L1, P1, M1 | strain gauges on the anterior, lateral, posterior and medial sides of the diaphysis, below the lesser trochanter |
| A5, L5, P5, M5 | strain gauges on the anterior, lateral, posterior and medial sides, at mid-diaphysis |
| EL1, EM1 | strain gauge embedded in the bone cement, on the lateral and medial sides, proximal level |
| EL2, EM2 | strain gauge embedded in the bone cement, on the lateral and medial sides, distal level |
| ITI ₁ | Implanted-To-Intact: Ratio between the maximum principal strain (ε_1) after implantation of the epiphyseal prosthesis, and the strain in the same location before implantation, for the same loading configuration. |
| ITI ₂ | Implanted-To-Intact: Ratio between the minimum principal strain (ε_2) after implantation of the epiphyseal prosthesis, and the strain in the same location before implantation, for the same loading configuration. |

1. INTRODUCTION

Many epiphyseal replacements have been proposed, with Charnley as one of the earliest proponents [1]. Epiphyseal prostheses in the seventies and eighties had extremely poor success (e.g.: Wagner [2], Freeman [3], and THARIES [4] prostheses). Stress-shielding and subsequent adverse bone remodeling is a potential cause of failure for hip replacement [5-7]. In fact, stress-shielding in the most proximal portion of the operated epiphysis was suspected to be responsible of the high failure rate for some early epiphyseal prostheses [8-11].

There is a recent resurgence of epiphyseal replacement [11, 12]. These designs have short-term satisfactory outcome, with success rates between 96% at two years and 98% at 5 years [12-17]. The most frequent reason for early revision for recent designs is neck fracture [12-14, 18]. Neck fracture has been associated to stress-concentrations caused by contemporary epiphyseal prostheses [18, 19], possibly in association with notching caused by sub-optimal implant positioning [15, 20]. Therefore, concerns exist about possible complications related to non-physiological load transfer of contemporary designs: on the short term, bone fracture caused by stress-concentration; on the long-term adverse bone remodeling caused by stress-shielding.

Unnatural stress patterns were found in the femoral head with a Finite Element (FE) model for the Wagner prosthesis [9]. In a later simulation [21] concluded that “the hypothesis osteopenia in the central head region is caused by stress-shielding is not supported”. Recent FE simulations [19, 22, 23] reported significant stress-shielding in some portions of the femoral head, and critical stress-concentration in others; the load transfer mechanism was greatly affected by the interface conditions (these FE results should be taken with caution as they were not supported by any direct validation). A comparative *in vitro* study [8] and a simplified biomechanical analysis of clinical cases [24] indicated that varying degrees of stress-shielding could be expected with the Wagner and Freeman prostheses, depending on implant orientation. Conversely, a DEXA study reported no significant early bone remodeling in relation to BHR implants [25]. Also *in vitro* results (based on a single operated femur being compared against a single non-operated one, obtained from different donors) seemed to indicate that the proposed epiphyseal prosthesis maintained a “normal femoral strain distribution” [26]. Recently, [27] reported a moderate strain increase in a Durom-implanted composite femur. Unfortunately, only limited results were presented (one specimen, only three strain measurement locations, using a composite femur which has not been validated for testing epiphyseal prostheses).

A comparison of the studies above highlights contrasting results. Such inconsistency is possibly explained by the limited sample size of experimental studies, and by the fact that FE models were quite crude (and only partly validated). Moreover, while stress-shielding of hip stems has been extensively investigated [28, 29], methods to assess load transfer of epiphyseal prostheses are rather inconsistent. Part of the common belief about stress-shielding and its detrimental effects is merely anecdotal. In fact, to date no experimental study reporting a sufficient number of specimen and strain measurement points, and no validated FE model, has been published to provide quantitative information about stress-shielding induced by epiphyseal prostheses.

This work aimed at assessing *in vitro* if epiphyseal prostheses induce concerning alterations to the stress distribution in the bone of the head and neck region. To this scope, a commercial device and a prototype were investigated using cadaveric femurs, when different loading configurations were applied.

2. MATERIALS AND METHODS

Cadaveric bone specimens were instrumented with strain gauges. They were subjected to a variety of loading configurations non-destructively. They were first tested in the intact condition, then under the same loading configurations after implantation of one of two types of epiphyseal prostheses. Bone strains were compared in the intact and implanted conditions to assess the stress-shielding effect of the implants. In addition, cement strains were measured for one of the implant types to provide additional information concerning the internal state of stress.

2.1 Bone specimens

Ten unpaired fresh-frozen human femurs were obtained through an international donation program (IIAM, Jessup, PA, USA) from male and female donors who did not suffer of musculoskeletal pathologies (Table 1).

Table 1 – Details of the femurs investigated (average, standard deviation and range over ten specimens). In the first three columns, details of the donors are listed (age, height and weight at death). In the last three columns details of the femurs are reported: Bone quality is reported in the 4th (bone density T-score computed respect the young reference population, and of the age-matched population, based on the Norland DEXA scanner reference population). Biomechanical dimensions [28-30] are reported in the last two columns (Biomechanical Length BL, and Head diameter, HD, see also Fig. 1).

| | DONORS' DETAILS | | | FEMURS' DETAILS | | |
|------------------------------|----------------------|-------------------|-------------------|-----------------|------------------------|-----------------------|
| | Age at death (years) | Donor Height (cm) | Donor Weight (kg) | DEXA T-score | Biomech length BL (mm) | Head diameter HD (mm) |
| Average ± standard deviation | 70 ± 8 | 171 ± 8 | 82 ± 20 | -2.08 ± 0.81 | 418 ± 7 | 49.2 ± 2.4 |
| Range | 51 to 83 | 157 to 178 | 48 to 164 | -3.42 to -0.11 | 408 to 466 | 46.6 to 54.4 |

They were DEXA-scanned (Excel-Plus, Norland, USA) and CT-scanned (HiSpeed, General Electric, USA) to document bone quality and lack of abnormality or defects. Anatomical dimensions (biomechanical length, BL, and head diameter, HD, Fig. 1) were measured as defined in [28-30]. The density values (Table 1) covered the entire range from physiological to osteopenic to osteoporotic bone according to [31-33]. The femurs were assigned to two sub-samples of five each, to be assigned to the two implant types (see below): no significant difference existed between the two sub-samples (unpaired t-test, $p > 0.2$) for the donor's details, biomechanical dimensions and bone quality (Table 1).

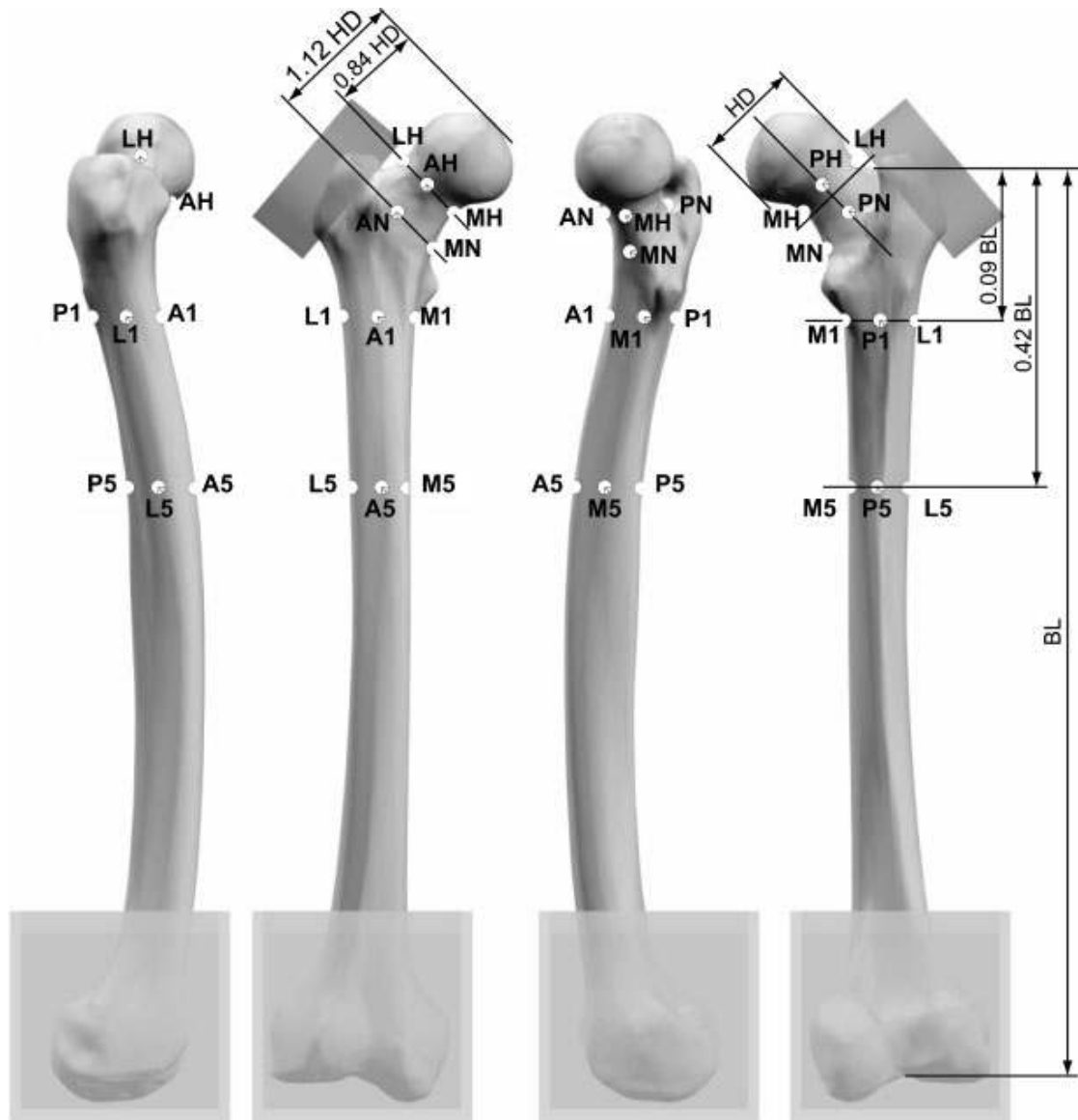


Fig. 1 – Right femur with an indication of the position of the strain gauges: lateral, anterior, medial, and posterior views. To allow comparable positioning between specimens, the levels were defined as a fraction of the femur dimensions (biomechanical length, BL, and head diameter, HD). The position around the neck of MH, MN, LH corresponded to the frontal plane [30]. The position around the neck of AH, AN, PH, PN corresponded to the mid thickness of the neck at the corresponding level. The position around the femur of A1, L1, P1, M1, A5, L5, P5, M5 corresponded to the mid thickness of the diaphysis. Also indicated is the epoxy pot on the greater trochanter used for application of the abducting force for loading configuration LCA (see Fig. 3).

The distal extremities of the femurs were potted with acrylic cement once the anatomical axes were identified [28-30]. During experimental tests, the femurs were wrapped in cloths soaked with physiological solution (room temperature: 27-30°C); they were stored sealed in bags at -25°C when not in use.

2.2 Strain measurement – bone surface

In order to measure principal strains (ϵ_1 and ϵ_2) and the angle (θ_p) of the principal planes, triaxial stacked strain gauges (KFG-3-120-D17-11L3M2S, Kyowa, Tokyo, Japan, grid length of 3mm) were bonded at fifteen locations (Fig. 1):

- Four around the head, close to the articular cartilage (Anterior, Lateral, Posterior, Medial sides);
- Three around the neck, distal to the previous ones (Anterior, Posterior, Medial: space on the lateral side was insufficient to host one additional strain gauge);
- Four around the proximal diaphysis, just below the lesser trochanter (Anterior, Lateral, Posterior, Medial).
- Four around the central part of diaphysis (Anterior, Lateral, Posterior, Medial). These gauges were not used for measuring the stress-shielding effect of the implant: they were placed at a sufficient distance from the implant so that they would not be affected by its. They served a control to verify that consistent loading conditions were applied to the intact and the implanted femur [28, 34]. For this reasons, readouts from these gauges are only briefly reported.

The actual position where the strain gauge was bonded sometimes was adjusted by some millimeters, when small defects (pores, ridges or grooves) made the bone surface unsuitable for bonding a strain gauge.

The measurement locations around the head (AH, LH, PH, MH) and neck (AN, PN, MN) were consistent with preliminary experience [35]. The measurement locations around the diaphysis (A1,L1,P1,M1,A5,L5,P5,M5) were consistent with previously published protocols for testing hip stems [28, 29]. The area for strain measurement was prepared with an established procedure for wet cadaveric specimens [36].

A grid excitation of 0.5V was selected to avoid heating. Strain was sampled at 10Hz, with a low-pass cutoff of 1Hz, using a multi-channel data logger (System-6000, Vishay Micro-Measurement, Raleigh, NC, USA).

2.3 Implants

Five femurs were implanted with Birmingham Hip Replacement (BHR, Midland Medical Technologies Ltd, Birmingham, UK). The BHR was chosen as a typical commercial epiphyseal prosthesis because it has been extensively implanted, reporting an excellent short-term outcome (97-98% positive follow-up at 2-3 years [13, 17], and stable implant [37, 38]).

The remaining five femurs were implanted with a prototype proximal epiphyseal replacement (Stryker Orthopaedics, Hérouville-Saint-Clair, France), simply referred to as “Prototype” in the following. This is a Cr-Co alloy device featuring a short curved stem (Fig. 2). The Prototype involved a slightly lower resection than the BHR, with complete removal of the epiphysis, to avoid the risk of necrosis of the residual most proximal epiphyseal bone as a consequence of loss of blood supply [39]. Because of its innovative design, it was suspected that the Prototype could alter the stress distribution in a significantly different way respect to other existing epiphyseal prostheses.

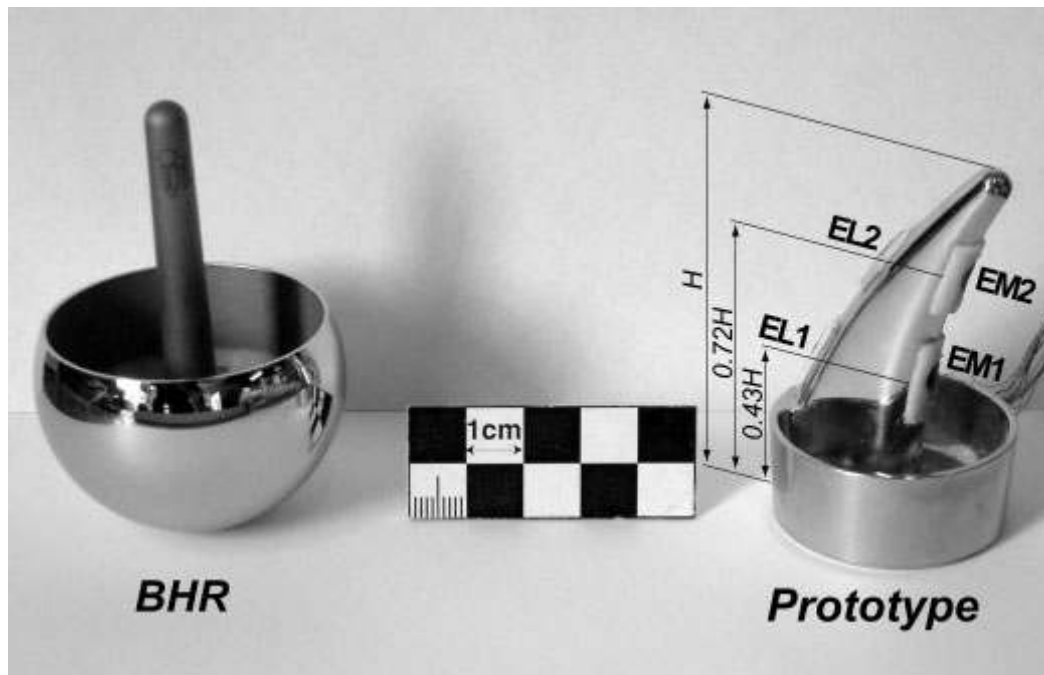


Fig. 2 – BHR (left) and Prototype femoral component (right, antero-posterior view). The BHR was axisymmetric. The Prototype was symmetrical about a frontal plane, and featured a short curved stem. The thin layers of pre-cured bone cement are visible on the Prototype, supporting the strain gauges to be embedded within the cement layer (two on the lateral side: EL1, and EL2, and two on the medial side: EM1, and EM2). The leadwires were included in the profile of the Prototype (and exited the prosthesis from the protruding proximal part) so as to minimize perturbation to the strain distribution [44]. The externally tapered quasi-cylindrical proximal part of the Prototype was coupled with a large sized modular ceramic ball (not visible here).

All implants were performed by experienced hip surgeons, following pre-operative planning (Hip-Op© software [40]), and according to the manufacturers' instructions. Both types of prosthesis were cemented with pre-chilled (+4°C) vacuum-mixed (Mixevac-II, Stryker, Mahwah, NJ, USA) acrylic bone cement (Simplex-P, Stryker). Correct implant positioning was assessed by post-operative X-rays.

2.4 Strain measurement – cement strain

As bone remodeling affects also the internal trabecular bone, and not just the outer cortical bone, it would be interesting to measure bone strain inside the bone. However, it is not possible to apply strain gauges on a porous material such as trabecular bone. To gain some information about the state of stress/strain inside the implanted bone, strain gauges were embedded inside the cement surrounding the Prototype stem (embedded strain gauges could not be placed on the BHR because it does not feature a proper cement mantle). As the Young's modulus of Simplex-P bone cement ($2.8 \pm 0.1 \text{ GPa}$, [41]) is comparable to trabecular bone ($1.5\text{-}4.0 \text{ GPa}$, [42, 43]), such strain values represent a good estimate of strain in the trabecular bone adjacent the cement layer. The technique for installing the embedded strain gauges included [44]:

1. Preparing thin grooves in the prosthesis to host the strain gauge leadwires inside the profile of the prosthesis;
2. Preparing a constant thickness layer ($1.0 \pm 0.05 \text{ mm}$) of pre-cured bone cement at the selected locations;
3. Bonding the triaxial stacked strain gauges (KFG-1-120-D17-11L3M2S, Kyowa, grid length of 1mm) with cyanoacrylate glue (CC-33A, Kyowa);

4. Sealing the grooves hosting the leadwires using talc-filled unsaturated polyester putty (140-Grifo, ICR, Reggio-Emilia, Italy)..

Four embedded strain gauges were placed on each Prototype stem, two on the lateral side (proximal: EL1, and distal: EL2), and two on the medial side (proximal: EM1, and distal: EM2), at a distance that was scaled according to the prosthesis size (Fig. 2).

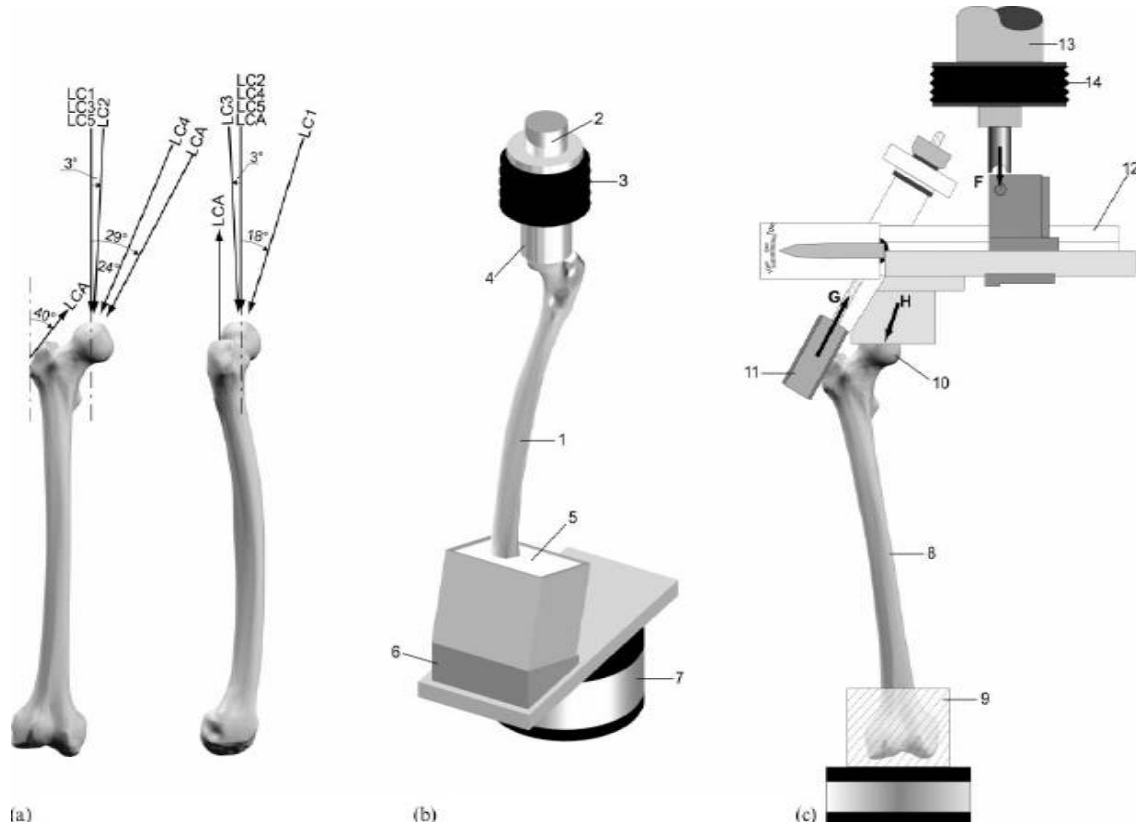
Signal from the embedded strain gauges were acquired using the same data logger (System-6000, Vishay) and settings as for those bonded on the bone surface.

2.5 Loading configurations

In order to investigate the strain distribution in the proximal femoral metaphysis, a set of simplified loading configurations was chosen (Fig. 3). The femur specimens were mounted on top of the load cell of the testing machine using interchangeable wedges to tilt the bone by the assigned angles. The force was applied vertical by the actuator of the testing machine to the femoral head through a system of rails to avoid transmission of horizontal force components, similarly to [28, 29]:

- LC1-LC4: To cover the physiological range of loading directions during a wide range of activities (including level walking at different speeds, single-leg-stance, stair-climbing and -descending, standing up from seated [45]), the cone spanned by the hip joint resultant force was calculated. Four loading configurations (LC1-LC4) were selected, to cover the extreme angle of the hip joint resultant force in the frontal and sagittal planes [46, 47]. A load was applied at the femoral head, simulating the hip joint resultant force. Muscle forces were not simulated, as experimental and Finite Element (FE) studies indicated they do not significantly alter the stress distribution in the proximal metaphysis [35, 48-51]. These configurations did not correspond to any specific motor task.
- LC5: To replicate a loading configuration frequently used in the literature (e.g.: [52, 53]), the femur was tested when the hip joint resultant force was parallel to the femoral diaphysis.
- LCA: As some studies [48, 54-56] suggest that muscle action significantly alters the stress distribution in the femoral diaphysis, to properly investigate the strain distribution around the distal portion of the implant, a configuration was included where the effect of the abductor muscles was simulated. The heel strike phase of gait was simulated, based on a previously validated procedure [28, 29].

Load was applied at a constant displacement rate of 2 mm/sec. To avoid bone, cement, or interface damage due to repeated loading, load was limited to 0.75 times the Body Weight (BW) of the relative donor [35, 46]. For all loading configurations the maximum force was held for thirty seconds to allow a constant time for a repeatable amount of creep to take place [Cristofolini, 1999 #60]. Each loading configuration was repeated six times on each



specimen. The specimens were allowed to recover for five minutes between repetitions.

Fig. 3 – A) Right femur (anterior and lateral views) with the direction of the applied force for the different loading configurations: LC1-LC4 covered the extreme directions of the hip joint resultant force in the sagittal and frontal planes; in LC5 the force was parallel to the diaphysis; LCA provided a validated simulation of the abductors [28, 29]. B) Setup for LC1-LC5 (postero-medial view) including: the femur (1); the actuator of the testing machine (2) with the system of rails to eliminate horizontal forces (3); the copy of the femoral head (4) to allow uniform load application; the distal pot holding the femur (5); the interchangeable wedges (6) to hold the femur at the assigned angles (LC4: 24° in the frontal plane and 0° in the sagittal plane, in this instance) on top of the load cell (7) of the testing machine. C) Setup for configuration LCA [28, 29]: the femur (8) was potted distally (9); the hip resultant force (H) was applied to the femoral head (10); the abducting force (G) was applied to the greater trochanter (11); the lever arms of a cantilever (12) were adjusted so as to obtain the desired hip joint and abducting force directions and magnitudes; a vertical force (F) was applied to the cantilever by the actuator (13) of the testing machine using a system of rails to eliminate horizontal forces (14).

2.6 Statistics

Linearity between force and strain was checked by linear regression separately for each strain gauge and each specimen. To obtain a single output for each strain gauge and each specimen, the average was calculated over all repetitions for the principal strains (ε_1 and ε_2) for the angle (θ_p) of the principal planes.

To provide an indication of the strain level in the intact condition, the strain distribution before implantation was examined (average over the ten femurs). This provided an

indication of the regions is larger/lower in the physiological conditions. The significance of the difference between the strain measurement locations, and between loading configurations in the intact condition were assessed by means of a factorial ANOVA, including a Fisher PLSD post-hoc where applicable.

To provide a quantitative estimate of the effect of the prosthesis on bone strain, the ratio was computed between the strain in the implanted femur, and the strain in the same location before implantation. The Implanted-To-Intact ratio (ITI_1 , ITI_2) was computed for both principal strain components (ϵ_1, ϵ_2), for each strain measurement location, each femur and each loading configuration. A value of ITI of 100% indicates no alteration with respect to the physiological condition; a value lower than 100% indicates stress-shielding; a value larger than 100% indicates an increased state of strain. Using the same femur as a control enabled reducing inter-specimen variability [28, 29]. Stress-shielding was computed separately for each strain measurement location, each specimen and each loading configuration. To avoid fictitiously large ratios due to close-to-zero data, the ITI was not computed where strain was lower than 50microstrain.

The significance of the effect of the two prostheses was assessed for each strain measurement location testing the hypothesis that ITI was different from 100% (one-group t-test). The significance of the difference between the stress-shielding induced by the two prostheses and by the different loading configurations was assessed by means of a factorial ANOVA, where the type of implant (BHR vs Prototype), the strain measurement location, the loading configuration were independent factors. For the cement strain measured by the embedded gauges in the Prototype implants, the significance of the effect of the different loading configurations and of the different strain measurement locations was assessed by means of a factorial ANOVA, where the strain measurement location, the loading configuration were independent factors. A Fisher PLSD post-hoc test was performed where applicable.

All statistical analyses were performed using dedicated software (StatView-5.0.1, SAS-Institute, Cary, NC, U.S.A.).

3. RESULTS

3.1 Quality of bone strain measurement

Load-strain linearity was excellent for each individual grid, and each loading configuration: $R^2 \geq 0.99$ for 98% of the cases where strains reached a value of 50microstrain or larger. This confirms that the bone can be assumed to behave linearly with good approximation[49].

Both for the BHR and the Prototype, strain in the distal region (gauges A5,L5,P5,M5) after implantation were within 20% of the strain before implantation for all loading configurations. This confirms that consistent loading conditions were applied to the intact and the implanted femur [28, 34]. For brevity, further details about these gauges are omitted as they provide little information about the effect of epiphyseal prostheses.

Measurement repeatability (intra-specimen variability) was good: the CoV between replicates under the same loading configuration was of the order of 1-4% (average: 0.4%) for the principal strain. Also, the angle (θ_p) of the principal planes varied on average by 0.3° (standard deviation) between replicates.

3.2 Strain distribution in the intact femurs (before implantation)

Both principal strains (ε_1 and ε_2) varied significantly (ANOVA, $p < 0.0001$, Fig. 4) between locations in the intact femurs. The direction of the applied force had a significant effect on both principal strains (ANOVA, $p < 0.0001$, Fig. 4). The location of the largest strains changed in relation to the direction of the applied force (Fig. 4). In general, the lateral part was the most stressed region in tension for most loading configurations, while the medial part was the most stressed region in compression (Fisher PLSD post-hoc, $p < 0.05$; Table 2).

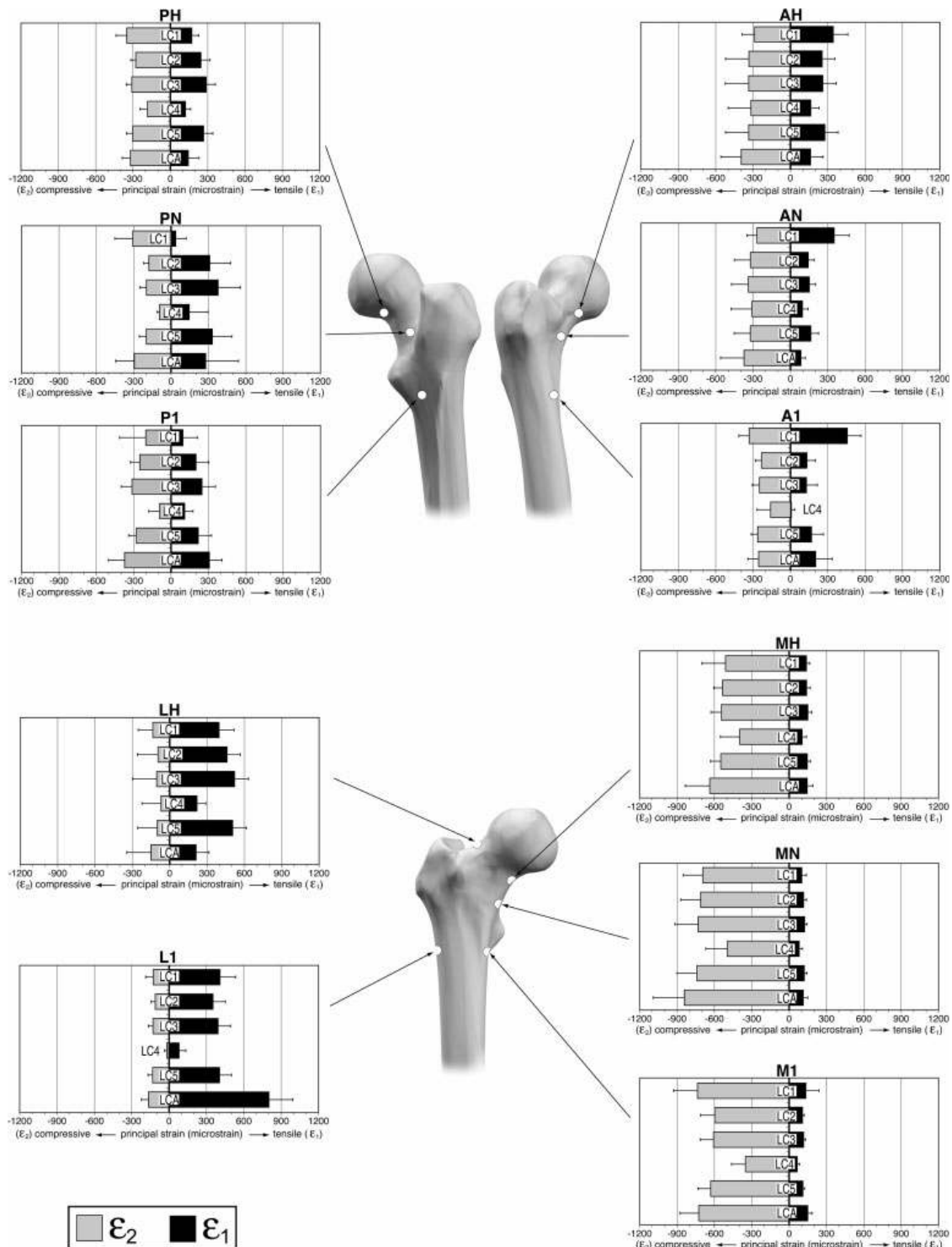


Fig. 4 – Maximum and minimum principal strains (ϵ_1 and ϵ_2) at 0.75 BW for the six loading configurations, for each measurement location. Average and standard deviation between 10 femurs is reported (all femurs going to be implanted with either implant type are pooled together to provide a reference of the strain in the intact condition).

3.3 Stress-shielding on the bone surface

In general, the strain distribution in the proximal implanted femur (both with the BHR and the Prototype) did not differ greatly from the intact: the Implanted-To-Intact ratios (ITI_1 and ITI_2) were close to 100% on most of the bone surface (Fig. 5-6); large differences were quite localized. While in most of the proximal femur the inter-specimen variability of the

ITI ratio was low, it was larger in the head region, and on the anterior side, especially where strain was low (<100microstrain).

Table 2 – Principal strains in the intact femurs. The average strain was computed over 10 specimens for each strain measurement location and for each loading configuration. Ranges are reported for each anatomical side of the femur.

| | ANTERIOR (AH, AN, A1) | LATERAL (LH, L1) | POSTERIOR (PH, PN, P1) | MEDIAL (MH, MN, M1) |
|---|----------------------------------|-----------------------------|-----------------------------------|--------------------------------|
| Maximum principal strain (ϵ_1) | 6 to 453 microstrain | 83 to 805 microstrain | 38 to 378 microstrain | 69 to 152 microstrain |
| Minimum principal strain (ϵ_2) | -159 to -396 microstrain | -14 to -161 microstrain | -91 to -373 microstrain | -348 to -840 microstrain |

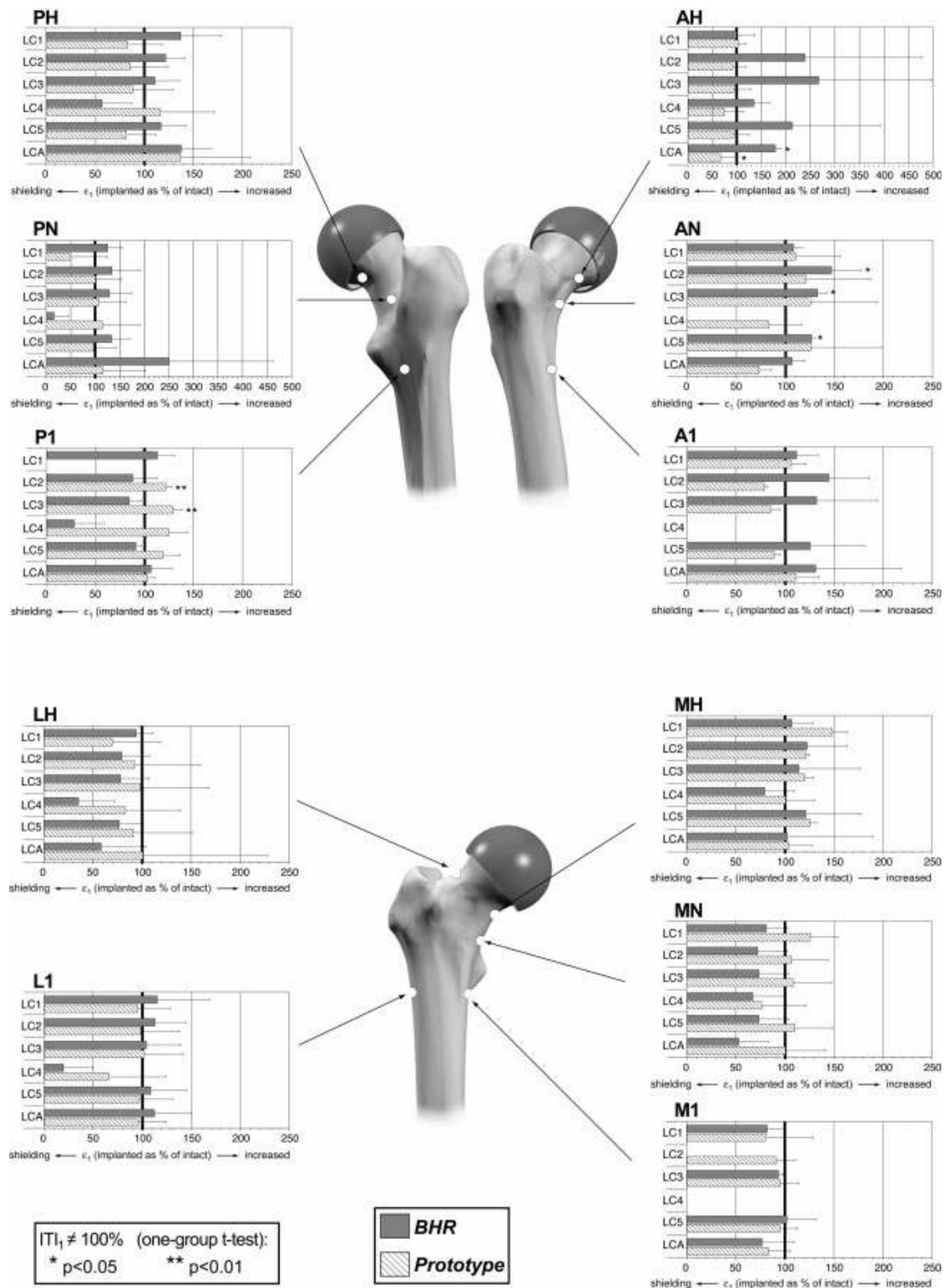


Fig. 5 – Alteration due implantation: IT_{I1} is the ratio between the maximum principal strain (ϵ_1) in the implanted and intact condition. IT_{I1}=100% indicates no alteration compared to the intact; IT_{I1}<100% indicates stress-shielding; IT_{I1}>100% indicates increased strain. Average and standard deviation between 6 BHR and 6 Prototype specimens are plotted for each measurement location, for the six load configurations. The distal locations (A5, L5, P5, M5) are not reported, as these gauges served as a control to ensure that identical loading was applied in the intact and implanted conditions. For each measurement location and each load configuration data was analyzed to assess if IT_{I1} was significantly different from 100% (one-group t-test).

NOTE: a different scale is used for AH and PN. Missing bars correspond to those locations where strain was lower than 50microstrain.

The Implanted-to-Intact ratio varied between loading configurations (especially with the BHR), but such effect was not statistically significant (Factorial ANOVA, $p=0.2$). In fact, if all strain measurement locations were averaged, the difference between the ITI for the different loading configurations never exceeded 30%, both for the BHR and the Prototype. In particular, the average ITI for LCA (simulation of abductor muscles) was always within the range for the remaining five loading configurations. LC4 was the loading configuration without simulation of the abductor muscles where the direction of the hip joint resultant force was closest to that of LCA (24° vs 29° in the frontal plane, Fig. 3). The difference between LCA and LC4 in terms of Implanted-to-Intact ratio (average of all strain gauges, Fig. 5-6) was less than 10%.

Both stress-shielding and stress-concentration were larger for the BHR than the Prototype: the Implanted-to-Intact ratio for the BHR was significantly different from 100% at several locations both on average (one-group t-test, Table 3) and for specific loading configurations (one-group t-test, Fig. 5-6); conversely, the Implanted-to-Intact ratio for the Prototype was significantly different from 100% only for specific loading configurations (one-group t-test, Fig. 5-6), but not on average (one-group t-test, Table 3). The alteration of the strain distribution greatly depended on the measurement location (Factorial ANOVA, $p=0.0002$ both for ITI_1 and ITI_2 ; Fig. 5-6). The difference between BHR and Prototype was statistically significant (Factorial ANOVA, $p=0.001$, both for ITI_1 and ITI_2 ; Fig. 5-6):

- The response of the BHR depended on the direction of the applied force: at some location (PH, PN) stress-shielding was observed for a given loading configuration, but stress-concentration was found for a different configuration. On average, the BHR caused stress-shielding in the posterior part of the head and neck (strain was nearly half the intact). A pronounced strain increase was observed in the anterior head and neck regions (on average strain was double than the intact). In one specimen a strain peak five times larger than the intact was found on the anterior side, when the hip joint force was close to the femoral axis (LC2, LC3, LC5).
- The load transfer of the Prototype seemed completely different: the largest stress-shielding was observed in the neck region (however, the amount of stress-shielding was lower than for the BHR, as it never exceeded 30%). Some stress-concentration was observed at the head region, close to the rim of the prosthesis (however, in no specimen such stress-concentration exceeded $ITI_1=250\%$). The different loading configurations had similar effects in terms of stress-shielding for the Prototype.

Table 3 – Summary of the largest alterations to the stress distribution (stress-shielding and stress-concentration) for both implant types. The localization is reported, together with the relative range of the ITI ratio.

| STRESS-SHIELDING | STRESS-CONCENTRATION |
|------------------|----------------------|
|------------------|----------------------|

| | | |
|------------------|------------------------------|------------------------------|
| BHR | PH, PN ITI = 53%- 57% ** | AH, AN ITI = 160%- 200% * |
| Prototype | AN, MN, PN ITI = 73%- 78% | LH, PH ITI = 126%- 147% |

NOTE: For each strain measurement location the six loading configurations were pooled and data were analyzed to assess if ITI was significantly different from 100% (one-group t-test):

* p<0.05

** p<0.01

It is remarkable that the alteration of the principal tensile strain (ITI₁, Fig. 5) and principal compressive strain (ITI₂, Fig. 6) were generally different: the average difference between ITI₁ and ITI₂ was 28%. ITI₁ was generally larger (i.e. less shielded) than ITI₂; stress-concentration affected most severely the principal tensile strains (ϵ_1).

The angle (θ_p) of the principal planes varied little between the intact and the implanted condition: variations of typically 0-20° (30-35° in two cases) were found for the BHR; variations for the Prototype never exceeded 16°.

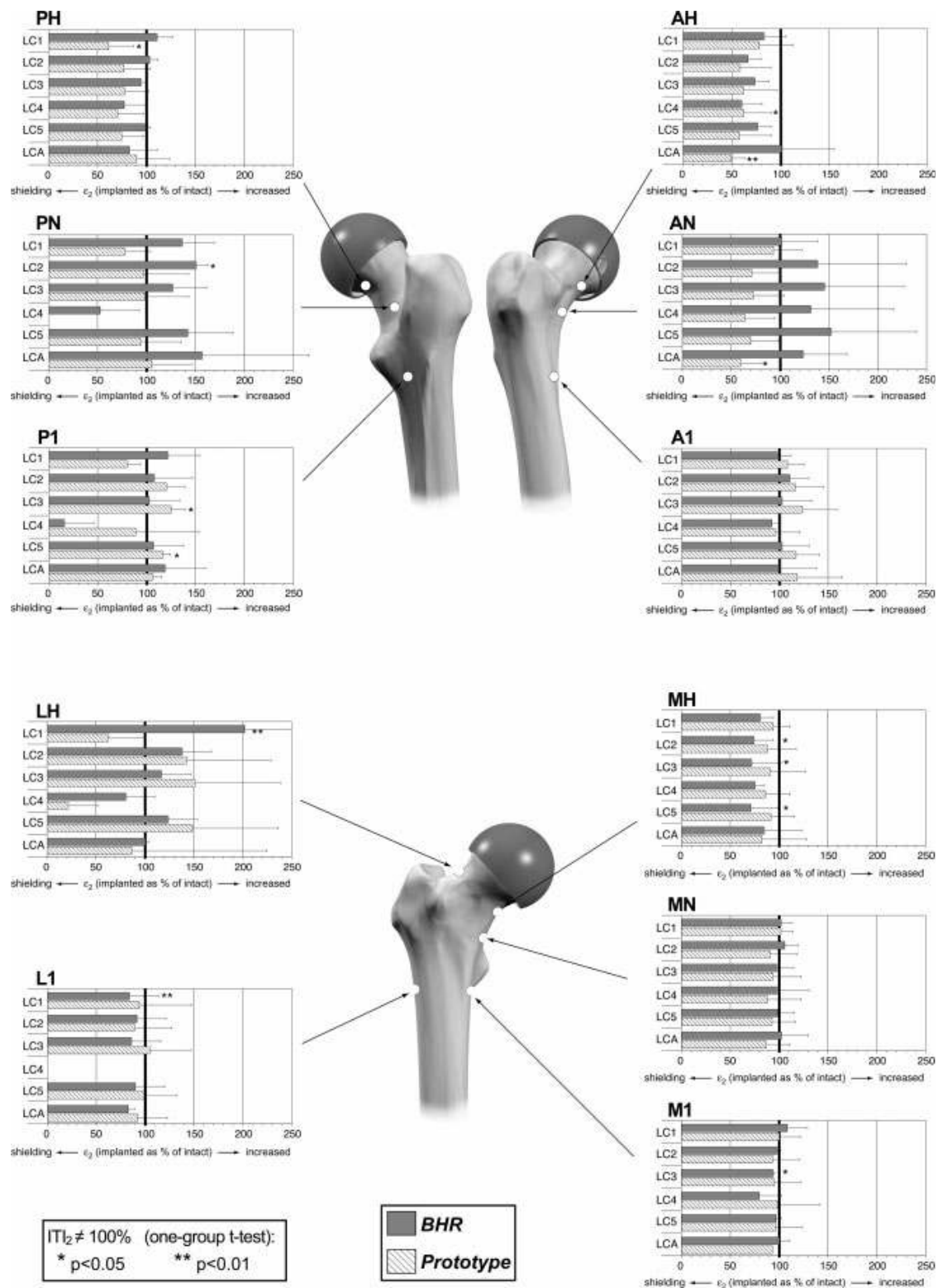


Fig. 6 – Alteration due implantation: ITI_2 is the ratio between the minimum principal strain (ϵ_2) in the implanted and intact condition. $ITI_2=100\%$ indicates no alteration compared to the intact; $ITI_2<100\%$ indicates stress-shielding; $ITI_2>100\%$ indicates increased strain. Average and standard deviation between 6 BHR and 6 Prototype specimens are plotted for each measurement location, for the six load configurations. The distal locations (A5, L5, P5, M5) are not reported, as these gauges served as a control to ensure that identical loading was applied in the intact and implanted conditions. For each measurement location and each load configuration data was analyzed to assess if ITI_2 was significantly different from 100% (one-group t-test).

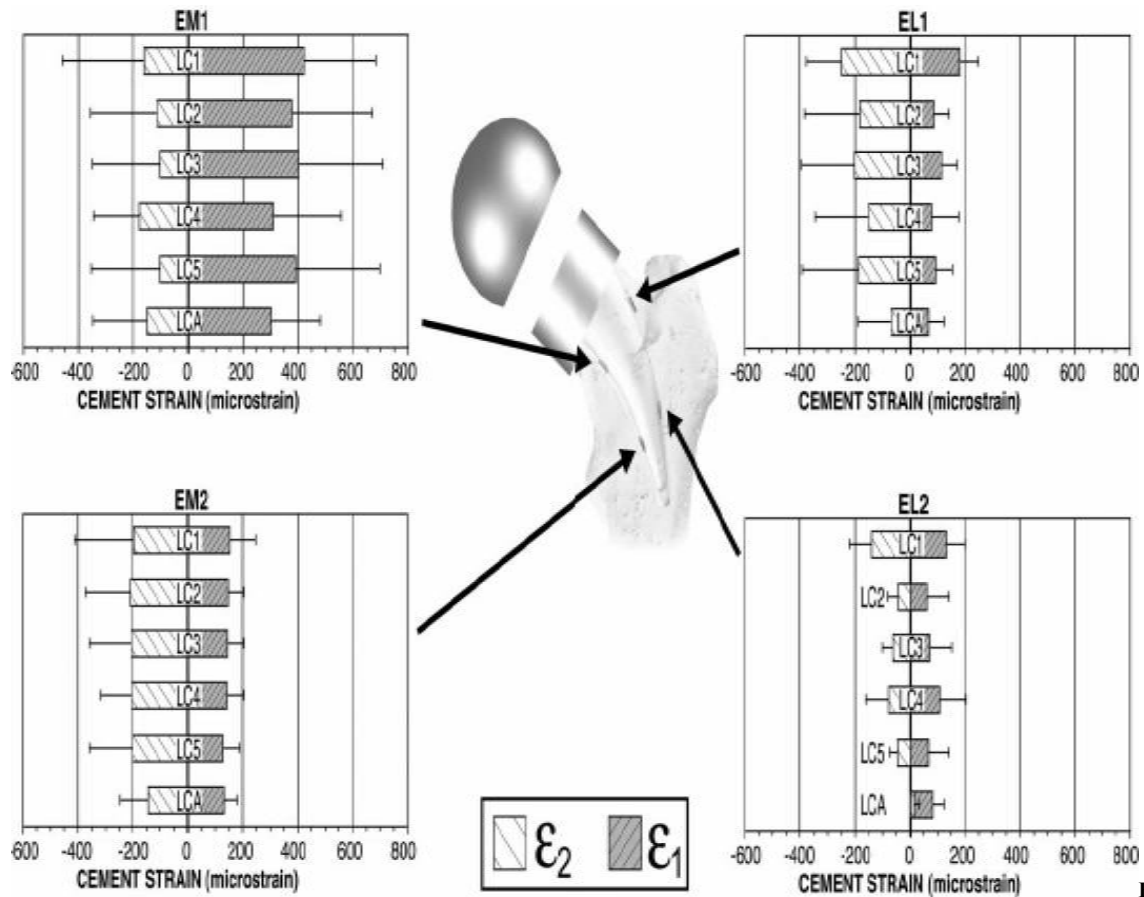


Fig. 7

– Principal strain in the cement layer of the Prototype (due to the limited amount of cement available, the BHR implants were not instrumented): average and standard deviation between 6 specimens. For each strain measurement location, the maximum and minimum principal strains (ϵ_1 and ϵ_2) are reported for the six load configurations (LC1-LC5 and LCA, see Fig. 3). As bone cement and trabecular bone have similar Young's modulus, such strain values represent an estimate of strain in the trabecular bone adjacent the cement layer.

3.4 Strain inside the implant structure

Cement strains were successfully recorded from all embedded gauges, with the exception of one gauge (EL1) that was damaged during implantation of one specimen. Principal strains in the cement ranged +61 to +417microstrain (ϵ_1) and +14 to -251(ϵ_2), and averaged (over all specimens, all strain gauges, all loading configurations) +178 and -139microstrain respectively (Fig. 7). The largest strains were always found in the proximal-medial location (EM1): these were almost twice as large as the strain recorded at the other locations. The strain at the different locations differed significantly (Factorial ANOVA, $p < 0.02$). The difference between loading configurations was not significant (Factorial ANOVA, $p = 0.8$).

Such values were recorded when a force of 0.75BW was applied. The typical load values recorded for physiological activities such as level walking at different speeds, single-leg-stance, stair-climbing and -descending, standing up from seated [45] are 1.9-2.6BW. If a proportion is applied considering a force of 2.5BW, the strain range recorded for ϵ_1 scale to 203-1391microstrain (average +592microstrain); the range recorded for ϵ_2 scale to +48 to -835microstrain (average -462microstrain).

Such strain values represent a good estimate of strain in the trabecular bone adjacent the cement layer.

4. DISCUSSION

After the first early unsuccessful designs, interest in epiphyseal replacement has greatly increased recently [11, 12]. No consensus has been reached as to whether stress-shielding-induced bone remodeling is a critical scenario for epiphyseal prostheses. Also, stress-concentrations associated with epiphyseal prostheses is a potential cause of bone fracture. This work aimed at assessing if contemporary epiphyseal prostheses induce concerning alterations to the stress distribution in the proximal femur. To this scope, a commercial device and a prototype were investigated using cadaveric femurs. A number of different loading configurations was simulated so as to explore the effect of a range of possible physiological activities.

Load transfer strongly varied between loading configurations for the BHR, but less for the Prototype. It is worth remarking that, while the strain distribution (both in the intact and in the implanted femur) was different when the abductor muscles were simulated (loading configuration LCA) if compared to any other loading configuration, the Implanted-to-Intact ratio for LCA was comparable to the other configurations (Fig. 5-6). This suggests that testing setups that do not feature abductor muscles can provide reliable estimates of the load transfer of epiphyseal prostheses.

Significantly different load transfer was found at different locations on the bone surface, for the two prosthetic designs. Alterations with respect to the intact conditions were generally small, with only some localized regions where strain was significantly altered. A highly significant difference was found between BHR and Prototype. Such difference was most pronounced in the anterior and posterior sides of the head and neck. The BHR caused stress-shielding in the posterior part of the head and neck; stress-concentration was found in the anterior head and neck regions. The largest stress-shielding for the Prototype was in the neck region. Moderate stress-concentration was observed for the Prototype at the head, close to the rim of the prosthesis. However, stress-shielding and stress-concentration for the Prototype were moderate: the average alteration respect to the intact never exceeded 20%.

For both devices, the regions where strain was most altered with respect to the intact (anterior and posterior, Fig. 5-6) corresponded to regions where strain was low in the intact femurs (Fig. 4).

The low resection level of the Prototype (complete removal of the epiphysis) in intended to avoid the risk of necrosis of the residual most proximal epiphyseal bone as a consequence of loss of blood supply [39]. This, in combination with the moderate alteration to the stress distribution, seems to indicate a low risk of adverse bone remodeling for the Prototype.

The alteration of the principal tensile strain (ϵ_1 , Fig. 5) and principal compressive strain (ϵ_2 , Fig. 6) were generally different. Therefore, if the alteration of the strain energy density (SED) is computed, a lower percentage variation can be expected than for the individual strain components. In fact SED is a combination of the different principal strain components (SED is often used as a predictor of bone remodeling in FE simulations, e.g.: [57-59]).

As it was not possible to measure strain in the trabecular bone, strain gauges were embedded in the bone cement where possible (i.e. along the stem of the Prototype). Strain measured in the bone cement represents a good estimate of strain in the adjacent trabecular bone, as the Young's modulus of cement (2.8 ± 0.1 GPa, [41]) is comparable to trabecular bone (1.5-4.0 GPa, [42, 43]). The cement strain recorded in this study were scaled to the typical load values recorded for physiological activities such as level walking at different speeds, single-leg-stance, stair-climbing and -descending, standing up from seated [45]: the strain range for ϵ_1 was to 203-1391 microstrain (average +592 microstrain); the range for ϵ_2 was to +48 to -835 microstrain (average -462 microstrain). Such strain values indicate that

the trabecular bone with the Prototype is stressed to a physiological level. In fact, strain during a number of physiological activities is in the range 300-1500microstrain [60, 61].

The strain reported here compare favorably with previous *in vitro* cadaveric studies: [26] measured tensile strain (ϵ_1) of 100-1200microstrain, and compressive strain (ϵ_2) of -100 to 1600microstrain with 1500N hip joint resultant force (unfortunately, load was not expressed in BW). In our BHR sample, the average tensile strain was +233microstrain; the average compressive strain was -337microstrain when a force of 0.75BW was applied. If a proportion is applied considering the average BW of the BHR sample, and scaling to 1500N, the strain values recorded here scale respectively to +476microstrain (ϵ_1) and -688microstrain (ϵ_2). Unfortunately more detailed comparisons are impossible because of the different sample size (1 vs 5), different strain gauge location, and different prosthetic device.

The generally moderate stress-shielding observed for the BHR on the bone surface is in agreement with previous studies: (i) *in vitro* studies [8, 26] found very low stress-shielding if the implant was correctly placed; (ii) no significant bone remodeling was observed with DEXA for BHR implants at 12 months [25] (to our knowledge, no similar long-term follow-ups are available).

Other studies conversely suggested that significant alteration to the strain pattern was induced by an epiphyseal prosthesis: (i) [9, 21] suggested that stress-shielding could be responsible of loosening of early resurfacing; (ii) [19, 22, 23] reported significant strain shielding in the superior femoral head for the ASR and BHR. All these studies were only numerical: results of FE models should be taken with extreme caution if they lack of quantitative experimental validation.

A pronounced stress-concentration was observed in the anterior and posterior sides of the head-neck region for the BHR for some loading configurations (up to five times the strain in the intact femur in some case). Such strain increase correlates with early fractures reported in implanted patients [14, 20, 62]. In fact, a recent study [18] correlated clinical fractures with stress peaks observed in FE models. This was also recently confirmed by an *in vitro* destructive test [35].

The main limitation of this study is that only the external bone surface is easily accessible for strain measurement. Therefore, reliable data were acquired for the alteration of the strain distribution only on the external bone surface. Internal strain was estimated exploiting strain gauges embedded inside the cement layer for one of the two devices. It is possible that some localized spots exist inside the trabecular structure where strain is significantly increased or shielded by the implant.

A typical limitation of strain gauges is that strain is measured only at the selected locations. This study featured a quite high number of strain gauges (fifteen triaxial strain gauges), higher than most published similar studies. However, in principle it is possible that very high localized shielding or concentration peaks existed at some points on the bone surface that were not observed because no strain gauge was attached to that point. However, an FE study carried out in parallel [35] confirmed that the alteration to the strain distribution on the bone surface is relatively smooth, with no highly concentrated peaks on the bone surface.

To prevent any possible bone, cement, or interface microdamage due to cyclic loading (6 loading configurations were repeated 6 times on each specimen), a low force was applied (0.75BW [35, 46]). Bone has been proven to behave linearly for this strain rate (this study, but also [49, 63]). Therefore, stress-shielding and stress-concentration computed as Implanted-to-Intact ratio do not depend on the actual load level.

The sample size was relatively small (five vs. five specimens). This increases the probability of false negatives (we might have failed to detect some existing effect).

Conversely, a small sample size does not induce false positives (if a difference is detected as significant, this difference is really significant). Most of our conclusions are based on statistically significant differences. We are not aware of any other *in vitro* study about load transfer of epiphyseal prostheses with five or more cadaveric femurs.

Finally, testing was intentionally limited to implants placed in the optimal position. In order to achieve an adequate sample size, all femurs were implanted in the best possible position, exploiting pre-operative planning [40]), and taking advantage of the *in vitro* conditions to optimize implantation reproducibility. It is possible that the patterns found here are altered in case of mispositioning, notching, etc.

In conclusion the BHR seems to somehow modify the strain distribution in the proximal femur. In fact, in some regions strain was remarkably shielded (although these were regions exposed to a generally low state of strain), while in other regions extremely high strain peaks were attained for specific directions of the applied load. The Prototype Proximal Epiphyseal Replacement seemed to transfer load in a more physiological fashion. In fact, strain in the implanted femur was closer to the strain in the intact femur, and stress peaks were less marked than for the BHR.

Acknowledgments

The Authors wish to thank Enrico Schileo, Saulo Martelli and Martino Pani for the valuable discussions; Elena Varini, Francesco Pallini and Mauro Della Motta for the support during the tests; Barbara Bordini and Manuela De Clerico for the statistical analysis; Luigi Lena for the artwork. This work was financially supported by Stryker Orthopaedics - Benoist Girard (Hérouville Saint Clair, France).

REFERENCES:

- 1 **Charnley, J. C.** Arthroplasty of the hip: A new operation. *Lancet*, 1961, **1**, 1129-1132.
- 2 **Head, W. C.** Wagner surface replacement arthroplasty of the hip. Analysis of fourteen failures in forty-one hips. *J Bone Joint Surg Am*, 1981, **63** (3), 420-7.
- 3 **Freeman, M. A. and Bradley, G. W.** ICLH surface replacement of the hip. An analysis of the first 10 years. *J Bone Joint Surg Br*, 1983, **65** (4), 405-11.
- 4 **Amstutz, H. C., Dorey, F. and O'Carroll, P. F.** THARIES resurfacing arthroplasty. Evolution and long-term results. *Clin Orthop Relat Res*, 1986, **213**, 92-114.
- 5 **Ahnfelt, L., Herberts, P., Malchau, H. and Andersson, G. B. J.** Prognosis of total hip replacement. A Swedish multicenter study of 4664 revisions. *Acta Orthop. Scand.*, 1990, **61**, 1-26.
- 6 **Coventry, M. B.** Lessons learned in 30 years of total hip arthroplasty. *Clin Orthop Relat Res.*, 1992, **274**, 22-29.
- 7 **NIH.** Consensus Statement on Total Hip Joint Replacement, NIH Consensus Statement, US Department of Health and Human Services, National Institute of Health, 1994 Sep 12-14; 12(5): 1-31.
- 8 **Crick, D., Wagner, J., Bourgois, R. and Dehu, P.** Comportement mécanique de l'épiphyse supérieure de fémur resurfacé et incidence des variations anatomiques et des différents types de cupules. *Acta Orthop. Belg.*, 1985, **51**, 168-178.
- 9 **Huiskes, R., Strens, P. H. G. E., van Heck, J. and Slooff, T. J. J. H.** Interface stresses in the resurfaced hip. Finite element analysis of load transmission in the femoral head. *Acta Orthop. Scand.*, 1985, **56**, 474-478.
- 10 **Head, W. C.** Total articular resurfacing arthroplasty. Analysis of component failure in sixty-seven hips. *J Bone Joint Surg Am*, 1984, **66** (1), 28-34.
- 11 **McMinn, D. and Daniel, J.** History and modern concepts in surface replacement. *Proc. Instn. Mech. Engrs. Part H: J. Engineering in Medicine*, 2006, **220** (2), 239-251.
- 12 **Amstutz, H. C., Beaulé, P. E., Dorey, F. J., Le Duff, M. J., Campbell, P. A. and Gruen, T. A.** Metal-on-metal hybrid surface arthroplasty: two to six-year follow-up study. *J Bone Joint Surg Am*, 2004, **86-A** (1), 28-39.
- 13 **Back, D. L., Dalziel, R., Young, D. and Shimmin, A.** Early results of primary Birmingham hip resurfacings. An independent prospective study of the first 230 hips. *J Bone Joint Surg Br.*, 2005, **87** (3), 324-329.
- 14 **Shimmin, A. J., Bare, J. and Back, D. L.** Complications associated with hip resurfacing arthroplasty. *Orthopaedic Clin. North America*, 2005, **36**, 187-193.
- 15 **Siebel, T., Maubach, S. and Morlock, M. M.** Lessons learned from early clinical experience of 300 ASR hip resurfacing implantations. *Proc. Instn. Mech. Engrs. Part H: J. Engineering in Medicine*, 2006, **220**, 345-353.
- 16 **Grigoris, P., Roberts, P., Panousis, K. and Jin, Z.** Hip resurfacing arthroplasty: the evolution of contemporary designs. *Proc. Instn. Mech. Engrs. Part H: J. Engineering in Medicine*, 2006, **220** (2), 95-105.

- 17 **Witzleb, W. C., Arnold, M., Krummenauer, F., Knecht, A., Ranisch, H. and Gunther, K. P.** Birmingham Hip Resurfacing arthroplasty: short-term clinical and radiographic outcome. *Eur J Med Res*, 2008, **13** (1), 39-46.
- 18 **Murray, D. W., Little, J. P., Steffan, R., Fouget, P., S., K., Gundle, R. and McLardy-Smith, P.** Femoral neck fractures following resurfacing. In *IMEchE Conference: Engineers & Surgeons: joined at the hip*, London, 2007, p[^]pp. 137-139.
- 19 **Taylor, M.** Finite element analysis of the resurfaced femoral head. *Proc. Instn. Mech. Engrs. Part H: J. Engineering in Medicine*, 2006, **220** (2), 289-297.
- 20 **Morlock, M. M., Bishop, N., R  ther, W., Delling, G. and Hahn, M.** Biomechanical, morphological, and histological analysis of early failures in hip resurfacing arthroplasty. *Proc. Instn. Mech. Engrs. Part H: J. Engineering in Medicine*, 2006, **220**, 333-344.
- 21 **Huiskes, R., Strens, P., Vroemen, W. and Slooff, T. J.** Post-loosening mechanical behavior of femoral resurfacing prostheses. *Clin Mater*, 1990, **6** (1), 37-55.
- 22 **Gupta, S., New, A. M. R. and Taylor, M.** Bone remodelling inside a cemented resurfaced femoral head. *Clin. Biomech.*, 2006, **21** (6), 594-602.
- 23 **Ong, K. L., Kurtz, S. M., Manley, M. T., Rushton, N., Mohammed, N. A. and Field, R. E.** Biomechanics of the Birmingham hip resurfacing arthroplasty. *J Bone Joint Surg Br.*, 2006, **88** (8), 1110-1115.
- 24 **Beaule, P. E., Lee, J. L., Le Duff, M. J., Amstutz, H. C. and Ebramzadeh, E.** Orientation of the femoral component in surface arthroplasty of the hip. A biomechanical and clinical analysis. *J. Bone Jt. Surg. Am.*, 2004, **86** (9), 2015-2021.
- 25 **Hayaishi, Y., Miki, H., Nishii, T., Hananouchi, T., Yoshikawa, H. and Sugano, N.** Proximal femoral bone mineral density after resurfacing total hip arthroplasty and after standard stem-type cementless total hip arthroplasty, both having similar neck preservation and the same articulation type. *J Arthroplasty*, 2007, **22** (8), 1208-13.
- 26 **Field, R. E. and Rushton, N.** Proximal femoral surface strain gauge analysis of a new epiphyseal prosthesis. *J. Biomed. Eng.*, 1989, **11**, 123-129.
- 27 **Ganapathi, M., Evans, S. and Roberts, P.** Strain pattern following surface replacement of the hip. *Proc. Instn. Mech. Engrs. Part H: J. Engineering in Medicine*, 2008, **222** (1), 13-18.
- 28 **Cristofolini, L.** A critical analysis of stress shielding evaluation of hip prostheses. *Critical Reviews in Biomedical Engineering*, 1997, **25:4&5**, 409-483.
- 29 **Cristofolini, L. and Viceconti, M.** Towards the standardization of in vitro load transfer investigations of hip prostheses. *Journal of Strain Analysis for Engineering Design*, 1999, **34** (1), 1-15.
- 30 **Ruff, C. B. and Hayes, W. C.** Cross-sectional Geometry of Pecos Pueblo Femora and Tibiae - A Biomechanical Investigation: I. Method and General Patterns of Variation. *Am. J. Phys. Anthropol.*, 1983, **60**, 359-381.
- 31 **NIH.** Consensus Statement on Osteoporosis, NIH Consens Dev Conf Consens Statement Online, US Department of Health and Human Services, National Institute of Health, 1984 Apr 2-4; 5(3):1-6.
- 32 **NIH.** Consensus Statement on Osteoporosis Prevention, Diagnosis, and Therapy, NIH Consens Statement Online, US Department of Health and Human Services, National Institute of Health, 2000 March 27-29; 17(1): 1-36.

- 33 **WHO.** Assessment of fracture risk and its application to screening for postmenopausal osteoporosis. Report of a WHO study group. WHO Technical Report Series, World Health Organization, Geneva, Switzerland, 843: 1-130. 1994.
- 34 **Cristofolini, L. and Viceconti, M.** In vitro stress shielding measurements can be affected by large errors. *Journal of Arthroplasty*, 1999, **14** (2), 215-9.
- 35 **Cristofolini, L., Juszczak, M., Pallini, F., Martelli, S., Taddei, F. and Viceconti, M.** Biomechanical testing of the proximal femoral epiphysis: intact and implanted condition. In *8th Biennial Conference on Engineering Systems Design and Analysis ASME-ESDA 2006*, Turin, 2006, p^pp.
- 36 **Viceconti, M., Toni, A. and Giunti, A.** Strain gauge analysis of hard tissues: factors influencing measurements. In *Experimental Mechanics. Technology transfer between high tech engineering and biomechanics* Ed E. G. Little, Elsevier Science Publisher B.V., Amsterdam, 1992, p^pp. 177-184.
- 37 **Glyn-Jones, S., Gill, H. S., McLardy-Smith, P. and Murray, D.** Roentgen stereophotogrammetric analysis of the Birmingham hip resurfacing arthroplasty. A two-year study. *J Bone Joint Surg Br.*, 2004, **86-B** (2), 172-176.
- 38 **Itayem, R., Arndt, A., Nistor, L., McMinn, D. and Lundberg, A.** Stability of the Birmingham hip resurfacing arthroplasty at two years. A radiostereophotogrammetric analysis study. *J Bone Joint Surg Br.*, 2005, **87** (2), 158-162.
- 39 **Steffen, R. T., Smith, S. R., Urban, J. P., McLardy-Smith, P., Beard, D. J., Gill, H. S. and Murray, D. W.** The effect of hip resurfacing on oxygen concentration in the femoral head. *J Bone Joint Surg Br*, 2005, **87** (11), 1468-74.
- 40 **Lattanzi, R., Baruffaldi, F., Zannoni, C. and Viceconti, M.** Specialised CT scan protocols for 3-D pre-operative planning of total hip replacement. *Med Eng Phys*, 2004, **26** (3), 237-45.
- 41 **Liu, C., Green, S. M., Watkins, N. D., Gregg, P. J. and McCaskie, A. W.** Some failure modes of four clinical bone cements. *Proc Inst Mech Eng [H]*, 2001, **215** (4), 359-66.
- 42 **Fung, Y. C.** Bone and cartilage. In *Biomechanics - Mechanical properties of living tissues*, Springer Verlag, New York, 1980, p^pp. 383-415.
- 43 **Ohman, C., Baleani, M., Perilli, E., Dall'Ara, E., Tassani, S., Baruffaldi, F. and Viceconti, M.** Mechanical testing of cancellous bone from the femoral head: experimental errors due to off-axis measurements. *J Biomech*, 2007, **40** (11), 2426-33.
- 44 **Cristofolini, L. and Viceconti, M.** Development and validation of a technique for strain measurement inside polymethylmethacrylate. *J. Strain Analysis in Engineering Design*, 2000, **35** (1), 21-33.
- 45 **Bergmann, G., Deuretzbacher, G., Heller, M., Graichen, F., Rohlmann, A., Strauss, J. and Duda, G. N.** Hip contact forces and gait patterns from routine activities. *J Biomech*, 2001, **34** (7), 859-71.
- 46 **Cristofolini, L., Varini, E. and Viceconti, M.** In-vitro method for assessing femoral implant-bone micromotions in resurfacing hip implants under different loading conditions. *Proc Inst Mech Eng [H]*, 2007, **221** (8), 943-50.
- 47 **Taddei, F., Cristofolini, L., Martelli, S., Gill, H. S. and Viceconti, M.** Subject-specific finite element models of long bones: An in vitro evaluation of the overall accuracy. *J Biomech*, 2006, **39** (13), 2457-67.

- 48 **Cristofolini, L., Viceconti, M., Toni, A. and Giunti, A.** Influence of thigh muscles on the axial strains in a proximal femur during early stance in gait. *J Biomech*, 1995, **28** (5), 617-624.
- 49 **Cristofolini, L., Juszczak, M., Martelli, S., Taddei, F. and Viceconti, M.** In vitro replication of spontaneous fractures of the proximal human femur. *J. Biomechanics*, 2007, **40** (13), 2837-2845.
- 50 **Keyak, J. H., Kaneko, T. S., Tehranzadeh, J. and Skinner, H. B.** Predicting proximal femoral strength using structural engineering models. *Clin Orthop Relat Res*, 2005 (437), 219-28.
- 51 **Cody, D. D., Gross, G. J., Hou, F. J., Spencer, H. J., Goldstein, S. A. and Fyhrie, D. P.** Femoral strength is better predicted by finite element models than QCT and DXA. *J Biomech*, 1999, **32** (10), 1013-20.
- 52 **Lotz, J. C., Cheal, E. J. and Hayes, W. C.** Fracture prediction for the proximal femur using finite element models: Part I--Linear analysis. *J Biomech Eng*, 1991, **113** (4), 353-60.
- 53 **Lochmüller, E.-M., Groll, O., Kuhn, V. and Eckstein, F.** Mechanical strength of the proximal femur as predicted from geometric and densitometric bone properties at the lower limb versus the distal radius. *Bone*, 2002, **30** (1), 207-216.
- 54 **Duda, G. N., Heller, M., Albinger, J., Schulz, O., Schneider, E. and Claes, L.** Influence of muscle forces on femoral strain distribution. *J Biomech.*, 1998, **31**, 841-846.
- 55 **Heller, M., Bergmann, G., Deuretzbacher, G., Dürselen, L., Pohl, M., Claes, L., Haas, N. P. and Duda, G.** Musculo-skeletal loading conditions at the hip during walking and stair climbing. *J Biomech.*, 2001, **34**, 883-893.
- 56 **Stolk, J., Verdonchot, N. and Huiskes, R.** Hip-joint abductor-muscle forces adequately represent in vivo loading of a cemented total hip reconstruction. *J Biomech.*, 2001, **34**, 917-926.
- 57 **Hollister, S. J., Kikuchi, N. and Goldstein, S. A.** Do bone ingrowth processes produce a globally optimized structure? *J Biomech*, 1993, **26** (4-5), 391-407.
- 58 **Weinans, H., Huiskes, R. and Grootenboer, H. J.** The behavior of adaptive bone-remodeling simulation models. *J Biomech*, 1992, **25** (12), 1425-41.
- 59 **Harrigan, T. P. and Hamilton, J. J.** Bone remodeling and structural optimization. *J Biomech*, 1994, **27** (3), 323-8.
- 60 **Aamodt, A., Lund-Larsen, J., Eine, J., Andersen, E., Benum, P. and Husby, O. S.** In vivo measurements show tensile axial strain in the proximal lateral aspect of the human femur. *J Orthop Res.*, 1997, **15** (6), 927-931.
- 61 **Lanyon, I. E.** Bone remodelling, mechanical stress, and osteoporosis. In *Osteoporosis* Ed H. F. De Luca, University Park Press, Baltimore, 1980, pp. 129-138.
- 62 **Amstutz, H. C., Campbell, P. A. and Le Duff, M. J.** Fracture of the neck of the femur after surface arthroplasty of the hip. *J. Bone Jt. Surg. Am.*, 2004, **86**, 1874-1877.
- 63 **Cristofolini, L., Taddei, F., Baleani, M., Baruffaldi, F., Stea, S. and Viceconti, M.** Multiscale investigation of the functional properties of the human femur. *Philos Transact A Math Phys Eng Sci*, 2008, **366** (1879), 3319-41.